Cold, Green and Clean:

Reduction of Parasitic Losses in Zero Emission Cryogenic Expanders

by

Iestyn Michael Nicholas Stead

A thesis submitted to the University of Birmingham

for the degree of DOCTOR OF PHILOSOPHY

Department of Mechanical Engineering

University of Birmingham

AUGUST 2020

Abstract

Dearman were a start up company manufacturing engines utilising a waste product, liquid nitrogen, to extract clean and cold power. The test case of the Dearman engine is a truck refrigeration unit (TRU), used on refrigerated delivery lorries; accounting for a large proportion of the total particulate emissions in refrigerated transport. The Dearman Engine reduces the total emissions from these refrigerated lorries however there is room for improvement and refinement to advance the technology closer to the maximum potential efficiency of the engine. This will reduce emissions from the system and the impact of refrigerated transportation on the environment. This thesis is focused on the tribology of the engine, reducing the parasitic losses through a three pronged approach: new materials, new lubricants and new designs. The Dearman Engine has a low power output compared to an internal combustion engine (ICE) and as such parasitic losses have the potential to absorb a significant amount of the power generated.

The cylinder liner — piston seal interaction was identified as the key contributor to friction in the engine. A material replacement investigation of the cylinder liner was undertaken through tribological specimen testing. A poly-tetrafluoroethylene (PTFE) cylinder, representative of the piston seal, was reciprocated against a number of polymer matrix composites (PMCs). The investigation compared the PMC to the current material used in the Dearman Engine: honed aluminium. The benchmark coefficient of friction at 12 °C under a contact pressure and reciprocating frequency representative of the Dearman Engine was 0.14. After investigation it was determined that unhoned poly-oxymethylene (POM) was the most beneficial polymer to implement in this area with a coefficient of friction of 0.08 at 12 °C. Unhoned POM also outperformed the benchmark in terms of settling time and percentage overshoot: summary statistics that were linked to the wear of the PTFE cylinder.

The potential of a laminated polymer as an alternative to the current piston seal, a composite, was also investigated: providing a saving in manufacturing costs and required energy of manufacture. Samples were tested under contact pressures representative of

the pressures in the Dearman Engine. There was no significant difference between the coefficient of friction and wear of a PTFE-PEEK composite and a PTFE-PEEK laminate at the same ratio of PTFE:PEEK (20%).

In an attempt to negate the need for an oil pump two fluids were examined as lubricants and potential heat exchange fluids (HEFs); one based on pectin and the other on bovine serum albumin (BSA). HEF is the working fluid that ensures efficient expansion of N_2 within the engine. It was shown that both fluids formed lubricating films and had the potential to be successful industrially viable lubricants. Pectin solutions were more sensitive to the concentration, where as BSA demonstrated less variation in the coefficient of friction between the two concentrations. At high loads BSA produced the lowest coefficient of friction; although at both loads tested $5\,\mathrm{mg\,ml^{-1}}$ pectin was capable of producing low coefficients of friction and as such in a complex system may be a better solution. The study identified that these lubricants have the potential to be a replacement for hydrocarbon based lubricants under the conditions tested.

Data analysis also led to improvements in the processing and potential insights inferred from tribological data: utilising a higher sample rate to investigate the effects of viscoelastic properties of polymers and lubricants on friction. Traditionally data is collected at a lower sample rate; this is a brute force approach to tribology and increasing this sample rate gives insights far exceeding the information present in traditional data analysis. The key feature that is missed in reciprocating tests is the area at the extremes of the stroke where a potential lubricant layer is broken down and there is stick-slip behavior resulting from asperity contact and a potential increased wear rate.

Combining a biomimetic lubricant/heat exchange fluid with a POM cylinder liner and a laminated PTFE/POM piston seal has the potential to reduce the parasitic losses and overall weight of the TRU. New analytical techniques will assist in future testing of viscoelastic materials and lubricants. This thesis has provided the inital steps in developing the Dearman Engine from a tribological perspective: potentially advancing the technology's industrial readiness and ensuring that the environmental ethos of the company is maintained.

To my Grandfathers, Bill and Roger

- who both encouraged me to pursue a career in engineering

Acknowledgements

I would like to first thank Prof. Karl D. Dearn, Prof. Thanos Tsolakis from the Department of Mechanical Engineering at the University of Birmingham and Dr. Henry Clarke from Dearman for their supervision and guidance over the past four years.

In addition I would like to thank Dr. David G. Eckold, Dr. Daniel Fennell, Mr. Nick Owen, Mr. Carl Hingley, Mr. Peter Thornton, Mr. Stephen Brookes and Mr. Lee Gauntlet for their academic and technical support without whom this thesis would be significantly shorter.

My thanks go to Dearman, The Institution of Mechanical Engineers, the Engineering and Physical Sciences Research Council and the Royal Commission for the Exhibition of 1851 for their technical and financial support, making my route to submission less stressful and allowing me to advance my research further. Without the support of members of the Mason Innovation and Tribology Group and the Biomedical Engineering Research Group I don't think I would have got this far. Thank you for the advice, ideas and most importantly: the coffee!

I would like to thank all those who provided the distractions that have been most welcome through the course of both my undergraduate and postgraduate studies; there are so many family members and friends to thank and it is impossible to get them all down!

The youth and leaders of Ariel Scout Group and the wider scouting community of Rea Valley District and Birmingham County have been invaluable in allowing me to escape from the office and reset (and occasionally providing inspiration) through the media of camping, hiking, and fire. I would especially like to thank Joe Hitchcock, Dan Loines

and Chris Wallace; the cause of a majority of my distractions (some beer may have been involved...).

Lastly, my family have also been a huge source of support, inspiration and fuel for procrastination; invaluable throughout the duration of my education. They have provided me with so much: a home, unfailing belief and a constant reminder that some things in life are apparently more important than the intricacies of Tribology (possibly).

IMNS 08/2020

Contents

List of Figures

List of Tables

Nomenclature

Subscripts and Superscripts

$\chi_{0,1,2,\ldots,i,\lambda,\ldots n}$ Index

$\hat{\chi}$ Maximum

$\widetilde{\chi}$ Median

Signal Processing

α Butterworth Filter coefficients

β_i Butterworth polynomial of order i

σ Rise time of a signal (s)

B Minimum frequency of observed effects (Hz)

f_s Sampling Frequency (Hz)

$R(s)$ Input Signal

s Laplace transfer parameter

T_s Time to steady state (s)

$Y(s)$ Transfer Function

Material and Lubricant Properties

γ Surface tension ($\mathrm{N\,m^{-1}}$)

γ_{LV} Surface tension between lubricant and the ambient air ($\mathrm{N\,m^{-1}}$)

ν Poisson's Ratio

θ Contact Angle ($^\circ$)

θ_0 Contact Angle for a smooth surface ($^\circ$)

A_F Area of A_{SL} projected onto flat plane ($\mathrm{m^2}$)

A_{SL} Area of solid-liquid surface ($\mathrm{m^2}$)

E Elastic Modulus or Young's Modulus (Pa)

E^* Equivalent Elastic Modulus (Pa)

R_f Roughness factor

W_{SL} Work of adhesion between a solid and liquid (J)

Physical and Mechanical Properties

δ Angular deviation of the valve stem

μ Coefficient of Friction

ψ Angle between connecting rod and axis of the cylinder bore ($^\circ$)

ξ Crank Angle ($^\circ$)

A Area ($\mathrm{m^2}$)

d Displacement (m)

E_μ Frictional Energy Dissipated (J)

F Force (N)

H Height (m)

K Spring Constant ($\mathrm{N\,m^{-1}}$)

L Length (m)

P Pressure (Pa)

R Radius (m)

T Temperature (°C)

V Volume (m^3)

v Velocity ($m\,s^{-1}$)

V_{CP} Contact Potential (mV)

Mathematical Notation

Δ Change in variable

$\varnothing$ Diameter

$\in$ In the set of

$[a, b]$ Greater than or equal to a and less than or equal to b

$|\chi|$ Absolute Value

$\perp$ Perpendicular or normal

$\prod$ Product operator

j $\sqrt{-1}$

x, y, z Cartesian coordinates

Acronyms

A Alanine.

BDC bottom dead centre.

BMEP brake mean effective pressure.

BSA bovine serum albumin.

C Cysteine.

CHP combined heat and power.

EDS energy-dispersive X-ray spectroscopy.

FMEP frictional mean effective pressure.

HEF heat exchange fluid.

HFRR high frequency reciprocating rig.

HSD high speed data.

ICE internal combustion engine.

IMEP indicated mean effective pressure.

K Lysine.

LiN liquid nitrogen.

LNG liquid natural gas.

LSD low speed data.

PA poly-amide.

PEEK polyether etherkeytone.

PMC polymer matrix composite.

POM polyoxymethylene.

PPA polyphthalamide.

PTFE poly-tetrafluoroethylene.

PTFE-L PTFE laminate.

PTFE-PEEK-C PTFE-PEEK composite.

PTFE-PEEK-L PTFE-PEEK laminate.

PTT polytrimethylene terephthalate.

SEM scanning electron microscope.

TDC top dead centre.

TRU truck refrigeration unit.

UHMWPE ultra high molecular weight polyethylene.

Chapter 1

Introduction

Fossil fuels and the issues surrounding their use are widely reported in the popular media. Headlines such as:

> "Air pollution particles found in mothers' placentas"
>
> (Carrington 2018)

and

> "Noxious air disappeared when London closed roads to cars for cycle event"
>
> (Reid 2018)

are never far from the front pages. Quoting alarming statistics is designed to apply political pressure on vehicle manufacturers, policy makers and consumers to be mindful of the impact of burning hydrocarbons for fuel. Whilst the statistics and measures reported by the media should be approached with caution, the underlying messages are very important.

The issues with crude oil fall into two categories: supply and usage. The drilling and extraction of crude oil is nearing a global production peak whilst the consumption of fossil fuel derived products is increasing with population growth and increased industrialisation (Sperling and Gordon 2009, pp. 5, 120). It is without a doubt that rapid technological development and increased production, as seen in Britain, during the 1850's would not have been possible without coal (Wrigley 2010) and later petrol, diesel and natural gas; however there is now a push to reduce reliance on these fuels.

There have been large steps in the past few decades to reduce emissions from the combustion of fuel in petrol and diesel engines. Legislation such as EU 2016/1628 restricts the levels of CO_2 and particulate matter allowed to be exhausted into the atmosphere by a variety of vehicle types. This new regulation, which came into force in 2018 and 2019, has widened the scope of previous regulation to include engines not involved in moving vehicles on the road. It is currently the most restrictive emission standard in the world (International Council On Clean Transportation 2016). Technological steps such as the installation of catalytic converters (Bhattacharyya and Das 1999), diesel particulate filters (Maricq 2007) and hydrogen fuel reforming systems (Fennell et al. 2014), to name a few,

have all reduced the levels of emissions but gasses such as CO_2 are still produced. The drive for reduced emissions is driven by two factors: public health and climate change; both equally as important for the improvement and continuation of the global community. Reducing reliance on fossil fuels and their impact on health and nature is a step in the right direction, however it is not the answer to solving the issues widely reported within the media and in more reliable sources.

There is also social and political pressure to reduce waste. One way to decrease waste is to use the resource in its most efficient manner. This idea was brought into the public domain by the publication of a report by the UK Department of Education and Science in 1966 (Jost et al. 1966). The report lists the huge cost to British manufacturing that is caused by improper lubrication and a lack of understanding of contacts between surfaces. In addition to these available savings, a technology that takes a waste product and can generate power or another useful product is hugely valuable on the path to reducing reliance on fossil fuels and in utilising the most energy from any power source. One example of this is combined heat and power (CHP) plants (Dentice d'Accadia et al. 2003). This technology takes the heat produced and subsequently wasted by the generation of electricity and use this energy to heat the premises and locality. This works well when the power generation plant is in the locality of where the heat is required such as in a residential neighbourhood.

Nitrogen is the most abundant gas in the atmosphere, making up $\approx$ 80% by volume (Lehninger 1982, p. 335). It is separated from air by the use of fractional distillation. This liquid nitrogen (LiN) can then be transported via tankers and stored for further use. LiN is used throughout the world for many different cooling purposes. The applications vary from medical science (Chian 2010), transport of food (Brown 2008) and machining (Ravi and Kumar 2012). In all of these the nitrogen is exhausted into the atmosphere at cryogenic temperatures returning it to where it was initially extracted. This wasted resource is a very useful energy vector (Private Correspondence, Dearman 2015).

The major issue with supply of LiN is that the infrastructure for widespread use is not currently available. This issue is more prevalent in the developing world. The Birmingham

Energy Institute proposed an interesting solution to this: liquid natural gas (LNG) being pumped off ships into storage and power generation plants as a source of waste cold that can be used to produce liquid air (Peters 2016). Communities and their industries would not benefit from such a system without technologies, such as the Dearman Engine — a cryogenic rankine cycle expander; that can exploit this waste cold to produce power. This engine has the most potential in applications where cooling and power are required such as data centres or refrigerated transport.

This thesis focuses on improving the efficiency of the Dearman Engine through studying the materials, fluids and designs currently used and testing alternatives.

Thesis Structure

Figure 1.1 shows the structure of the thesis working to improve the efficiency of the Dearman Engine.

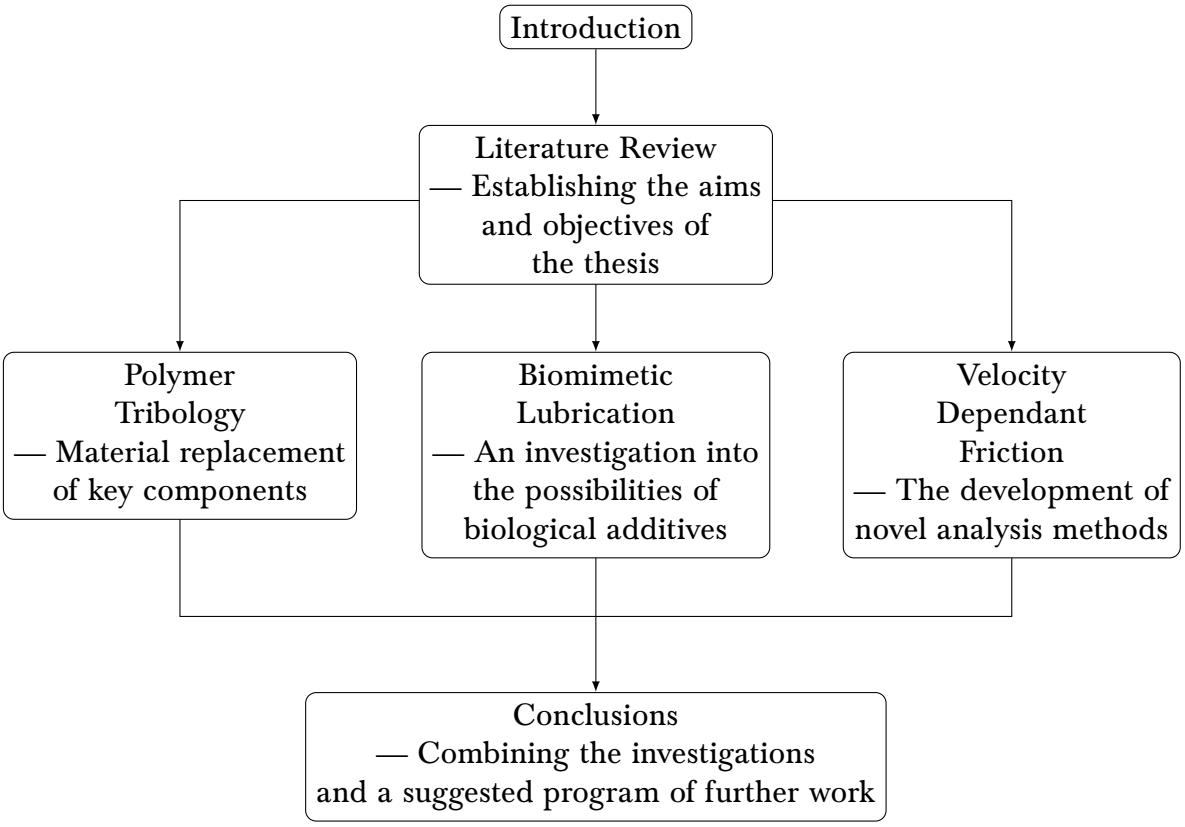

Figure 1.1: The structure of this thesis.

Chapter 2

Literature Review

The Dearman Engine is one addition to the global attempts to reduce the impact of engineering on the natural world. In order to utilise its full potential, research into reduction of parasitic losses, such as friction, is critical. Minimising lost energy, increasing longevity of parts and reducing the complexity of the engine are all imperative for successful industrialisation in the future.

2.1 The Dearman Engine

This section has been developed using personal correspondence with Dearman dating from 2015 to the date of submission.

The Dearman Engine is a cryogenic expander, shown in Figure 2.1; it operates on a cycle similar to the Rankine Cycle as shown in Figure 2.2 (Walshaw 1946, p. 135). The initial test case for the effectiveness of the system was a refrigerated goods truck resulting in the Dearman truck refrigeration unit (TRU).

The engine uses two working fluids: liquid nitrogen (LiN) and a heat exchange fluid (HEF). These fluids work synergistically within the cylinder to provide a near isothermal expansion (Igobo and Davies 2014). This combination of fluids within the cylinder was the brain child of British Inventor: Peter Dearman (Dearman 2006). LiN is evaporated within a heat exchanger external to the engine. In the case of the TRU the heat exchanger is located within the food storage area of the truck and is the initial cooling step in the system. The LiN enters the engine at high pressure (30 bar to 50 bar) and ambient temperature after passing through the exchanger.

The power cycle is as shown in Figure 2.3. As soon as the N_2 enters the cylinder and comes into contact with the HEF, the pressurised gas expands resulting in a power stroke. Due to the HEF, the expansion is nearly isothermal. As the piston rises the expanded mixture is exhausted. The dual phase fluid that is removed from the cylinder is then separated in the exhaust system. As the piston nears top dead centre (TDC) HEF is injected into the cylinder ready for the injection of the N_2 just after TDC.

In the TRU the power generated by the expansion is used to power a conventional

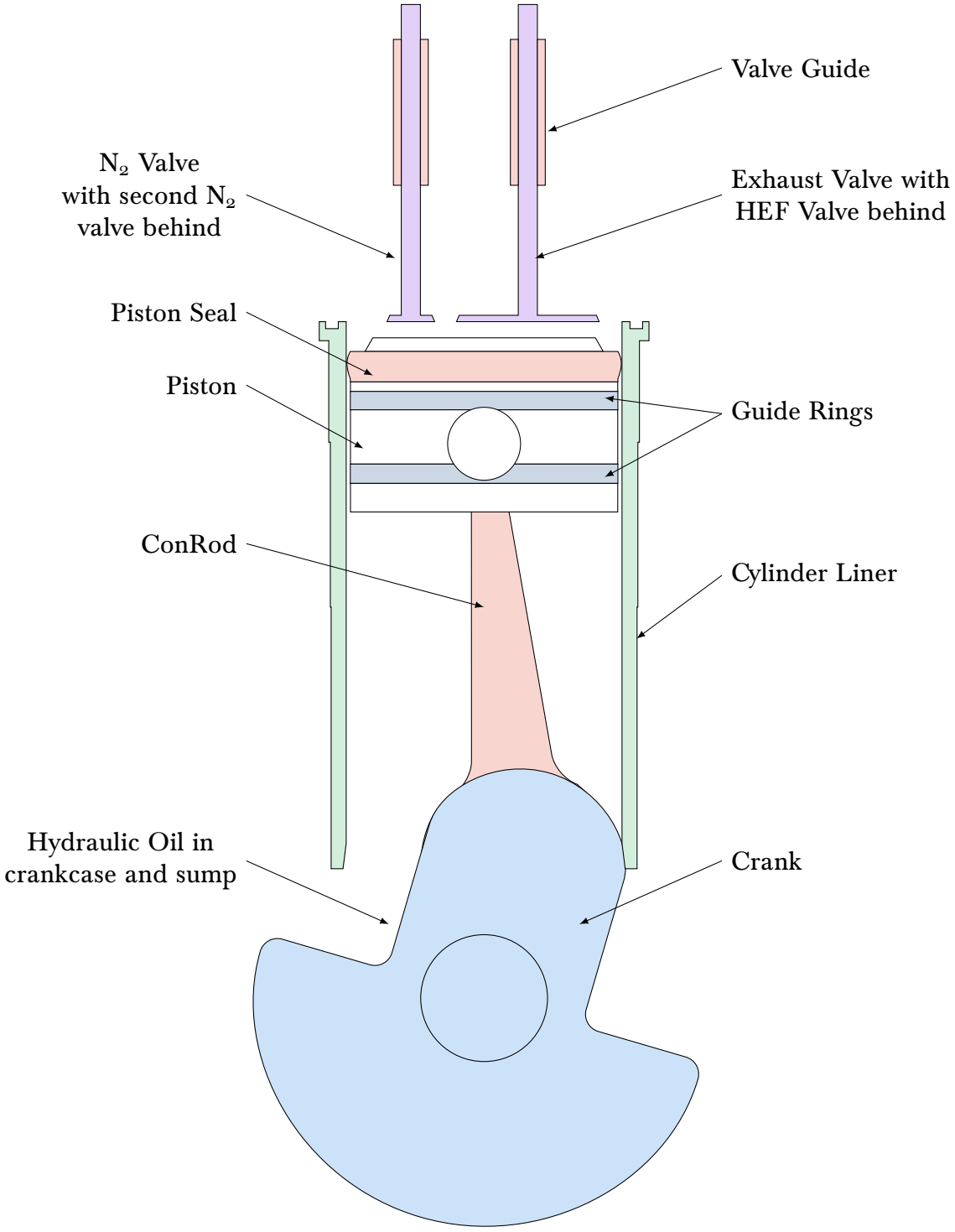

Figure 2.1: The key components of the Dearman Engine addressed in this thesis. Not to scale.

vapour compression refrigeration system. This process doubles the coefficient of performance of a standard diesel powered refrigeration device; this is due to the fact the evaporation of the N_2 removes heat from the food storage area of the truck and then

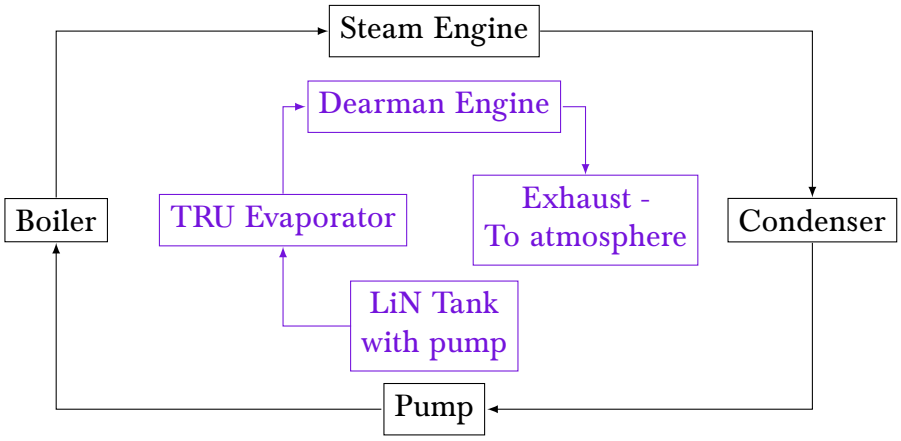

Figure 2.2: The Rankine Cycle for a steam engine (adapted from Walshaw 1946) with the Dearman Engine terminology annotated.

is used to generate power. This power can then be used to provide more cooling. In other applications the power may be used for other purposes such as electricity generation.

The power output from the Dearman Engine is around 5 kW. Analysis of a standard durability dynamometer test performed by Dearman resulted in a mean indicated mean effective pressure (IMEP) of 9.5 bar and a mean brake mean effective pressure (BMEP) of 7.2 bar. This led to a calculated value of frictional mean effective pressure (FMEP) of 2.3 bar and an efficiency of 75.9%. There is a large potential for bringing the IMEP and BMEP closer together through a tribological study. With the engine producing significantly lower power output than a conventional internal combustion engine (ICE) parasitic losses are more detrimental to the performance of the Dearman Engine.

Engine Friction

Figure 2.4 shows the contribution to friction of the major sub-assemblies within the Dearman engine. The data was collected by motoring a fully assembled 1st generation engine coupled to a dynamometer; the power consumed by the dynamometer was then measured by Dearman Test and Development Engineers. The 1st generation engine is the original configuration of the Dearman Engine where a large number of the components are 'off-the-shelf' ICE components, this configuration was designed as a proof of concept. The engine was disassembled and the power recorded as the subsequent sub-assemblies

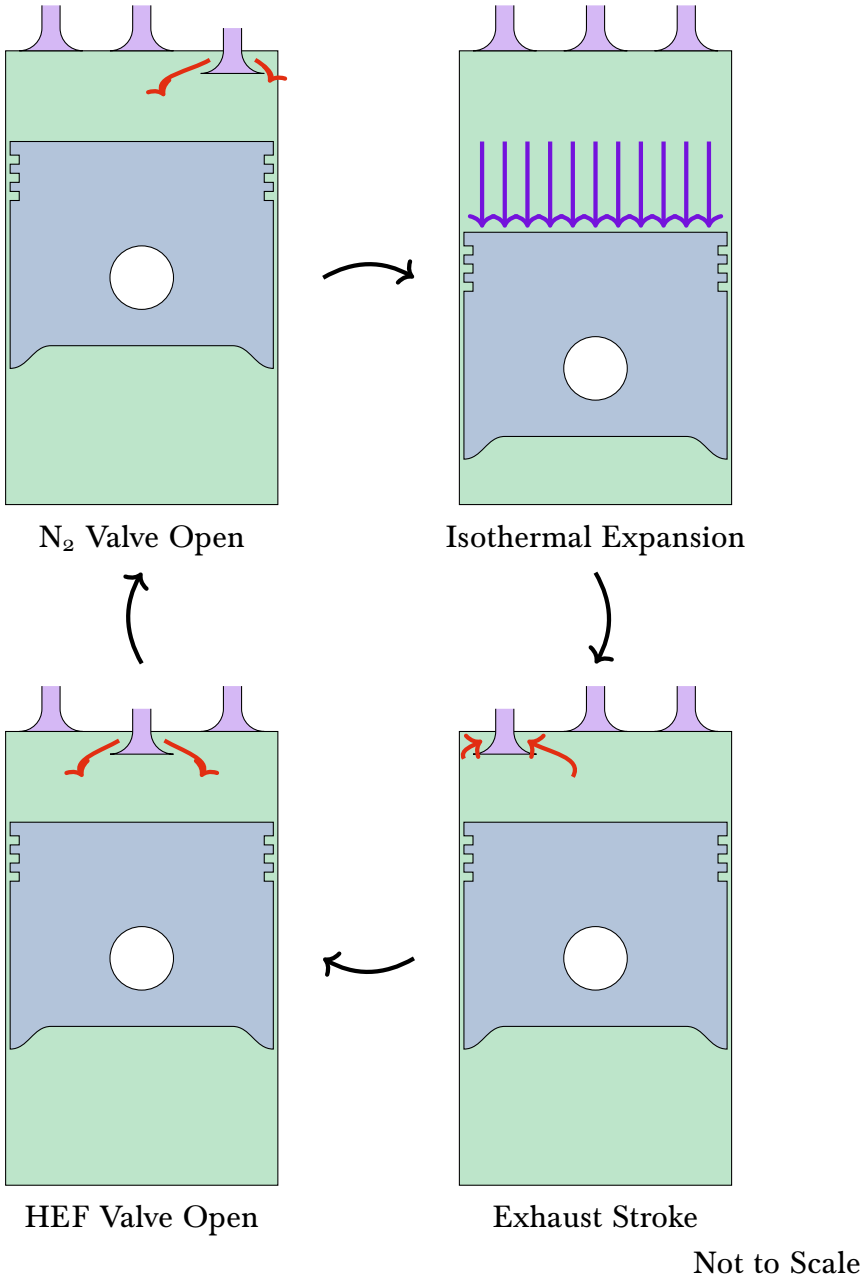

Figure 2.3: The Dearman Cycle (stylised). Starting top left: 1) N_2 valve opens 2) In contact with the heat exchange fluid (HEF) the N_2 expands 3) As the piston returns to TDC the expanded gasses are exhausted 4) HEF is allowed into the cylinder just before TDC to prepare the cylinder for the next expansion.

were removed for a comparison of the contribution to the total losses of the engine. The major contributor to frictional losses was the piston ring, accounting for nearly a third of the total. This piston ring, also known as the piston seal, is critical to efficient expansion and thus efficient power generation.

Originally the Dearman Engine was manufactured from mass produced ICE

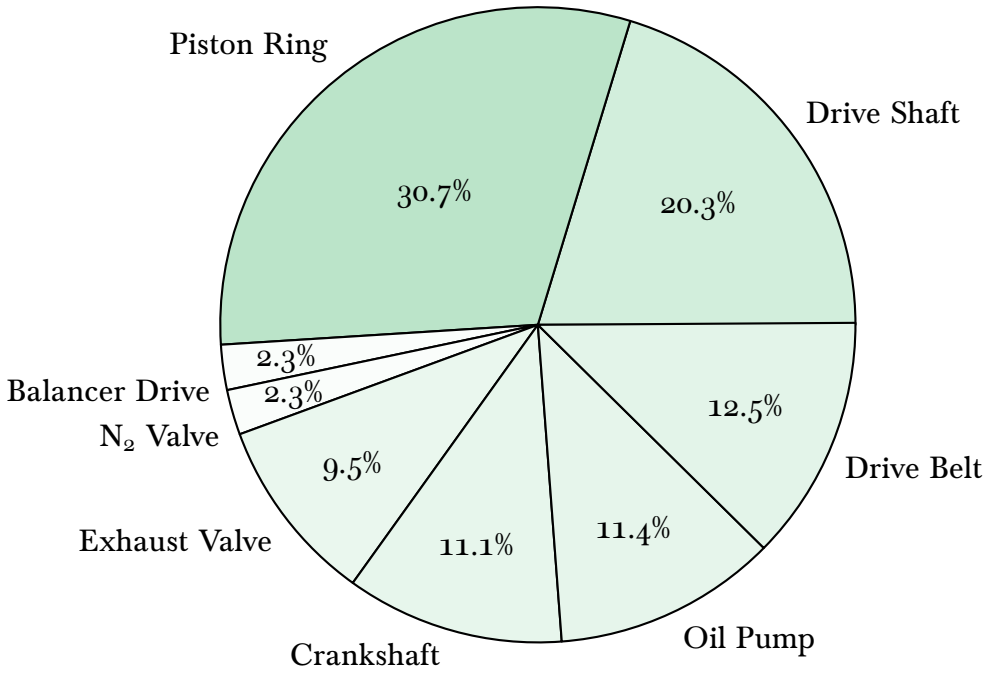

Figure 2.4: The contribution of constituent sub-assemblies to overall friction within the Dearman Engine derived from a frictional teardown performed by Dearman of a 1st generation engine (Private Correspondence 2015).

components, adapted to allow the flow of N_2 and HEF into the cylinder to provide a quasi-isothermal expansion. This design worked as a proof of concept but as the technology is inherently different in its nature to an ICE it follows that there should be a design process to advance the technology reflecting these differences. Later generations of the Dearman engine developed the 1st generation engine moving the technology further from a traditional ICE and closer to a fully bespoke design. The change in temperature from $\approx 150\,^{\circ}C$ in an ICE (Priest and Taylor 2000) to $\approx 25\,^{\circ}C$ in the Dearman Engine, working fluids and loads involved open up the possibility of utilising new materials, new lubricants and new designs. These potential improvements include polymers: known for their low density and high strength (Mark 2009) and biomimetic lubricants: based on lubricants found in biological organisms with the potential to provide an alternative to hydrocarbon based oils (Ahlroos et al. 2011).

2.2 Polymer Tribology

Advances in material science have produced new materials that have been used in many applications, however polymers are not widely used in sub-ambient temperatures (< 20 °C). Prime examples of applications operating that could benefit from the properties of polymers are compressors (Yeo and Polycarpou 2012; Nunez and Polycarpou 2015; Cannaday and Polycarpou 2005) and gearboxes (Dearn, Hoskins, Petrov, et al. 2013a; Dearn, Hoskins, Andrei, et al. 2013; Meuleman et al. 2007). Polymers are used in these applications for two main reasons: mass and friction reduction. The polymers discussed in the rest of this chapter were all selected for their high relative stiffness and suitability for the application.

There have been many studies that have examined the tribology in an oil-less compressor, these tend to operate at similar temperatures and loads to the Dearman Engine. A study performed by Yeo and Polycarpou assessed the performance of polymer coatings on the bore of a compressor (Yeo and Polycarpou 2012), this focused on the use of polyether etherkeytone (PEEK) and poly-tetrafluoroethylene (PTFE) coatings between −20 °C and 120 °C. PTFE was shown to outperform PEEK as a bulk coating when the coefficient of friction was observed. However impregnating PEEK with PTFE improved the performance over that of the two materials on their own. It was hypothesised that the PTFE formed small particles that created a solid lubricant layer.

Polymers can be combined with reinforcing fillers to improve both the mechanical and tribological properties of the polymer matrix composite (PMC) as shown in Figure 2.5. Glass fibres and carbon fibres are commonly impregnated into a thermoplastic matrix to improve the wear resistance (Friedrich et al. 2005). These also have the benefit of increasing the thermal conductivity of the material reducing the flash temperature of the interaction. Hoskins et al. found that an increased flash temperature increased the coefficient of friction (Hoskins et al. 2014) through the melting of the surface. By implication, increasing the thermal conductivity can reduce the coefficient of friction. Other solutions exist for the improvement of the wear resistance but glass and carbon

fibres are more readily available and are often cheaper. Carbon fibres are stiffer but using them has a higher cost penalty than glass (Chuah 2012). Glass fibres are supplied in short chopped and long fibre variants. Under normal running short chopped fibres can lead to many exposed fibres running against the counter surface when the matrix material wears, significantly increasing the overall wear (Karger-Kocsis and Friedrich 1988); this can be mitigated through careful selection of manufacturing process. Short chopped fibres are easier to incorporate into a material but longer woven fibres are more effective at reinforcing the material (Chuah 2012).

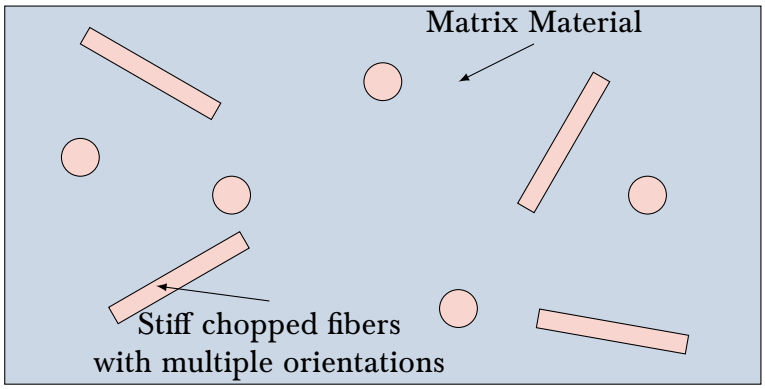

Figure 2.5: An example polymer matrix composite.

Lu and Friedrich demonstrated that between 0 °C and 50 °C the coefficient of friction of PEEK increases with an increase in temperature for an unreinforced sample. The coefficient of friction decreases with short carbon fibre reinforced samples with an increase in temperature with a minimum value at the glass transition temperature of PEEK ($\approx$ 150 °C) (Lu and Friedrich 1995).

Polymers are rarely used for power generation components inside ICEs due to the high temperatures involved (Priest and Taylor 2000) meaning that their weight and power saving advantages can not be exploited. However, the much lower operating temperatures of the Dearman engine (<30 °C) mean that this technology has many potential applications and one key material of interest is poly-ether-ether-ketone (PEEK) (Z. Zhang et al. 2004).

All of these factors must be considered when applying PMCs in tribological applications. This research aimed to assess the tribological properties of polymers and

composites that may be used to manufacture a cylinder liner for a reciprocating low temperature engine by replicating the conditions in the engine.

HEF, the fluid mixed with pressurised nitrogen in the engine to ensure quasi-isothermal expansion, is an aqueous solution made up of 70% water and 30% poly-ethylene glycol in the current Dearman Engine configurations. So whilst the engine is currently mainly lubricated with hydraulic oil the polymers must also be compatible with aqueous solutions due to the HEF present in the cylinder. Some poly-amides (PAs), are well known for absorbing moisture and expanding, however they are among some of the polymers commonly utilised for tribological applications (Mark 2009). Polyphthalamide (PPA) is a subset of PA used for its improved performance with moisture and chemical resistance and has been produced mainly for the automotive industry (DuPont 2008). Polytrimethylene terephthalate (PTT) is mechanically similar to PA but has been relatively unused due to a large cost in the manufacture but DuPont developed a process utilising corn starch to produce 1,3-propandiol. This is a major step in the commercialisation of the polymer as previously this was produced from petrochemical sources. This novel process allows PTT to be manufactured economically (Kurian 2005).

One of the major benefits of using polymers is the ability to produce composites utilising the desirable properties of each individual material (Lu and Friedrich 1995). Traditionally a stiff polymer is used in combination with a soft lubricious polymer in order to provide a material that is durable and has a low coefficient of friction under certain conditions (Khedkar et al. 2002). This combination tends to be produced by embedding the softer polymer into a stiffer matrix material. Although PMCs come with a few downsides: they tend to be more expensive compared to unreinforced polymers and the inter-facial boundary between each component material can adversely affect the mechanical properties.

PTFE-PEEK composites (PTFE-PEEK-Cs) have been investigated in a variety of different ratios of PEEK:PTFE. When the PTFE percentage is larger than that of the PEEK, they do not perform favourably an undesirable phenomenon known as grooving occurs; where the PTFE wears more than the PEEK and causes cavities to appear on the

surface (Lu and Friedrich 1995). The tribological film produced during grooving also has a lower thickness resulting in lower lubricity.

Although composites are widely used to obtain properties of multiple materials, there is some evidence to suggest that using laminated materials can provide comparable friction with composites; a schematic is shown in Figure 2.6. Qi et al. investigated the tribological performance at elevated temperatures using a pin on laminated aluminium oxide with molybdenum, the friction was 60% lower than the monolithic material (Qi et al. 2012). However, at ambient temperature the AlO_3/Mo composite gave better results than the laminate.

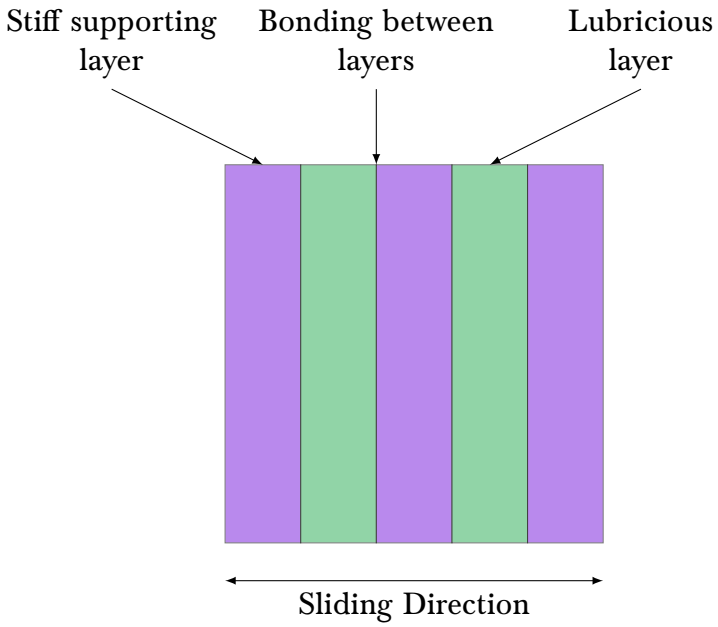

Figure 2.6: A schematic for a laminated polymer concept.

The investigation of friction pre dates the formal study into Tribology in 1966. Pioneers in the subject include da Vinci, Amontons, de la Hire and Coulomb. Da Vinci is often credited with the earliest scientific experiments in analysing the coefficient of friction. Amontons published four laws of friction in his paper 'De la resistance cause'e dans les machines' (Amontons 1699) that were later investigated in depth by Coulomb. De la Hire developed a the first theory of the mechanism that causes friction. These pioneering works led to the development of the three fundamental laws of dry friction that are widely accepted, however there are limits to their validity (Schnurmann 1942; Hutchings and

Shipway 2017; Popova and Popov 2015):

1. Friction is directly proportional to the applied normal load.

2. Friction is not dependant on the apparent area of contact.

3. Friction of a sliding object is not dependant on its velocity.

These laws can be condensed mathematically into Equation 2.1; Figure 2.7 demonstrates the notation used. It is now understood that these laws are a good 'rule of thumb' but they are idealised. The coefficient of friction depends on many factors such as the materials involved, the temperature of the surfaces and the topography of the surface.

$$F_\mu = \mu F_\perp \tag{2.1}$$

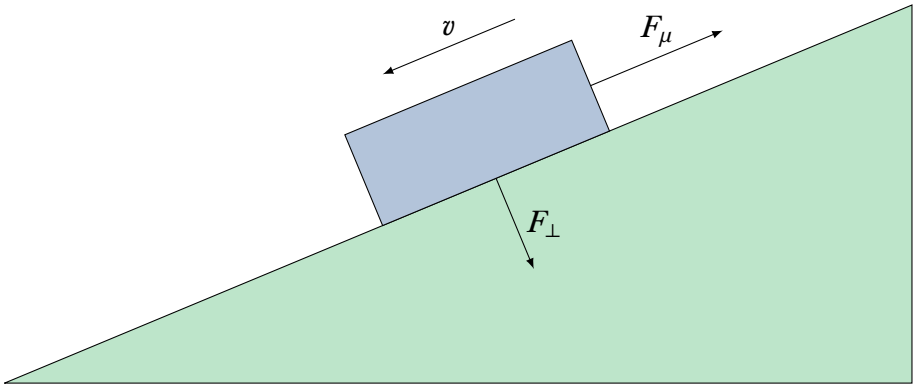

Figure 2.7: A schematic of the notation used in Equation 2.1.

The above laws fail to hold during extreme conditions; high velocity and force experiments do not respect them (Bevan 1939). In the case of polymers there are other factors that impact the coefficient of friction. The visco-elastic nature of polymers and their change in crystallinity during heating means that the mechanisms and conduction of heat is significantly different to that of metals and so their behaviour under friction is different (Johnson 2003, pp. 184–195) (Dearn, Hoskins, Petrov, et al. 2013a).

Visco-elastic materials are those that undergo an elastic and plastic deformation during an applied strain (Roeder 2013). This introduces a hysteresis in their use as supporting surfaces. As plastic deformation is related to the rate of strain applied as well as the magnitude; polymer friction is dependant on the relative speed of the contacting surfaces. This is a major deviation from Coulomb's law of friction.

In traditional tribological studies the friction and wear properties are measured at low sample rates ($\approx 1\,\text{Hz}$) and summarised in statistical descriptors such as maximum, minimum, mean and median friction or post test measurements such as wear volume. These all have their place in describing the tribological performance of materials and lubricants but do not give insight into the non-linear effects of materials.

In addition to non-linear properties, frictional data can also give more insight into the transient wear of materials. The frictional energy dissipated during motion is converted into other forms: heat (Carslaw and Jaeger 1959, pp. 266–270), sound, vibration and the most important tribologically — wear (Hu et al. 2013; Rymuza 1996). Frictional energy dissipation can be calculated using the coefficient of friction, however the higher the sampling frequency, the more accurate the reported value.

The Nquist-Shannon sampling theory (Nyquist 1928) describes the minimum frequency (B) effects that can be described by observations at a given sample rate (f_s) as shown by Equation 2.2. For example, in order to observe effects that occur at, say, 1 Hz a sampling frequency of 2 Hz must be used. This implies that in pursuit of fully understanding non-linear effects of materials and lubricants a low sample rate is unsuitable.

$$f_s > 2B \tag{2.2}$$

2.3 Lubrication

Another approach to reducing the parasitic losses of the Dearman Engine is to address the lubricant currently used: hydraulic oil. Traditional lubricants, derived from hydrocarbons

(Mang 2007) do not fit the ecological and environmental focus of the Dearman Engine. The polymers discussed above are also derived from the same sources however they are expected to have a significantly longer life span than the lubricant during operation. For these reasons there was a focus on searching wider than the traditional sources of lubricant.

A lubricant within an engine needs to operate under a wide variety of conditions as it is in contact with a number of different components. They operate under boundary and hydrodynamic lubrication and a mix between the two, known as mixed lubrication. Boundary lubrication is when the two surfaces are fully supporting each other and the asperities of the two materials come into contact (Komvopoulos et al. 1985). Friction under boundary lubrication loosely follows Amontons' laws for dry contacts and is not significantly dependant on velocity. Again this falls down when the materials are visco-elastic. It is a common form of lubrication in both the natural and engineering world. These kind of contacts occur under high pressure and low velocity conditions such as: bearings, gears and synovial joints (Bart et al. 2013; Schmidt et al. 2007). As boundary lubrication results in partial contact between the two surfaces it can lead to high levels of adhesive wear due to the cold welding of asperities (Mang 2007, p. 17).

Boundary lubricant additives react chemically with the surface of materials through polar bonds (Komvopoulos et al. 1985). In the human body fatty acids, proteins and polysaccharides all make up synovial fluid, these chemicals all react and are absorbed into cartilage to make a lubricious surface for low friction, low velocity, high contact pressure motion within joints. The exact make up of these fluids is highly complex and varies due to species, age, health and environmental factors of each subject but the breaking down of these fluids has been linked to debilitating conditions such as arthritis (Schmidt et al. 2007). In ICEs boundary lubrication regimes can be found between the camshaft and followers and piston rings briefly at TDC and bottom dead centre (BDC). Due to the higher temperatures present in the system ($\approx$ 150 °C to 200 °C) the lubricants involved tend to be based on crude oil and are also subject to oxidation within the contact around the piston ring causing contamination of the oil (Lee et al. 2006).

Hydrodynamic lubrication occurs when the pressure or velocity in the fluid rises

high enough to fully separate the two surfaces. When this lubricating layer becomes contaminated with wear debris, or other particles, abrasive wear occurs. This regime is found under high velocity contacts such as the crank bearings and piston rings (Priest and Taylor 2000). The coefficient of friction is dependant on the velocity and pressure between the surfaces in this situation due to the changes in viscosity in the lubricant caused by the applied conditions.

2.4 Biomimetic Lubrication

It is known that animal fats and water were used to grease doors and axles in wagons and carts in antiquity. It is no wonder that the Latin and Greek word for lard '*axungia*' ($\alpha\xi o\nu\gamma\gamma i\alpha$) is rooted in the Latin word for an axle '*axem*'. There is also evidence of the Romans using the dregs of olive oil mixed with water, left over from olive oil production, being boiled down and used as a lubricant (Harris 1974). Lard and Olive oil are both mixtures of fatty acids with long carbon chains. The major difference between the two substances is the concentration of saturated and unsaturated fatty acids. Olive oil has a saturated C_{16} concentration of 7 g/100g to 16 g/100g (mass of compounds with chains of 16 carbon atoms per 100 g of oil) whereas lard has a saturated C_{16} concentration of 24 g/100g to 30 g/100g (Thomas et al. 2015). The differences change the physical properties of the lubricant but the fundamental chemistry of the fluids is the same.

During autumn across the globe there are issues with leaf abscission reducing the traction available on road surfaces and rail track. This loss in traction has been attributed to pectin, a type of polysaccharide (Cann 2006). Pectin is a complex mix of polymerised chains of sugars, found in plant cell walls (Bauer 2012). The structure of pectin varies with species of plant, time of year and where the cell is on the plant, however it is present in all live plant cells. Approximately 60% of the cell wall is made up of homogalacturonan a main constituent of pectin (Caffall and Mohnen 2009). The interaction between the pectin in the leaves and the wheel/rail contact forms a layer (Zhu et al. 2014) that is difficult to remove, due to bonding between the leaf matter and the steel, and significantly reduces

the coefficient of friction (Li et al. 2009). This phenomenon is potentially beneficial as a way to generate a boundary lubricant coating harnessing the adhesion between the pectin and steel to reduce the contact between the two surfaces and reducing the friction.

Pectin tends to be used as a viscosity modifier and emulsifier in food chemistry. It is starting to be more prevalent in other sectors from the manufacture of polymer films for convenience food (Silva et al. 2009) to corrosion inhibiting coatings (Fares et al. 2012) however it has never been used as a lubricant additive for an engineering application.

There are other examples of long chained organic molecules in nature that have lubricating properties. Synovial joints use synovial fluid to lubricate themselves. This fluid is largely made up of proteins (long chains of amino acids), mostly serum albumin. Higher concentrations of these proteins have been detected in patients who are suffering with arthritis, demonstrating their importance in lubricating joints (Hui and Mccarty 2013). Bovine serum albumin (BSA) has been found to be approximately 13× 3 nm in size (Lehninger 1982, p. 170) and molecular weight of $66\,000\,\mathrm{g\,mol^{-1}}$ (Lehninger 1982, p. 707). BSA is used in blood to move fatty acids, metals and other compounds around the body (Huang et al. 2004). Synovial joints operate at a significantly lower contact pressure than a rail and wheel but the fluids contain the same long chained structure as pectin and so may be capable of running under similar loads.

In all of these cases these fluids consist of a long chemical chains constituting of fatty acids, amino acids (in the case of proteins) or polymeric sugars (polysaccharides). The other similarity is that in these situations the environment is aqueous. There is an interaction between these chemicals and the water present to form a boundary lubricant, reducing the coefficient of friction and heat in a contact, whilst washing debris out of the contact. This is observed over a range of contact pressures from the knee at ≈3.5 MPa (Haut Donahue et al. 2003) to the contact between the rail and train wheel at ≈1200 MPa (Li et al. 2009).

The ability for long chained biological compounds to lubricate mechanical components over a wide range of conditions is clear; opening the possibility of alternatives to hydrocarbon based lubricants. Biolubricants — lubricants sourced from biological matter

and biomimetic lubricants — fluids mimicking a natural lubricant by using a constituent compound from a biolubricant. Hydrocarbons are derived from either crude oil or synthesised from those derivatives (Mang 2007, pp. 1–6). The use of hydrocarbon based lubricants adds to the carbon footprint of the end product and also has the possibility of contaminating the environment (Boyde 2002). A bio- or biomimetic- lubricant derived from living sources, when sourced sustainably, can reduce the carbon footprint and impact of the lubricant on the environment.

Biological lubricants are complex chemicals and so the effects of temperature, load and velocity have not been fully studied. In order for industrial and wide scale implementation of bio- and biomimetic- lubricants these effects need assessing. A critical factor in the utilisation of biomimetic polymers is the stability and longevity of the lubricant, controlling the chemical degradation. Effects of both temperature and pH have been shown to affect the chemistry of biomolecules. Above 70 °C BSA forms complex structures and denatures above 55 °C (Schmitt et al. 2009). Whilst the denaturing of proteins is not critical to the formation of a lubricating layer, complex structures could form detrimental detritus that may end up trapped between the two surfaces. The properties of pectin are well reported and are dependant on the pH of the surrounding solution, changes in viscosity such as gelling are due to the levels of pH or the introduction of Ca^{2+} ions into a solution (EndreSS and Christensen 2009). Unless the solution is taken above a high temperature and the molecules begin to oxidise; pectin solutions are not reported as having major changes in their chemistry.

Chemistry of Pectin

Pectin is abundant and present in most plant matter, and as such if it could be proven to be a potential industrial lubricant it is a renewable alternative to hydrocarbons. Leaves are made up of multiple carbohydrates and polysaccharides, in some leaves pectin is used to cement the cellulose fibres together. Pectins are polysaccharides (literally many sugars) found in the cell walls of all plant cells. The levels of pectin vary dependant on where

the cell is located on the plant. Homogalacturonan, a constituent part of pectins, is a polymer of α-1,4-linked-*D*-galacturonic acid, the structure is shown in Figure 2.8 (Caffall and Mohnen 2009).

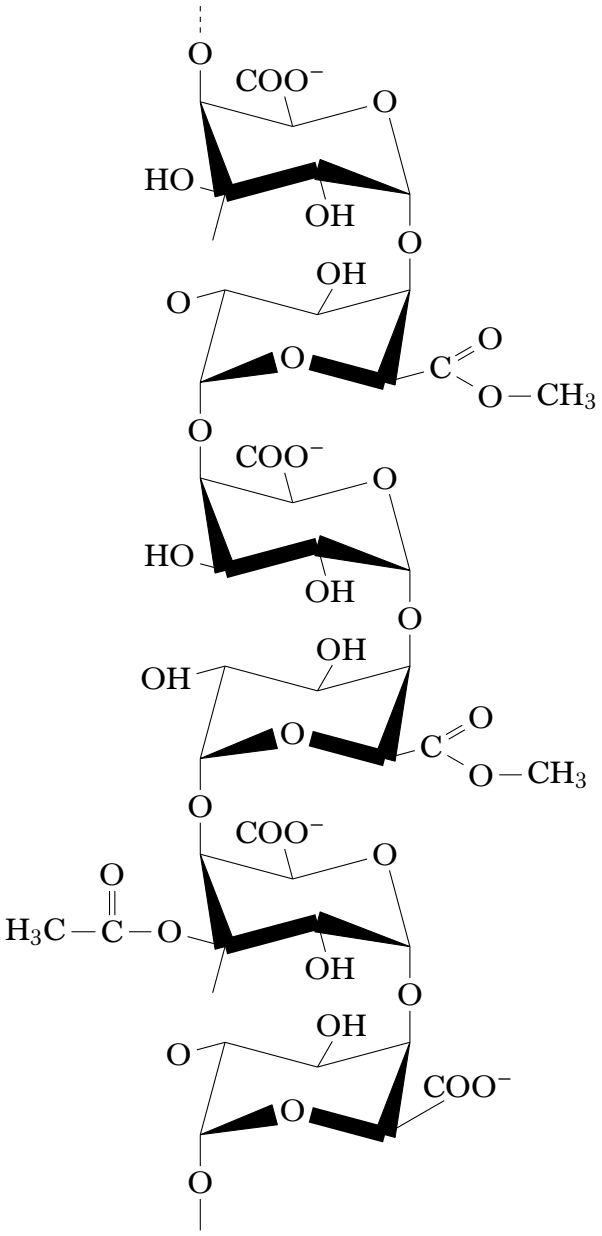

Figure 2.8: The skeletal structure of homogalacturonan (adapted from Ochoa-Villarreal et al. 2012).

This polymer has sections with carboxylic acid groups spread along the chain. It has been hypothesised by that between these carboxylic acid groups ionic bonds form with Ca_2^+ ions. These bonds form the polymer into a parallel chain. This model is known as the 'Egg Box Model' shown in Figure 2.9 (Grant 1973). In general pectin requires Ca_2^+

or a complex molecules, such as sugars and acids to form a gel (Thakur et al. 1997).

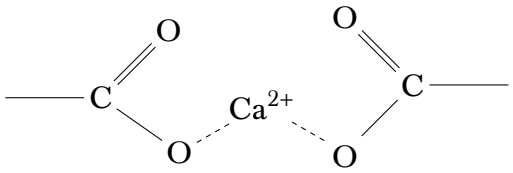

Figure 2.9: The 'egg box' model of bonding between Pectin and Ca_2^+ ions (adapted from Ochoa-Villarreal et al. 2012).

Metals and bacteria have been shown to bond through the use of polysaccharides. This has been shown for a large variety of polysaccharides and metals (Kotrba 2011). There is also a drive to develop green polymers to replace polymers derived from crude oils. Silva et al. developed a polymer based on pectin and one on alginate. They used glycerol as a plasticiser and a CaCl solution to crosslink the polymer. CaCl is used as it helps to make the resulting polymer insoluble in water but makes the film brittle (Silva et al. 2009).

Chemistry of Proteins

Proteins make up a large amount of the biochemistry present in the natural world. Despite the large variety of organisms ranging from bacteria to plants these proteins are made up of 20 building blocks known as amino acids (Lehninger 1982, p. 121). These are organic compounds that consist of an amino group ($-NH_3$) and a carboxylic acid group ($-COOH$). These amino acids form a peptide bond between a $-N^+H_2$ and COO^- groups on subsequent acids to form chains known as proteins (Daintith 1966, p. 402). This process is shown in Figure 2.10 (Lehninger 1982, p. 111).

Proteins form very complex structures determined by the order of these amino acids. The peptide bonds form what is known as the primary structure of the protein, a back bone of amino acids (Daintith 1966, p. 442). When describing proteins each of the 20 amino acids is abbreviated to a single letter allowing sections of the back bone to be represented by a sequence of letters (Lehninger 1982, p. 134). Figure 2.11 shows this process. In the figure, a section of a protein containing Alanine (A), Lysine (K) and Cysteine (C) is shown with the peptide backbone running along the top of the figure. Hanging off the

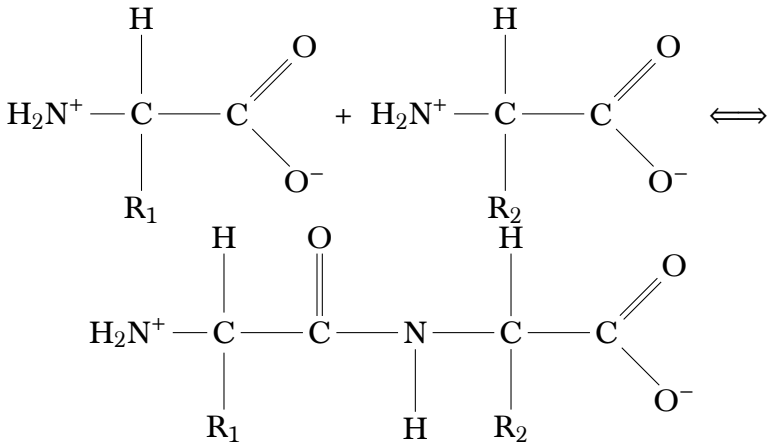

Figure 2.10: The formation of a peptide bond.

chain between each peptide bond is a tail. These tails are what makes each amino acid unique (Lehninger 1982, p. 56).

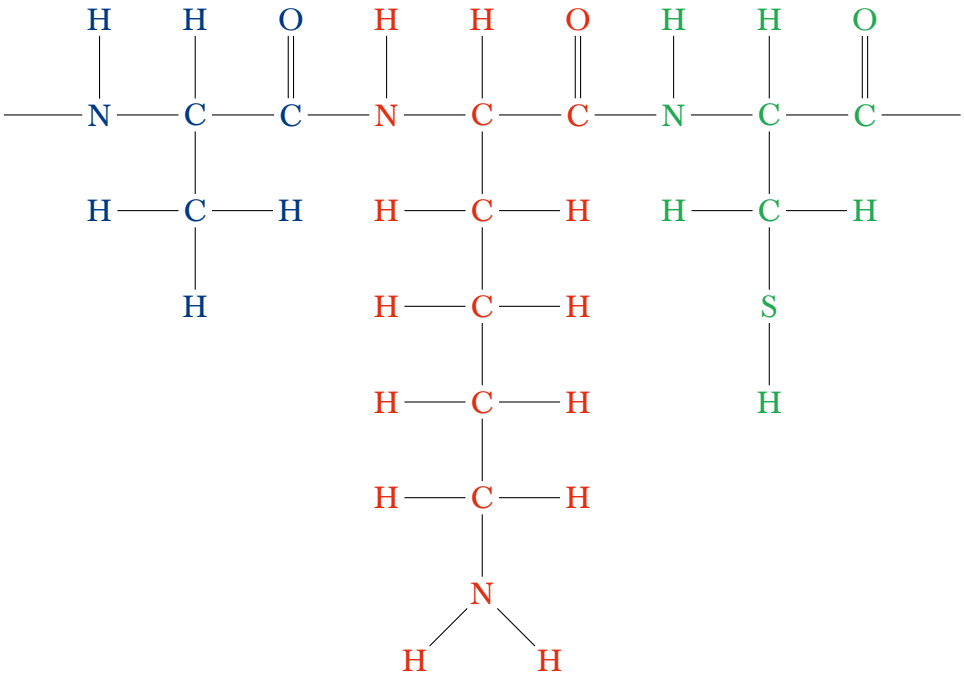

Figure 2.11: The primary structure of proteins. Example shown is AKC (Alanine - Lysine - Cysteine). Adapted from (Campbell et al. 2017, p. 125).

There are two major forms of secondary structures: alpha and beta. Alpha structures form helical sections within the protein and beta structures form folds within the structure causing the peptide chains to run parallel to each other. The secondary structures are formed via hydrogen bonding between the carboxylic acid and amino groups as shown in Figure 2.12 (Campbell et al. 2017, p. 128). Due to the individual chemistry of each tail

forming electron rich and electron deficient areas of the chains the tails form hydrogen bonds between sections of the chain creating the tertiary and quaternary structures of the proteins (Lehninger 1982, pp. 147–206).

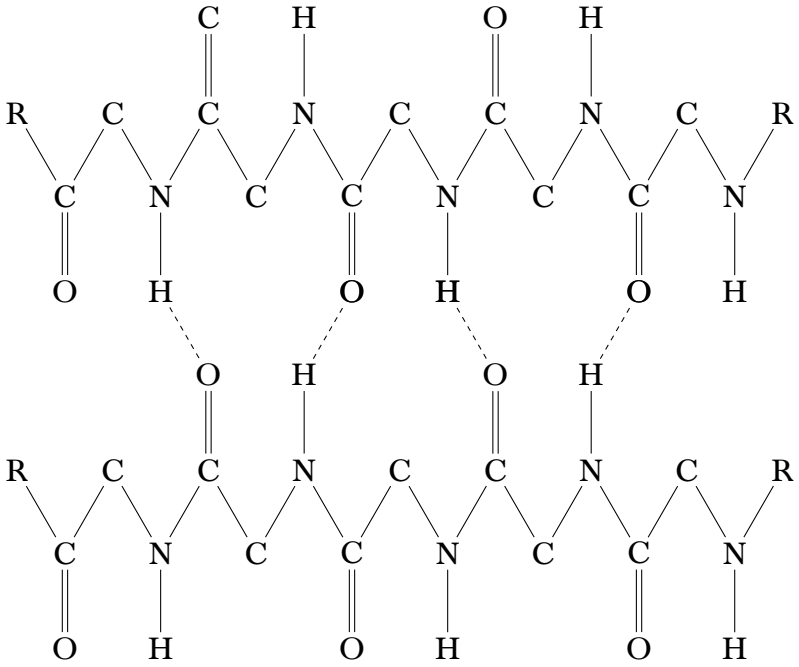

Figure 2.12: Hydrogen bonding between peptide chains forming parallel peptide chains.

2.5 A Synergistic Approach - Aims and Objectives

In order to reduce the parasitic losses found within the Dearman Engine an approach that addresses materials, lubrication and design in conjunction with each other is needed. It is clear that with an engine designed to be an adapted ICE there is a large amount of room for improvement to ensure the engine is adequately designed for the working fluids employed. In the case of the TRU reduction of weight is key in increasing the efficiency of the prime mover as more of the energy produced will go into accelerating the payload and not the vehicle itself.

The literature has shown that there is a significant potential for the reduction of parasitic losses through material replacement with polymers and the introduction of biomimetic lubricants. Combining this with improved analysis methods designed to provide insight into the velocity dependant non-linear material properties such as

visco-elasticity. These need to be applied synergistically ensuring that each of the areas of the research work together and no unwanted effects are produced.

Aim: To reduce parasitic losses in the Dearman Engine

Objectives:

i) A tribological assessment of a polymer cylinder liner.

ii) The testing of a laminated polymer piston seal as a method of reducing upstream energy usage and increasing the efficiency of the piston seal - cylinder liner interaction.

iii) Development of biomimetic fluids capable of operating as a lubricant and as a HEF.

iv) Improvement of the materials and lubrication in the cylinder head to reduce the need for an oil pump thus reducing the weight of the system.

v) Develop novel analysis methods to assess the impact of visco-elastic properties on the friction and wear.

Chapter 3

General Materials and Methods

3.1 Introduction

The following chapter sets out the key materials and methods used in order to facilitate the reduction of parasitic losses within the Dearman Engine. Following the literature review and the establishment of aims and objectives the materials and methods presented below all facilitate the completion of those aims.

3.2 Materials

Table 3.1 shows all of the materials used in this thesis with key data. Initially polymers for Chapter 4 were selected through a Pugh analysis: quantifying and prioritising key material properties, shown in Table 3.1. Further details of the Pugh Analysis are given in the appendices. The materials for later chapters were selected for their practicality in the application and to exploit their properties as stated in Chapter 2.

Table 3.1: The materials used in this thesis listed alphabetically, data is taken from manufacturers' datasheets and other sources. Where the data was unavailable in the public domain or not supplied by the manufacturer the table was left blank. (Diversified Enterprises 2018; Yan et al. 2017; Design 2014; M. Pelagade et al. 2012).

Material Name	**Grade**	**Young's Modulus**	**Poisson's Ratio**	**Density**	**Surface Free Energy**
		E	ν	ρ	
		GPa	—	$kg\,m^{-3}$	$mJ\,m^{-2}$
Al	6063 T83	68.9	0.34	2700	—
PEEK	450G	4.0	0.39	1300	—
PEEK	Ketron 1000	4.3	0.39	1300	42.1
POM	Delrin 100AL NC010	3.0	0.35	1400	38.6
POM w/ PTFE	Delrin 500AF (20% PTFE)	2.8	0.35	1530	—
PPA	Zytel HTN51 G35HSL NC010 (35% Glass reinforced)	12.0	0.35	1470	—

Material Name	Grade	Young's Modulus	Poisson's Ratio	Density	Surface Free Energy
		E	ν		
		GPa	—		
PTFE		0.47	0.45	2170	72.8
PTT	Sorona 3030G NC010 (30% Glass reinforced)	11.0	0.35	1560	—
Ti	6Al-4V	113.8	0.34	4433	59.2
UHMWPE	Tivar Dryslide	0.65	0.33	935	—
20% PTFE PEEK Composite	Ketaspire Solvay	—	—	—	—

3.3 Methods

Friction and Wear

The aim of tribological laboratory testing is to produce friction and wear data in various forms that relate to an application. Various methods exist for producing results in the laboratory that are scalable back to the technology being modelled. Test rigs exist that model a specific motion or application but they are limited to that mechanism and do not necessarily produce results that are transferable to wider applications. The Institution of Mechanical Engineers Tribology Group defines five types of tribological test (Institution of Mechanical Engineers 2014):

1. Machinery Field Tests — Testing of live machinery
2. Machinery Bench Tests — Testing of machinery under simplified operating conditions
3. Systems Bench Tests — Testing of sub-assemblies under simplified operating conditions
4. Component Bench Tests — Testing of components under simplified operating conditions
5. Specimen Tests — Testing of materials under laboratory conditions or conditions representative of simplified operating conditions

The further down the list the cheaper the testing is to perform but the more widely applicable the results to other applications. Standards such as ASTM D6079, ASTM D7688 and ISO 12156 exist to assess the lubricity of fuels in a variety of internal combustion engines (ICEs). However the testing parameters in these standards are significantly less harsh than the conditions within an ICE. For example ASTM D6079 states the parameters set out in Table 3.2. This exists as a way of comparing fuels lubricity and does not give results of how a fuel will operate within a specific ICE. This is the key

to tribological testing: producing comparable results through testing that emulates the mechanisms present.

Table 3.2: The test parameters as listed in ATSM D6079 (ASTM International 2012).

Fluid Volume	2.0 ± 0.2 ml
Stroke Length	1.0 ± 0.2 mm
Frequency	50 ± 1 mm
Fluid Temperature	60 ± 2 mm
Relative Humidity	30 to 85%
Applied Load	200 ± 1 g
Test Duration	75.0 ± 0.1 min
Bath Surface Area	6 ± 1 cm^2

Equipment exists that will perform tests according to the standards listed above however they do not allow the user to run tests under conditions dissimilar to the parameters defined within the standard. For example the PCS high frequency reciprocating rig (HFRR) (London, UK) allows for variation in frequency in the range of 10 Hz to 200 Hz over 0.02 mm to 2 mm. This allows for a wide range of velocities but will only accept a 6 mm ball as an upper specimen and a 10 mm diameter disc as a lower specimen. This limits the relevance of results to applications where the contact pressure is within a specific range.

Equipment such as the Phoenix Tribology TE77 (Hants, UK) have a large level of customisability allowing the rig to be used to model biomechanical contacts such as hip joints (Choudhury et al. 2013; Novak et al. 2007). For this adaptability, the TE77 was used in this thesis in order to adequately model the contacts being studied.

The rig can be set up to accept different shaped geometries for testing. The three most common are: ball on flat which was not used in this thesis but is used in ASTM D6079 (shown in Figure 3.1a), flat on flat (also known as low pressure and shown in Figure 3.1b) and cylinder on flat (also known as line contact and shown in Figure 3.1c).

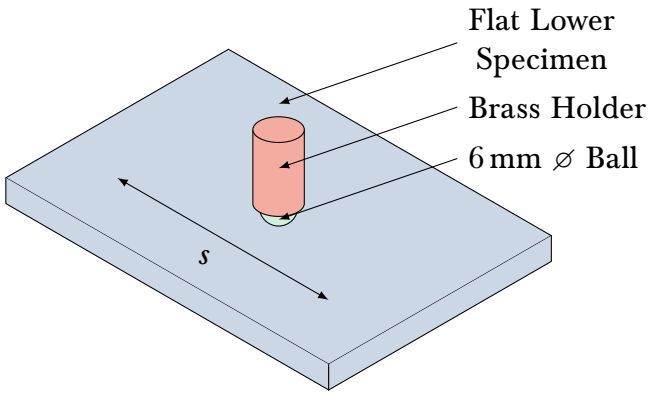

(a) The TE77 ball-on-flat configuration; used in ASTM D6079 not utilised in this thesis.

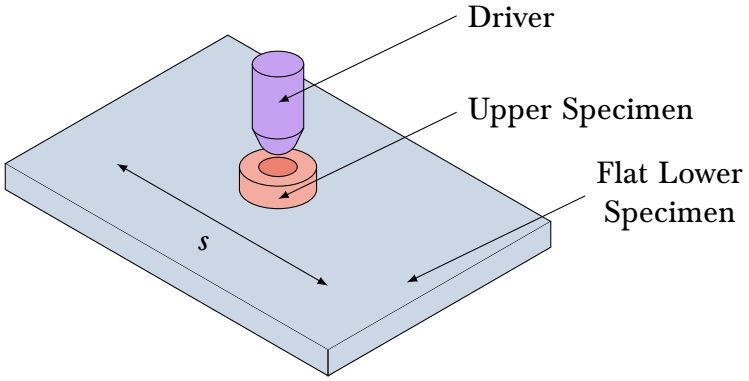

(b) The TE77 low-pressure configuration; used in Chapter 6. A modified version of this configuration is used in Chapter 4.

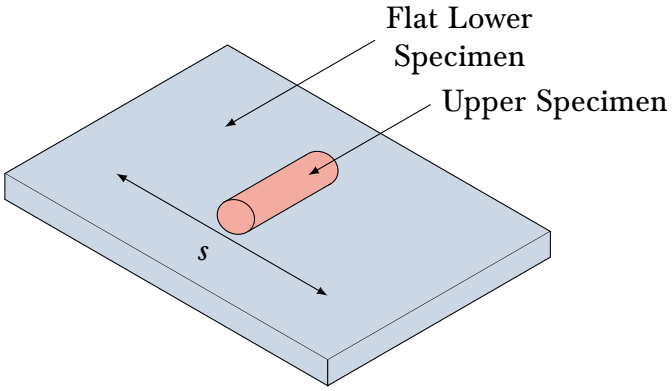

(c) The TE77 line-contact configuration; used in Chapters 4 & 5.

Figure 3.1: The TE77 configurations used in this thesis.

In each of these configurations the force is applied to the upper specimen through the holder attached to the reciprocating arm.

Also shown in the schematic is the cooling plate of the TE77. This plate can be interchanged with a heating plate allowing the rig to be controlled to an accuracy of ± 2 °C within a range of −10 °C to 300 °C. The cooling plate has channels running through

it that allow for the flow of a heat exchange fluid (HEF) through them. These channels are connected to a Thermo Scientific Haake A40 chiller with AC200 controller (Thermo Fisher Scientific, MA, USA) in order to control the temperature of the HEF. The heating plate is controlled by the TE77 operating software, COMPEND 2000, utilising heating elements embedded in the plate. Temperature feedback is provided through a K-type thermocouple mounted in the lubricant bath.

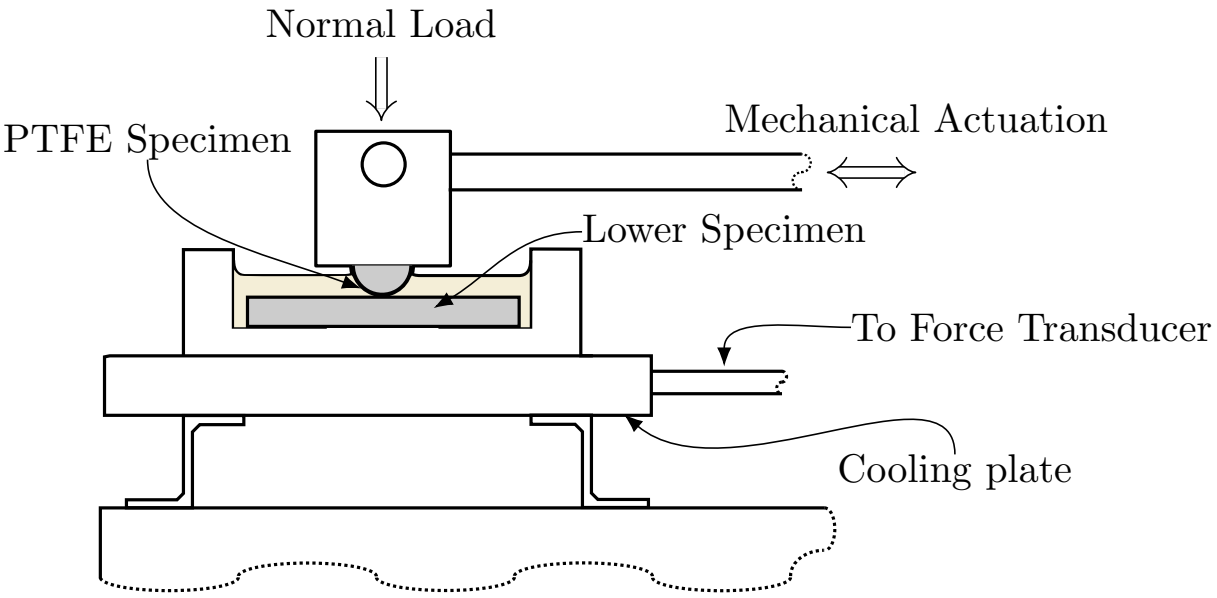

Figure 3.2: A profile schematic of the TE77 with labels in the line contact, cylinder on flat configuration. Image taken from I. M. Stead et al. 2019.

In cases where a variable volume of lubricant during a test is required a syringe pump (KDScientific Legato 110, MA, USA) was utilised. The outlet of the syringe was connected to a pipe attached to the reciprocating head; drip feeding lubricant directly to the contact zone.

TE77 Data Files

Data can be collected in two ways by the TE77, controlled by COMPEND 2000, a proprietary program developed by Phoenix Tribology. Low speed data (LSD) is stored at a rate of 1 Hz throughout this thesis. Each data point is the mean of the signal over the previous second. This is useful in order to monitor the trends that may occur during the duration of the test. Table 3.3 shows the data collected in the LSD file.

Table 3.3: The contents of the LSD file as recorded by the TE77.

Signal	Unit	Description
Time	-	Timestamp of when the data line was taken
This Step	-	Step number relating to the test control program
Step Time	s	The duration of the current step
Test Time	s	The time elapsed since the start of the test
Friction Force	N	The measured friction force
Frequency	Hz	The frequency of rotation of the motor
Load	N	The normal contact force applied to the upper specimen
Specimen Temp	°C	The temperature of the specimen measured by a thermocouple situated in the lubricant bath
Friction Coeff	-	The coefficient of friction as calculated by $\frac{F_\mu}{F_\perp}$
Friction Range	N	The measurement range of the frictional force The voltage range of the force transducer is 10 V, the conversion from a potential difference to frictional force is $F_\mu = \frac{F_{Input}}{10\,\mathrm{V}} \times F_{Range}$. Varying the Friction Range will adjust the resolution of the measurement.
Contact Potential	mV	The potential difference between conductive specimens. Supplied voltage is 50 mV

Signal	Unit	Description
Force Input	V	The raw voltage signal from the force transducer

High speed data (HSD) is collected periodically throughout the test rather than continuously. In this thesis the HSD is collected at 20 kHz, each sample is the raw value of the signal; recorded at 0.050 ms intervals. The data collected is shown in Table 3.4.

Table 3.4: The contents of the HSD file as recorded by the TE77.

Signal	Unit	Description
HSD Friction Volts	V	The raw signal from the force transducer
HSD Stroke	mm	Signal from an linear variable differential transducer situated on the back of the reciprocating arm reporting position of the arm
HSD Contact Potential	V	The potential difference between the upper and lower specimen (not useful when either specimen is non-conductive)
HSD Friction Force	N	The friction force

In both files reference is made to the contact potential between the two specimens. This can be used in lubricated tests to analyse the film thickness between two conductive specimens. The signal maximum is 50 mV.

TE77 Data Analysis

Coefficient of Friction - Steady State The steady state coefficient of friction was determined by finding the median of the coefficient of friction data for the whole of each test.

Steady State Descriptors The time to steady state was assessed by using settling time and percentage overshoot of a smoothed signal. These concepts were derived from control engineering analysis (Ogata 1997). These descriptors, settling time and percentage overshoot, tend to refer to a desired value of a control system. However in this analysis they have been compared to the steady state coefficient of friction.

Equation 3.2 and Equation 3.3 demonstrate the calculation process for the time to steady state. The settle percentage was found at each point along each coefficient of friction trace in the data set. Before the settle percentage was calculated the signal was smoothed using Tukey's (running median) smoothing function ($3RS3R$) as seen in Equation 3.1. The data is passed through the algorithm as a whole dataset and as split sections until convergence (Tukey 1977).

$$\begin{aligned} x_1^{3M_e} &= x_1 \\ x_i^{3M_e} &= \text{median}[x_{i-1}, x_i, x_{i+1}], \ i \in [2, n-1] \\ x_n^{3M_e} &= x_n \end{aligned} \tag{3.1}$$

The last time where the settle percentage is larger than the threshold was deemed the time to steady state.

$$\text{Settle\%} = \frac{\mu - \widetilde{\mu}}{\widetilde{\mu}} \tag{3.2}$$

$$\text{Settle Time} = \max\left(|\text{Settle\%}| > \text{Threshold}\right) \tag{3.3}$$

The threshold for this analysis is defined as the settling time or the time taken for the system to reach an equilibrium where variation is less than 10% of the median value of the coefficient of friction. The percentage overshoot was calculated using the comparison of the peak value (highest measured value) and the median of the coefficient of friction. This is shown graphically in Figure 3.3. This was important to demonstrate the stability of the tribological interaction.

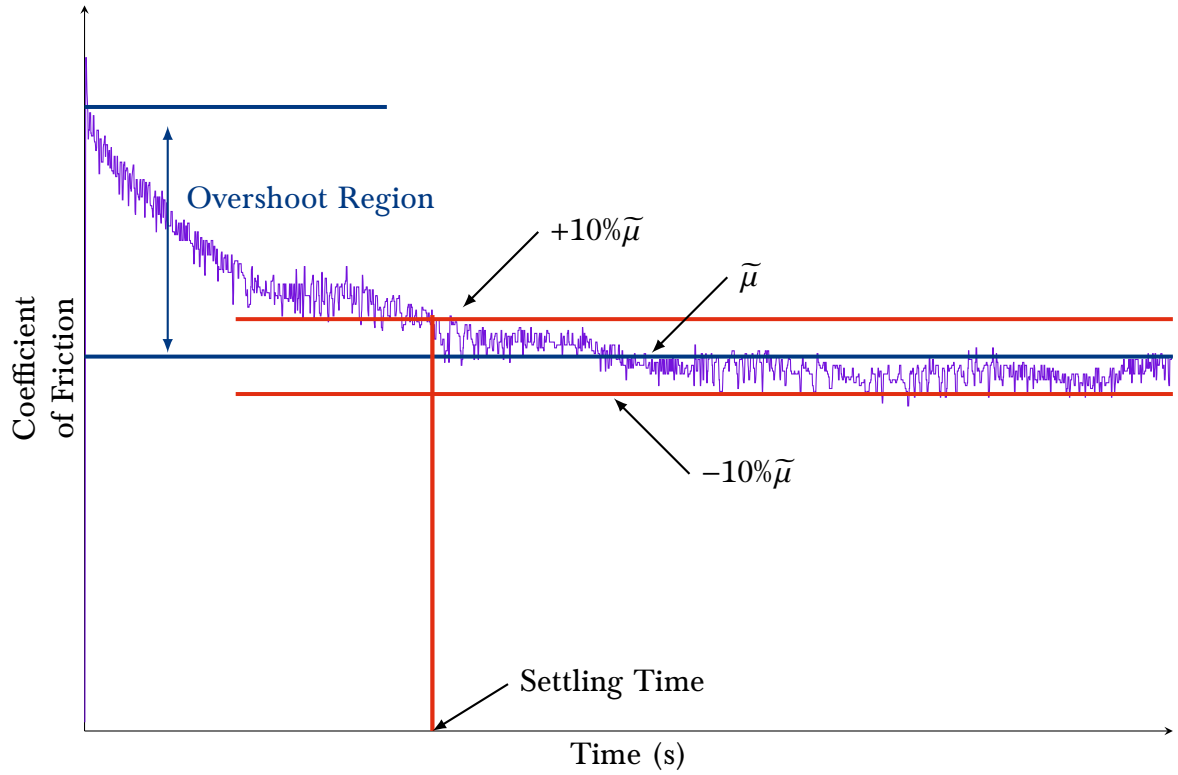

Figure 3.3: An example analysis of the coefficient of friction. The overshoot region and settling time are annotated on the diagram.

Frictional Energy Dissipated

Friction force was recorded in the HSD file as positive and negative values to reflect the change in direction. The signal was filtered using a Butterworth filter to remove as much of the high-frequency noise as possible from the frictional data. 5th order Butterworth polynomials were generated using the Python 3 function *butter* from the *scipy.signal* package. A low pass filter with a critical frequency of 5 mHz was applied to the 20 kHz sample rate high-speed data. This filter attenuated any oscillation higher than 1 kHz. These frequencies are outside those that would be expected from the testing; filtering these changes out corrects for the error in measurement.

Equation 3.4 to Equation 3.6 show the form the Butterworth polynomials take and the corresponding transfer function (Hashumoto et al. 1989), in this case each set of factors calculated the average friction. Equation 3.4 denotes the standard form for a transfer function in the s space where: σ represents the rise time of the signal; α_i are coefficients of the filter; β_n are the Butterworth polynomials; unless otherwise defined j is $\sqrt{-1}$ and s

is the transfer space represented by $s = \sigma + j\omega$.

$$Y(s) = \frac{1}{\alpha_0 + \alpha_1(\sigma s) + \ldots + \alpha_\lambda(\sigma s)^\lambda} R(s); \lambda \in [2,5] \tag{3.4}$$

$$\alpha_i = \left(\frac{\beta_i}{\beta_0}\right)\left(\frac{\beta_0}{\beta_1}\right)^i \tag{3.5}$$

$$\beta_0 + \beta_1 s + \ldots + \beta_n s^n = \prod_{i=1}^{n}\left(s - e^{\frac{j(-n-2i+1)\pi}{2n}}\right) \tag{3.6}$$

Each high-speed data set contained multiple oscillations averaged by degree. The circular integral was then extracted from the average using Equation 3.7, giving the frictional energy cost of a reciprocation stroke, where: μ is the coefficient of friction; d is displacement, F represents force, y the integrating variable and E_μ denotes work done by friction also known as the dissipated frictional energy.

$$E_\mu(d) = \oint_0^d F_\mu(y)\mathrm{d}y \tag{3.7}$$

Surface Topography and Morphology

Analysis of the surface pre- and post-test allows for better understanding of the mechanisms that are present during testing. Three types of method were used that have varying levels of resolution.

Optical Methods

The Alicona InfiniteFocus (Graz, Austria) can be used in order to assess: the form of a surface, the profile of a wear scar and the surface roughness of a sample. The surface morphology is measured by moving an objective lens with a very narrow focal length through a range of heights and, by processing the images, a 3D image of the surface is produced.

Scanning Electron Microscopy and Energy Dispersive X-ray Spectroscopy

An scanning electron microscope (SEM) can be used to generate a 2D image of a surface. In this thesis a Hitachi TM3030 (Krefeld, Germany) was used, a table top microscope. In contrast to the Alicona the SEM does not provide any data on the topography of the surface but provides information on the morphology. The TM3030 has a back scatter electron detector, which detects changes in composition rather than detailed analysis of differences in surface height. It can be used to identify scratching and pitting on the surface. In conjunction with energy-dispersive X-ray spectroscopy (EDS) more information on these features can be obtained. EDS provides information on the elements present in the measuring field; this measuring field can be a point, line or area of the SEM image. Two EDS units were used one manufactured by Bruker (MA, USA) and one by Oxford Instruments (High Wycombe, UK).

In polymer based testing it was possible to use EDS in order to examine the transfer of poly-tetrafluoroethylene (PTFE) onto the counter surface. A majority of the polymers used did not contain F^- ions unlike PTFE and so detecting these ions on the surface suggests the presence of a PTFE transfer layer.

Physical Methods

A Mitutoyo Surftest SJ-310 (Hampshire, UK) was used to measure the surface roughness of samples. This benefit from being easy to take quick measurements but is limited by the size of the stylus and is unable to deal with large changes in surface height.

Surface Roughness Parameters

Ra is a surface topography descriptor of the average roughness of a surface. Mathematically this can be represented as in Equation 3.8.

$$\mathrm{Ra} = \frac{1}{L}\int_0^L |z(x)|\, dx \tag{3.8}$$

Abbott-Firestone curves plot the cumulative distribution of the surface height; this relationship is shown in Figure 3.4. A useful statistic in the analysis of these curves is the gradient of the interquartile range. A less steep gradient indicates that the surface is more consistent and is made up of similarly sized asperities; whereas a higher gradient would suggest a wider spread of asperity sizes (G. W. Stachowiak and A. W. Batchelor 2014, pp. 477–479).

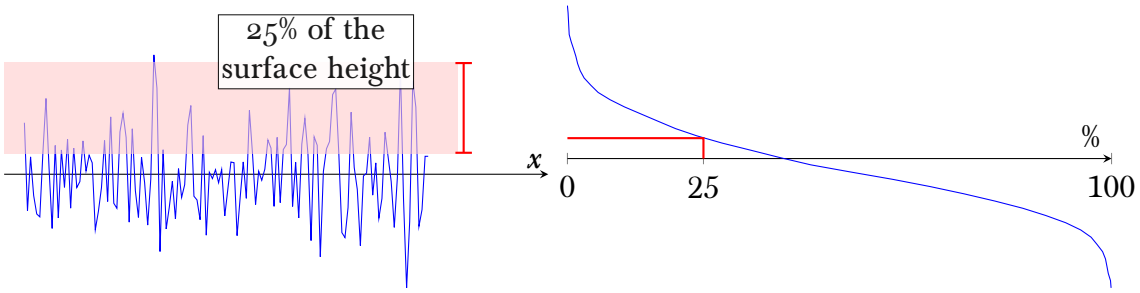

Figure 3.4: An example Abbott-Firestone curve, where the red line shows the calculating procedure. The highest 25% of the observations are shaded in red on the left, and the corresponding cummulative probability shown on the right.

Quantifying Wear

Wear can be quantified volumetrically and gravitametrically. The volumetric wear measurement method of cylinder upper specimens is shown in Figure 3.5. The wear volume was calculated using Equation 3.9 where V_{Wear} is the wear volume, V_{Total} is the total volume of the sample of the cylinder before testing, $V_{Cylinder}$ is the volume of the cylinder after testing. The average standard deviation of the mean for this process is $0.31\,\mathrm{mm}^3$ which is equivalent to an error in the measurement of 13% [1]. Taking the measurement multiple times along the length of the sample allows for any misalignment in the tribometer. Graviametric wear was observed by measuring the mass of the sample pre- and post-test.

$$V_{Wear} = V_{Total} - V_{Cylinder} \tag{3.9}$$

[1] These results are presented in section 4.2

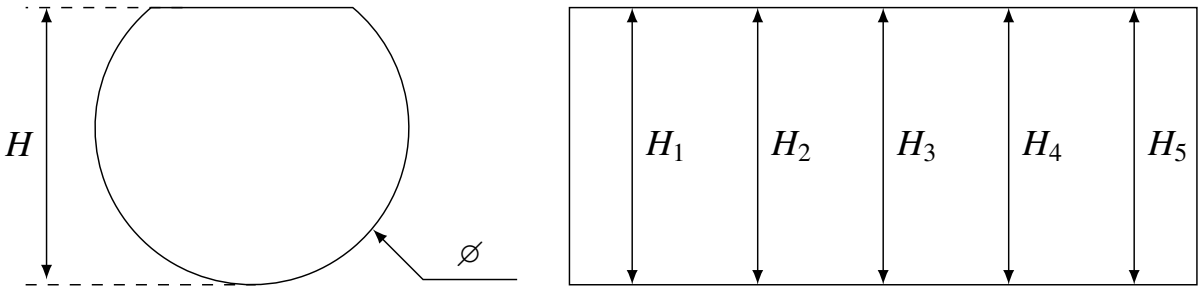

Figure 3.5: Post-test measurement technique to determine wear volume in the cylinder upper specimens. Each measurement was taken five times at different points along each sample.

Wettability

A transfer layer can help to further lubricate a contact, especially if the transfer layer consists of a self lubricating material such as PTFE (Jain and Bahadur 1978). Jain and Bahadur concluded that the transfer would occur from a material with low cohesive energy to a higher energy material. In addition to this using the Young - Dupré equation (Equation 3.12) materials with a lower contact angle will encourage transfer. Nunez and Polycarpou found that to create a continuous and uniform film, the optimum for a consistent contact, a smoother counter surface was ideal due to the higher adhesion forces causing cohesion. They also reported that a smoother surface caused smaller wear particles and less ploughing, this also promoted a more consistent counter surface (Nunez and Polycarpou 2015). There is a limit to this, some roughness is required in order to promote adhesion of the transfer layer on the alternative surface (Hutchings and Shipway 2017).

The surface roughness affects the contact angle formed by a droplet of lubricant on a material surface. This spreading, or wettability, is influenced by the surface roughness, viscosity of the lubricant and the surface energy of the material (Bhushan and Jung 2008; Kalin and Polajnar 2013).

The fundamentals of this theory are encompassed in Equation 3.10 where R_f is defined in Equation 3.11, where A_{SL} is the real area of the surface and A_F is the projected area

(Whyman et al. 2008).

$$\cos\theta = R_f \cos\theta_0 \tag{3.10}$$

$$R_f = \frac{A_{\mathrm{SL}}}{A_{\mathrm{F}}} \tag{3.11}$$

The effect of this change in contact angle reduces the adhesion of the lubricant to the surface of the material leading to more spreading of the lubricant and a lower film thickness. This relationship is described in the Young-Dupré equation — Equation 3.12 where: W_{SL} is the work of adhesion between the solid and liquid and γ_{LV} is the surface tension between the lubricant and air (Schrader 1995). The work of adhesion can also be written as in Equation 3.13 (S. Wang et al. 2009). γ_S is also known as the surface free energy and is displayed in Table 3.1. An increase in γ_S will lead to an increase in the work of adhesion.

$$W_{SL} = \gamma_{LV}\,(1 + cos\,(\theta)) \tag{3.12}$$

$$W_{SL} = \gamma_S + \gamma_L - \gamma_{SL} \tag{3.13}$$

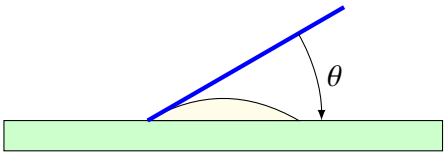

Figure 3.6: Contact angle measurement procedure.

Figure 3.6 shows the procedure used to measure the contact angle that the lubricant made with the surface. The surface was first cleaned with ethanol, then acetone and then hexane. In between each cleaning process the solvent was allowed to evaporate for 10 min. A 10 µl drop of lubricant was placed onto the surface and an image was taken every 5 s

for 10 min. The angle (θ) of the edge of the drop was measured, shown as a blue line in Figure 3.6. The droplet was imaged using a telecentric lens, this accounted for any parallax errors in the measurement.

Surface Tension

A SITA T15 bubble tensiometer (SITA Messtechnik GmbH, Dresden, UK) was used to measure surface tension of lubricants. The surface tension was measured at a range of bubble life times for each lubricant. The measurements were repeated 3 times each.

Surface tension and contact angle are highly linked as shown in Equation 3.14 where γ denotes surface tension and θ the contact angle; the subscripts S and L refer to the solid and liquid boundaries. The higher the inter-facial energy (γ_{SL}) the thicker the lubricant film and the lower the coefficient of friction (Liu et al. 2008). At the start of the test the solid surfaces of the same material will have similar values of γ_S and so the parameter $\gamma_L cos\,(\theta)$ is indicative of inter-facial energy; an increase in $\gamma_L cos\,(\theta)$ will reduce γ_{SL} and increase friction when comparing lubricant performance between identical materials. In this case the effect of solid contact between identical materials will be constant and so comparing the parameters in this way results in a description of the lubricant performance.

$$\gamma_{SL} = \gamma_S - \gamma_L \cos\theta \tag{3.14}$$

As the tension and wettability of a lubricant is dependant on temperature, these tests were conducted at the same time over a few hours on the same day. This ensures only minor variation in the ambient temperature reducing the error in the measurement.

3.4 Contact Mechanics

In order to accurately simulate the Dearman Engine on the TE77 the contact pressure of the pertinent interaction was modelled. Working from Dearman technical drawings and

data from engine testing the contact pressure between the piston seal and cylinder liner and the valve stem and valve guide was calculated.

Many theories of contact mechanics have been presented in literature, in this thesis a purely elastic contact was assumed for the calculations using the theory set forward by Hertz (Hertz 1896). In the case of polymers the true contact area will deviate from the Hertzian contact as represented by theories such as JKR (Johnson 2003) however, these deviations are small. Many assumptions were made in simulating the Dearman engine on the TE77 caused by limitations in the geometry of the lubricant bath and the motion of the motor that drives the upper specimen. As such a minor variation in contact area is negligible and Hertzian contact pressure can be assumed.

Piston Seal - Cylinder Liner

Figure 3.7 shows the cross-section of the piston seal of the Dearman Engine. The following calculations determine the contact pressure acting upon the outer lip of the seal, the mechanics is based on the free body diagram shown in Figure 3.8.

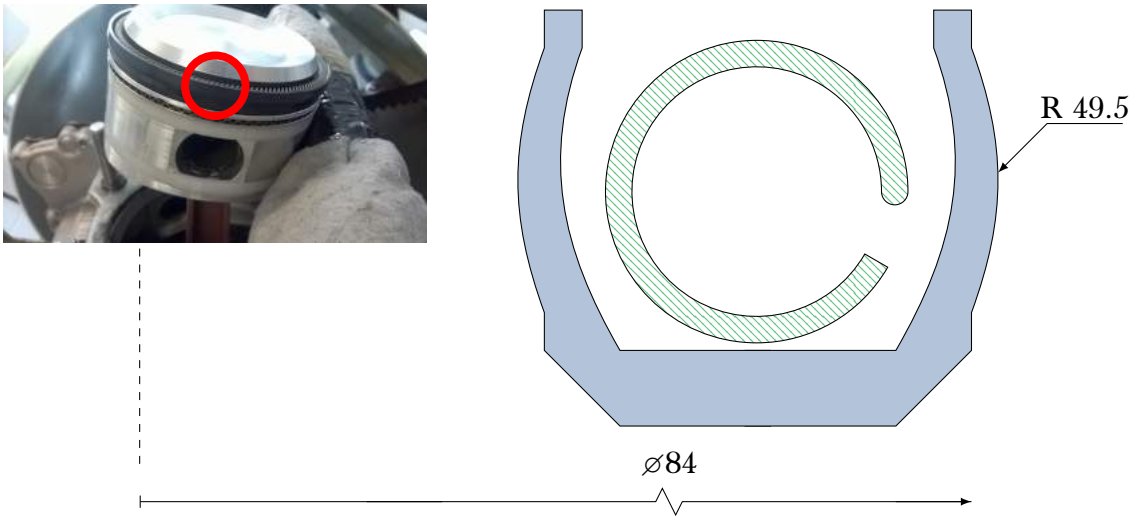

Figure 3.7: Cross-section of the piston seal showing the polymeric outer and spring in the centre of the seal circumference. An image of the piston is shown in the top left of the schematic with a circle to show where the cross-section has been taken (not to scale, all dimensions are in mm).

The maximum pressure and resulting force was calculated from the data represented in Figure 3.9. This data was collected from a generation 1.5 Dearman Engine at 40 bar N_2

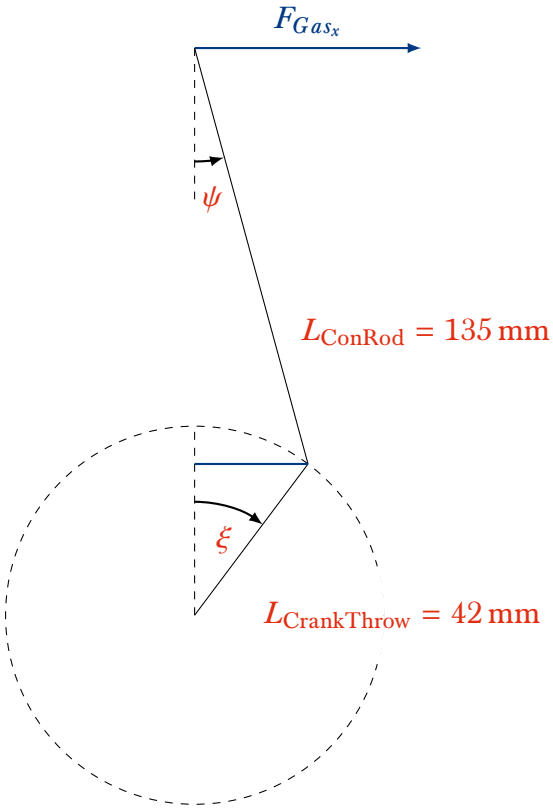

Figure 3.8: A free body diagram of the force acting on the cylinder wall transmitted via the connecting rod.

supply pressure, 800 rpm and a cylinder temperature of 12 °C: representative of a standard operating conditions for the engine installed on a truck refrigeration unit (TRU). The generation 1.5 engine is identical to the 1st generation from the bottom end of the engine to the top of the cylinder, the cylinder head is a bespoke unit designed for the flow of nitrogen and HEF.

The maximum contact pressure within the seal was calculated using Equations 3.15 to 3.26 (Johnson 2003, p. 101), assuming the seal is manufactured from PTFE and the cylinder from Aluminium 6063. The equations first calculate the force on the cylinder wall from the expansion of the gas and then convert it into a contact pressure. It was assumed that the length was equal to $84\,\pi$ mm and the radius was taken from the seal geometry shown in Figure 3.7.

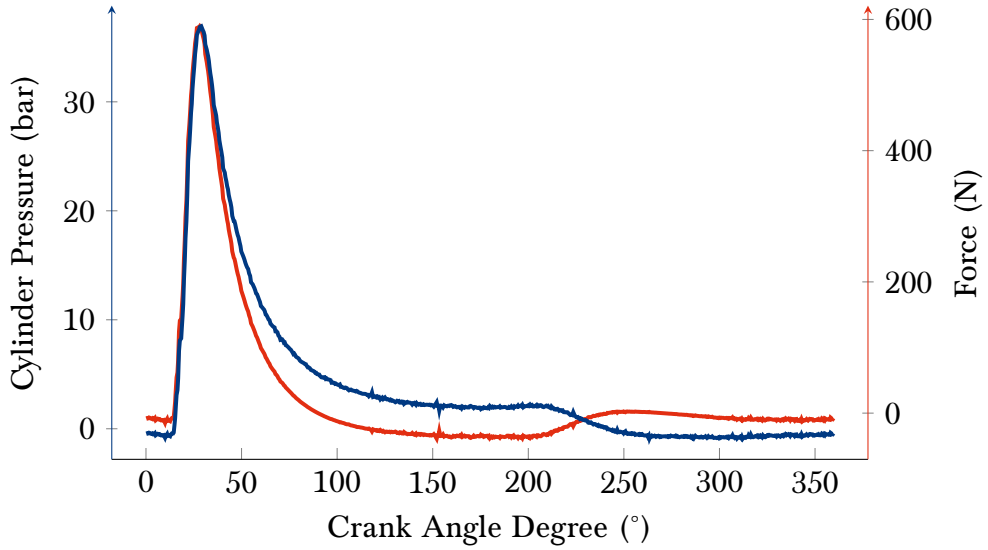

Figure 3.9: The cylinder pressure and force relative to crank angle degree as measured on a generation 1.5 Dearman Engine during normal running conditions.

$$F_{\text{Cylinder Wall}} = F_{\text{Gas x}} + F_{\text{Seal}} \tag{3.15}$$

$$F_{\text{Gas x}} = P_{\text{Gas}} A_{\text{Piston}} \tan(\psi) \tag{3.16}$$

$$\psi = \sin^{-1}\left(\frac{L_{\text{CrankThrow}}}{L_{\text{ConRod}}}\right) \tag{3.17}$$

$$L_{\text{Crank Throw x}} = L_{\text{CrankThrow}} \cos(\xi) \tag{3.18}$$

$$F_{\text{Gas x}} = P_{\text{Gas}} A_{\text{Piston}} \tan\left(\sin^{-1}\left(\frac{L_{\text{CrankThrow}} \cos(\xi)}{L_{\text{ConRod}}}\right)\right) \tag{3.19}$$

$$\hat{F}_{\text{Gas x}}\Big|_{\substack{\hat{P}_{\text{Gas}}=36.9\times10^5\,\text{Pa}\\ \xi=28.9^\circ}} = 590\,\text{N} \tag{3.20}$$

$$F_{\text{Seal}} = P_{\text{Gas}} A_{\text{Seal Inner Lip}} \tag{3.21}$$

$$F_{\text{Seal}}\Big|_{\substack{\hat{P}_{\text{Gas}}=36.9\times10^5\,\text{Pa}\\ A=3.7\times10^{-5}\,\text{m}^2}} = 136\,\text{N} \tag{3.22}$$

$$\hat{F}_{\text{Cylinder Wall}} = 726\,\text{N} \tag{3.23}$$

$$\hat{P}_{\text{Cylinders with parallel axes}} = \sqrt{\frac{F_{\text{Cylinder Wall}} E^*}{\pi L R}} \tag{3.24}$$

$$E^* = \left(\frac{1 - \nu_1^2}{E_1} + \frac{1 - \nu_2^2}{E_2} \right)^{-1} \tag{3.25}$$

$$\hat{P} = 3.33\,\text{MPa} \tag{3.26}$$

The maximum contact pressure ($\hat{P}$), 3.33 MPa, was used in Chapter 4 as a target contact pressure to achieve in testing.

Valve Stem - Valve Guide

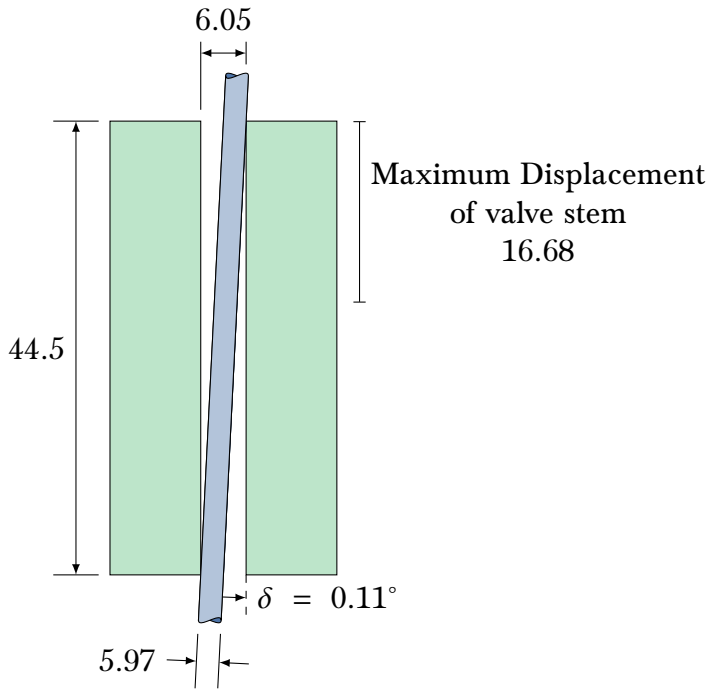

Figure 3.10: A schematic of the valve stem and valve guide, all dimensions in mm.

Figure 3.10 and Figure 3.11 were used to calculate the maximum contact pressure imparted on the valve guide as calculated below. The spring rate of the valve spring was calculated from data collected by Ricardo (Shoreham-by-Sea, West Sussex, UK) on behalf of Dearman. This was then integrated to calculate the force applied down the valve stem and then the maximum force in the x direction calculated.

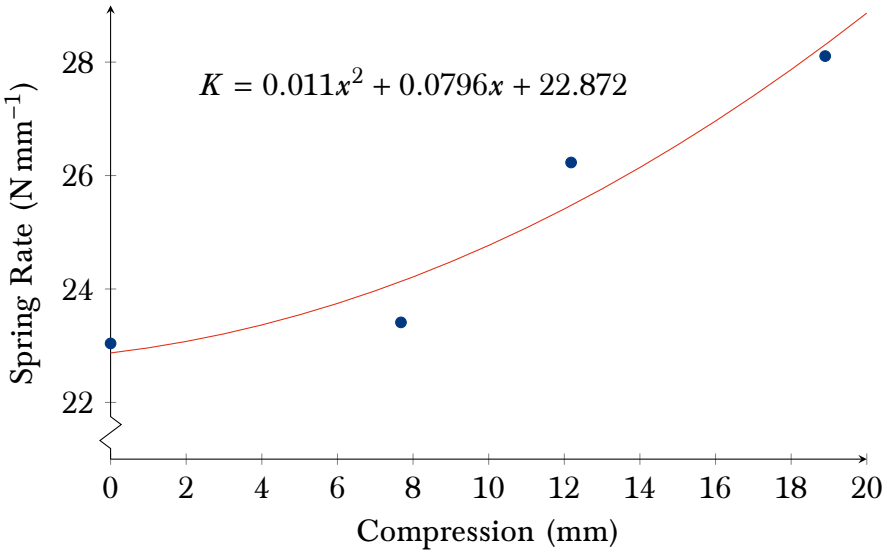

Figure 3.11: A graph of compression length against spring rate shown in blue is the actual spring rate and a quadratic polynomial fit with the equation also shown.

$$K = 0.011x^2 + 0.0796x + 22.872 \tag{3.27}$$

$$F_\Sigma = \int_{\check{x}}^{\hat{x}} K \, \mathrm{d}x \tag{3.28}$$

$$F_\Sigma\Big|_{\substack{\hat{x}=16.68\,\mathrm{mm} \\ \check{x}=0\,\mathrm{mm}}} = 410\,\mathrm{N} \tag{3.29}$$

$$\hat{P} = \frac{F_x}{A} \tag{3.30}$$

$$\hat{P} = \frac{F_\Sigma \tan\delta}{A} \tag{3.31}$$

$$\hat{P}\Big|_{\substack{\delta=0.11^\circ \\ A=1.13\times10^{-4}\,\mathrm{m}^2}} = 6.96\,\mathrm{kPa} \tag{3.32}$$

The maximum contact pressure of the valve stem, 6.96 kPa on the valve guide is used in Chapter 6.

3.5 Conclusions

This chapter has set out materials and methods used throughout this thesis. It set out a variety of methods for assessing tribological performance of materials and lubricants and analysing the resulting data and surfaces. These methods all contribute to the delivery of

the aims and objectives set out at the end of Chapter 2 in order to reduce the parasitic losses within the Dearman Engine.

Chapter 4

Polymer Tribology: A Material Replacement Study

The content of this chapter is based on the following papers:

Iestyn M.N. Stead et al. (July 2019). "Towards a plastic engine: Lowtemperature tribology of polymers in reciprocating sliding". In: *Wear* 430-431.January, pp. 25–36. ISSN: 00431648. DOI: 10.1016/j.wear.2019.04.008,

Iestyn M. N. Stead et al. (2019). "Cold, clean and green: improving the efficiency and environmental impact of a cryogenic expander". In: *IOP Conference Series: Materials Science and Engineering* 502, p. 012157. ISSN: 1757-899X. DOI: 10.1088/1757-899X/502/1/012157

4.1 Introduction

The following chapter explores the implementation of polymers within the Dearman Engine cylinder-piston interaction. This was undertaken in order to utilise the advantageous tribological properties of polymers when compared to the original materials used within the engine. The first investigation was into the replacement of the cylinder liner, originally manufactured from aluminium. The second investigation in this chapter concentrated on the piston seal assessing if a cheaper and less complex design utilising laminated polymers as an alternative to a composite material.

4.2 Cylinder Liner

Materials and methods

The materials used in this phase of testing are shown in Table 4.1 where aluminium is a benchmark for comparison representing the current engine block.

Currently, the piston of the Dearman engine employs a poly-tetrafluoroethylene (PTFE) composite seal to separate the cylinder from the bottom end—this was modelled using a PTFE cylinder (pin) for the upper specimen. The lubricant used was Lubron ISO 10 Hydraulic Oil (Lubron Advanced Oils Ltd., Northamptonshire, UK).

Table 4.1 also shows a summary of the testing parameters. These were designed to simulate conditions within the Dearman engine. 10 ml of lubricant was used as it flooded the contact, this was the closest to splash lubrication that could be replicated on the TE77. Before testing the specimens were chilled to the required temperature; during the testing the chiller and controller kept the specimen bath at the required temperature (±2 °C).

The PTFE upper specimens were cut from long lengths using a jig to guarantee consistency in length, after the sample was cut the edges were de-burred and cleaned in ethanol.

The lower specimen samples were systematically honed using 320 grit wet dry paper to formulate a cross hatched surface. Aluminium, polyphthalamide (PPA), polytrimethylene

Table 4.1: The parameters used in the testing on the TE77 HFRR. The testing was split into two phases, one hour and twelve hour testing. Values are taken from the Dearman standard operating conditions, the calculations for derived parameters are presented in Chapter 3

Parameter		**Value**
Frequency		13.3 Hz
Stroke Length		25 mm
Contact Pressure		3.33 MPa
Sliding Distance		2394 m / 28 728 m
Time		1 h / 12 h
Temperature		−8 °C / 12 °C
Upper Specimen	Material	PTFE
	Size	∅ 6 mm × 15 mm
Lower Specimen	Material	Aluminium 6063 T83, PPA, PTT, PEEK, POM, POM with PTFE and UHMWPE
	Size	58 mm × 20 mm × 4 mm
Lubricant		10 ml Lubron 10, Hydraulic Oil

terephthalate (PTT), polyoxymethylene (POM) and POM with PTFE were all also tested unhoned to compare the effect of the honing on the samples. Where materials were supplied as plates less than 4 mm thick, shims were used to make up the thickness for the lower specimen samples. When the samples were prepared for testing on the TE77 they were cleaned in an ultrasonic bath with ethanol and the excess solvent was allowed to evaporate. Ethanol was used as it was one of the few solvents that were suitable to use with all of the materials.

The TE77 was used for two different phases of testing. i. A one hour test with three repeats was used to ascertain the coefficient of friction and to screen the materials. ii. A 12 h durability run for each material, this allowed data about the wear volume to be collected and to explore transfer of materials between specimens.

Results

Steady State Coefficient of Friction

Figure 4.1 shows the mean coefficient of friction of each material at both temperatures tested. The honed glass reinforced materials (PPA and PTT) both had a noticeable increase in friction with a decrease in test temperature, although PPA had a larger variance in the data. The other polymers did not demonstrate a large change in coefficient of friction with temperature. This is significant as they are both reinforced with glass and all of the others were unreinforced polymers. The POM with PTFE also demonstrated an increase in coefficient of friction but this effect was reduced, this demonstrates that the reinforcing of materials directly affects the tribological performance in low temperature reciprocating sliding. Out of the polymers, the PPA and PTT demonstrated the lowest coefficients of friction. The materials in Figure 4.1 have been ordered in reducing Young's modulus. It can be seen that the coefficient of friction is affected by the Young's modulus of the honed materials. In general the stiffer materials demonstrate a lower coefficient of friction. This trend is not replicated in the unhoned materials.

The effect of the honing process can also be determined from Figure 4.1. For all of the materials other than the PTT, honing the samples has increased the coefficient of friction.

Time to Steady State

Figure 4.2 shows the time to steady state for each material during the 1 h tests. The aluminium shows a long settling time for the friction signal but with a wide spread of data. PPA at 12 °C has a long settling time, this is not an ideal trait for a bore material as the system is not stable and this can promote excessive wear during the bedding in process but this effect is also affected by other factors such as surface roughness. The transition to steady state is a balance between the wear mechanism determining the frictional properties and *vice versa*. For instance the excessive flash temperatures can cause increased plastic deformation and more adhesion increasing the wear rate. A shorter transition is not guaranteed to reduce the wear rate but it can be loosely correlated (Ian Hutchings et

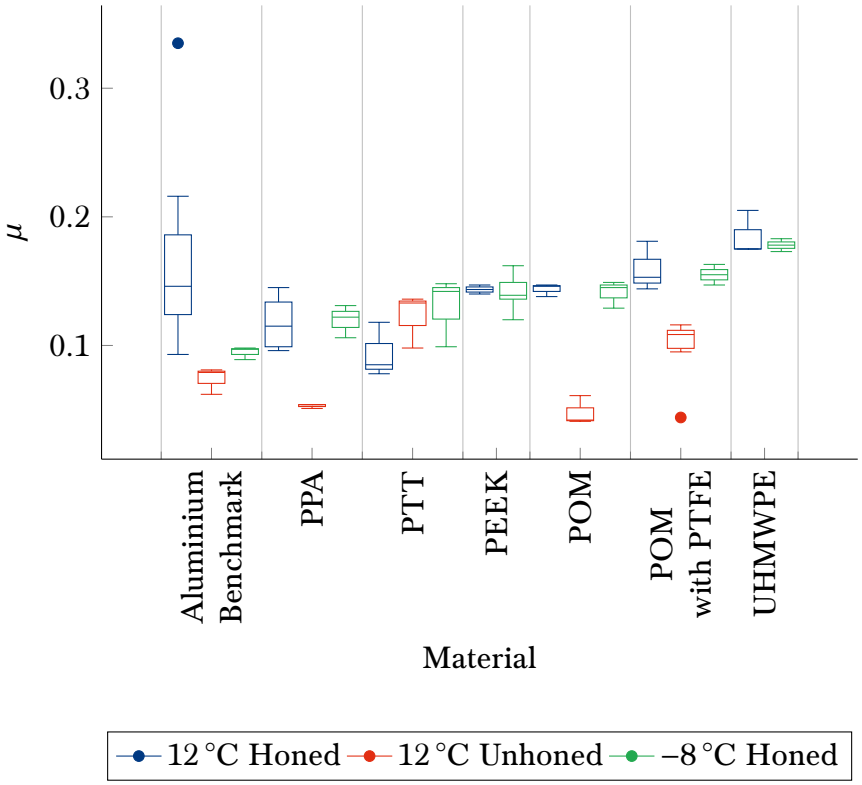

Figure 4.1: A comparison of the steady state coefficient of friction at the two different temperatures and surface preparations, 12 °C in red and −8 °C in blue. The materials are ordered in decreasing stiffness from left to right.

al. 2011). In general the −8 °C tests show a lower settling time. The only material that does not follow this trend is polyether etherkeytone (PEEK). PTT, POM and ultra high molecular weight polyethylene (UHMWPE) all show a short settling time, which is a promising property for reduction of wear and system stability. POM with PTFE had a consistently short settling time.

Figure 4.3 shows the percentage overshoot of the coefficient of friction over the steady state coefficient of friction. It can be seen that aluminium overshoots by at least 15%, this increased coefficient of friction could increase the flash temperature of the material and therefore increase wear in the seal. At 12 °C PPA has a high overshoot and this combined with a long settling time may promote excessive wear over a long period of time. At −8 °C overshoot is less than 20%. Again PTT, POM and UHMWPE all show similar trends with a low overshoot and clustered data. This data point corresponds with the sample that displayed a high settling time.

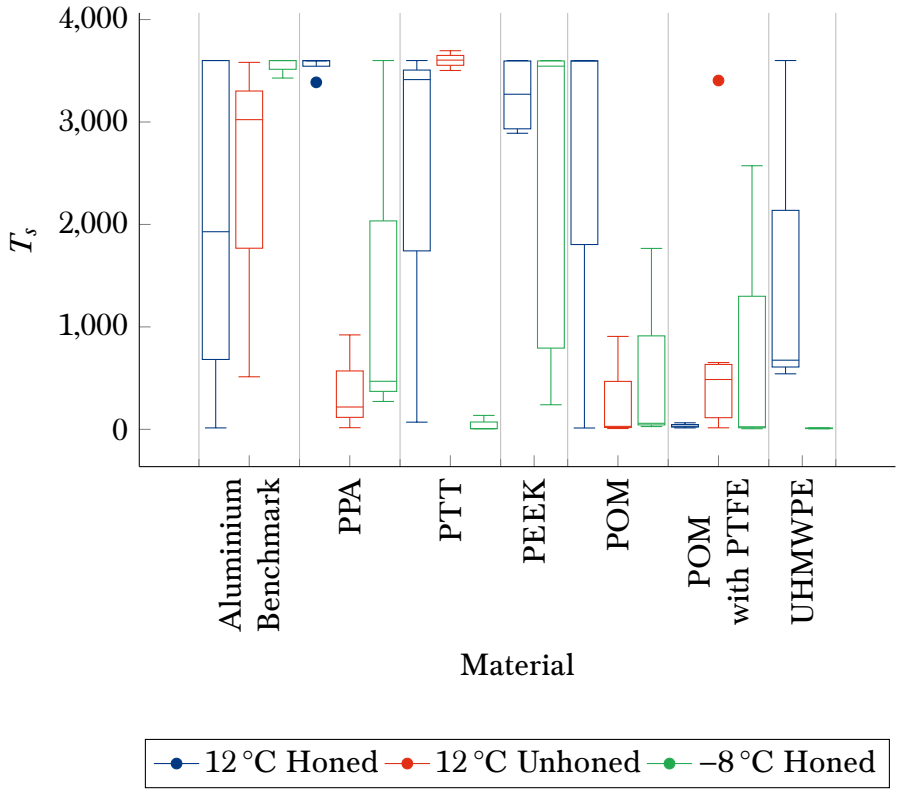

Figure 4.2: Time to steady state (s) calculated from tests conducted for one hour.

Wear Volume

Figure 4.4 shows the average coefficient of friction plotted against the wear volume of the PTFE upper specimen. This does not show a strong trend but suggests that the wear volume is related to the coefficient of friction, this corroborates trends seen by Chattopadhyay and Barrell et al. (Chattopadhyay 2001; Barrell and M. Priest 2003). PTT has the lowest coefficient of friction, wear volume and percentage overshoot out of all the honed materials that were tested.

There are some datasets where the coefficient of friction has a broad spread as shown by large error bars. This is likely caused by misalignment of the upper specimen in the specimen carrier of the TE77.

The POM impregnated with PTFE has a higher coefficient of friction than the standard POM. It appears that the PTFE impregnation worsened the wear rate and friction. Burris and Sawyer reported that the wear rate for filled polymers was dependant on the percentage of reinforcement by weight. They reported that there is a 'sweet spot' in the

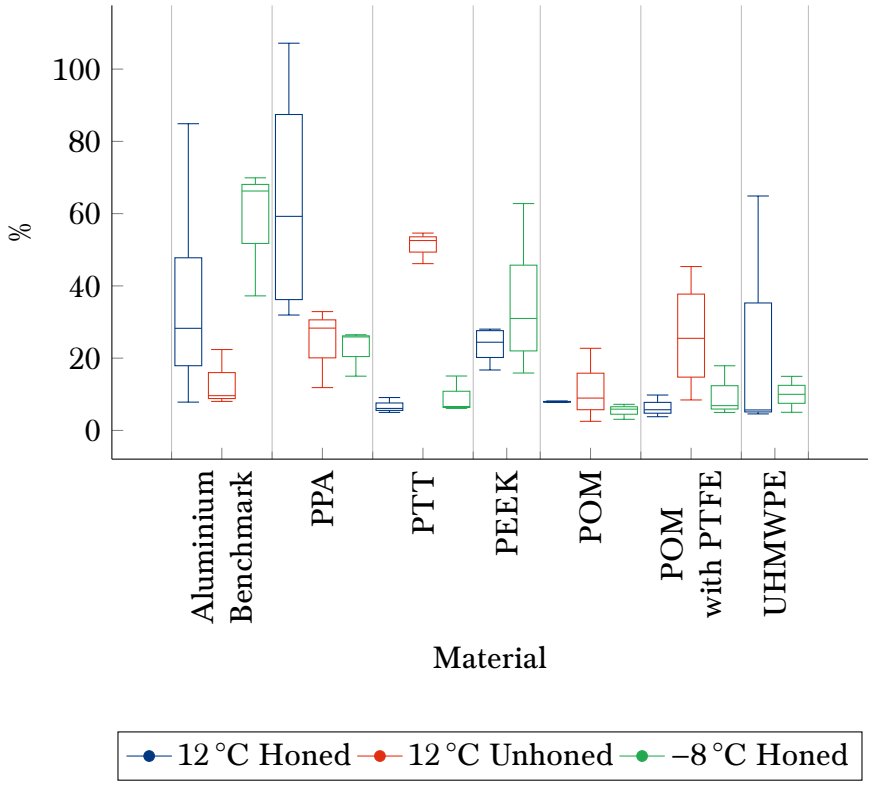

Figure 4.3: Percentage overshoot calculated from tests conducted for one hour.

reinforcement percentage at which wear would be the lowest (Burris and Sawyer 2006). It can be surmised that the level of impregnation used in the POM with PTFE is unsuitable and a different level of impregnation may improve the wear volume observed.

PPA had the highest wear rate out of the polymers relative to the coefficient of friction. This was likely to be due to the trend shown in Figure 4.2 and Figure 4.3 where the coefficient of friction overshot by the largest amount the steady state coefficient of friction and took longer to settle to the steady state. Honed PEEK also has one of the lower coefficient of friction's but the second highest wear rate out of the polymers.

Figure 4.5 shows the mean wear volume of the PTFE upper sample for each condition plotted against the overshoot of the coefficient of friction during the testing. It can be seen that there is a loose correlation between the variables, the calculated coefficients were honed: $R^2 = 0.31$ and unhoned: $R^2 = 0.77$. This is not unexpected but supports the notion that a large overshoot can lead to excessive wear rates through asperity smoothing. The likely explanation of this phenomenon is that the reduction of coefficient of friction

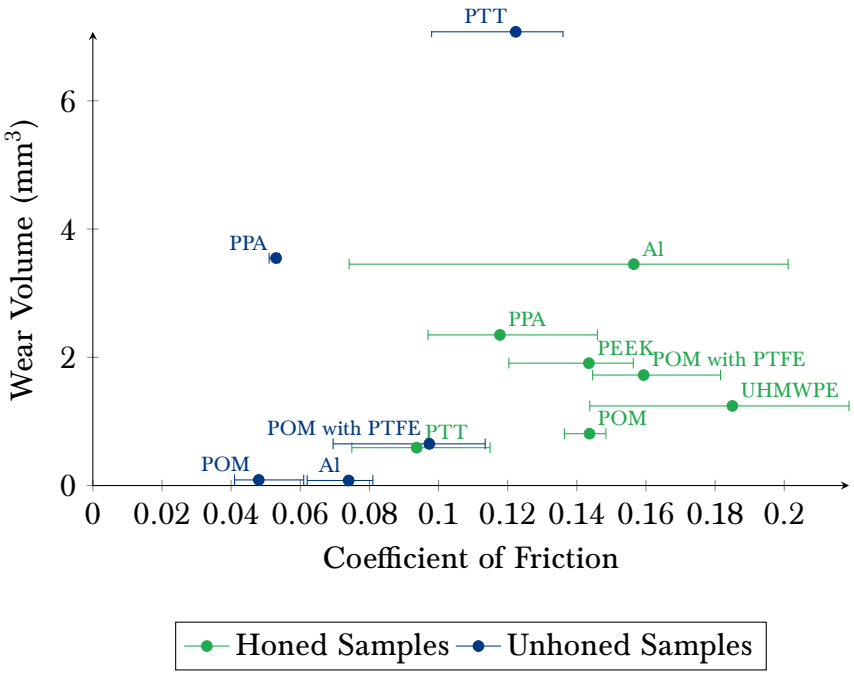

Figure 4.4: The wear volume of PTFE upper specimen plotted against the coefficient of friction during the 12 h durability runs. The error bars are one standard deviation in each direction of the measurement.

to steady state is due to the transfer of PTFE onto the counter-surface and so a higher overshoot leads to more transfer of PTFE.

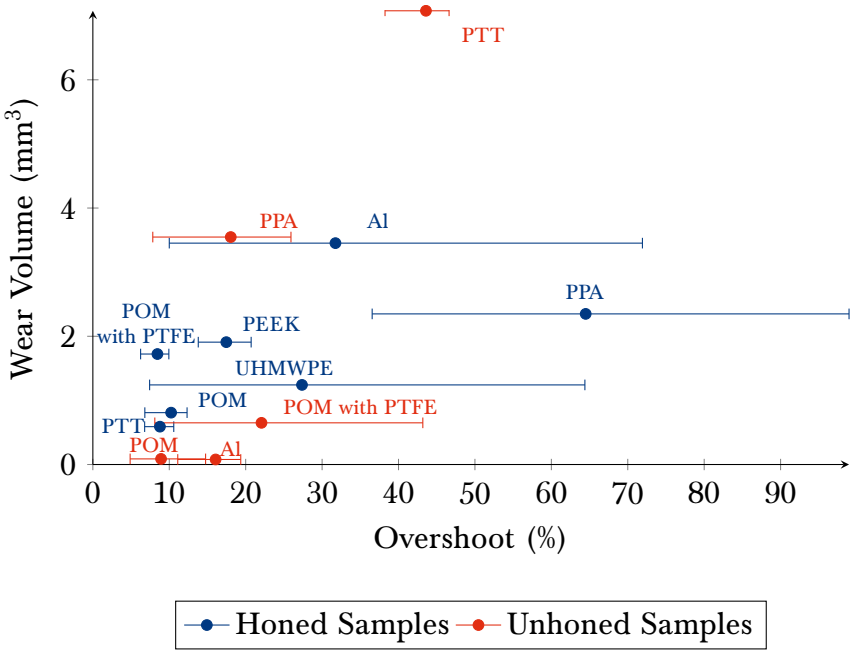

Figure 4.5: The mean wear volume of PTFE upper specimen plotted against the percentage overshoot of coefficient of friction during the 12 h durability runs. The error bars are one standard deviation in each direction of the measurement.

The method through which the overshoot leads to high wear rates is likely to be due to a higher coefficient of friction causing a higher flash temperature (Hoskins et al. 2014). This higher flash temperature will reduce the activation energy required to remove the asperities promoting an increased wear rate. This can also be linked to work by Kubiak et al. where a higher dissipated energy in contact was linked to a higher wear rate (Kubiak et al. 2011). A higher flash temperature is indicative of a higher dissipated energy.

In this study only one repeat of the durability tests were undertaken. This provides some limitation in the conclusions that can be drawn from the data. However, the wear data was compared with literature as a check to support the validity of the data. Whilst the numerical data cannot be directly compared, the trends are able to be analysed. The comparative wear (ie. PEEK causing more wear in the PTFE sample than POM) between UHMWPE, PEEK, POM and PTFE composites is corroborated in literature (Friedrich et al. 2005; Cannaday and Polycarpou 2005; Mens and Gee 1991).

Wettability

The wettability of the materials measured with the hydraulic oil compared to the wear volume is shown in Figure 4.6. It can be seen that there is a PTT data point that is an outlier in the data. Honed PTT displays more oleophobic behaviour, the drop of oil did not spread across the surface. In the more oleophilic materials the wear volume roughly increases with an increase in wettability, although surface roughness and morphology effects will be present. Unhoned POM and aluminium were the most oleophillic and have a low wear volume. Higher wear volumes occur with a higher contact angle in these materials. Physically, the lower the contact angle, the better the spread of the lubricant across the sample, the oil is theoretically able to better lubricate the bearing surfaces. Borruto et al. showed a low contact angle allows the oil to 'wash' wear debris away and reduce the coefficient of friction. To promote low coefficient of friction and wear the seal and cylinder liner should have significantly different contact angles (Borruto et al. 1998). This is also supported by more fundamental work undertaken by Schertzer and Iglesias where it was determined that a spreading of the lubricant in low film thickness

contacts reduced the coefficient of friction and therefore the frictional energy dissipation and adhesive wear (Schertzer and Iglesias 2018). In the case of honed PTT with a high contact angle, more energy will be required to remove material from the surface. A high contact angle and a low wear rate means that the lubricant is not coating the surface well but that the materials are suitable to be run against each other in starved lubrication. However, poor retention of the liquid lubricant can be counteracted by lubrication from a solid lubricant, in this case PTFE from the upper specimen. This may lead to excessive wear in the seal. A low wear volume would suggest that the honed PTT and the PTFE with the hydraulic oil lubricating the contact is ideal. Unhoned PTT has a high wear volume and a low contact angle. This would suggest that the system is unstable, this also coincides with a large percentage overshoot.

Both POM and POM with PTFE have a low contact angle. As discussed in Section 4.2 the pure POM has a lower wear volume but a comparable contact angle. This low contact angle may allow for adequate lubrication, producing a low wear volume compared to the other materials that are not reinforced ie. UHMWPE, PEEK.

In general the materials with a lower contact angle have a lower wear volume; this also coincides with the lower overshoot materials as demonstrated in Figure 4.5. The only material that does not fit the trend is the PTT but it is significantly more oleophobic and so the mechanisms of lubrication are likely to be significantly different from the other materials.

Surface Roughness

Figure 4.7 shows the Abbott-Firestone curve for each material with the upper and lower quartiles marked. The Ra is shown in Table 4.2 and the uncertainty in the Ra is one standard deviation of the mean. Measurements were taken after tribological testing.

Aluminium has the smoothest Ra and the lowest gradient for the interquartile range for both the honed and unhoned samples. For honed PTT the Ra is 0.790 µm but the bearing area curve suggests a large proportion of the roughness is significantly consistent, this is demonstrated by its low gradient. This may be one of the reasons PTT displayed

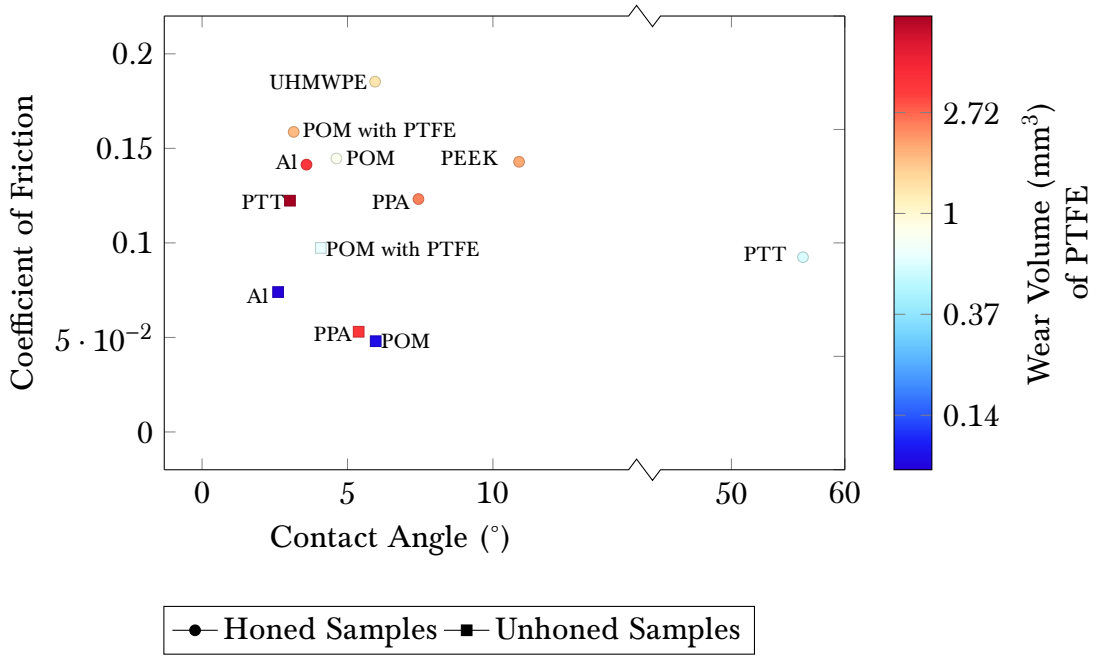

Figure 4.6: The contact angle plotted against the coefficient of friction from tests operated at 12 °C. The wear of the PTFE upper sample is shown using the colour bar on the right. The wettability was tested using Lubron ISO10 at ambient temperature.

low coefficient of friction as well as a low wear rate. Smaller asperities and a better bearing surface will reduce the coefficient of friction as long as the lubricant can be held at the surface. The surface of the PTT was the best solution for coefficient of friction and wear resistance out of the honed polymers tested. Rohm et al. reported that the bearing area curve affects the coefficient of friction. In the study they demonstrated that the difference was more prevalent with a higher velocity but that close to 0 °C a lower gradient in the bearing curve reduced the coefficient of friction (Rohm et al. 2016). As the piston velocity is high the effect of bearing area is important to the running of the engine. It can be seen that the surface roughness of the samples also correlates with the trend seen in the steady state coefficient of friction in Figure 4.1; the surface roughness appears to increase with an reduction of Young's Modulus and the increase in coefficient of friction. This is likely to be due to material preparation, a stiffer material will be harder to hone and so less fatigue is introduced into the surface during the initial preparation.

Honed PPA had a similar Ra and a similar Abbott-Firestone curve to the honed PTT although the PPA wear volume shown in Figure 4.4 was significantly higher. The honed

PPA had a higher percentage of glass filler than the PTT tested; a higher percentage of glass filler has been shown to increase wear resistance (Khedkar et al. 2002). This may also explain why the honed PPA is smoother than the unhoned PPA after testing as the hard glass will wear the PTFE further and lead to a transfer layer forming faster. However a shorter fibre length increases the wear rate (Friedrich et al. 2005). This effect may have been caused by the honing process exposing some of the fibres increasing the abrasive wear. UHMWPE has the highest surface roughness of the materials which corresponds with the highest coefficient of friction, this was due to the honing process damaging the surface rather than causing a cross hatching pattern but the material resists wear.

The honing process does not appear to have changed the roughness of the samples by a large amount. In general the honing makes the surface roughness increase. Figure 4.8 and Figure 4.9 show the relationship between coefficient of friction and the surface roughness parameters. It can be seen that a higher surface roughness and higher gradient of the interquartile range can be correlated with a higher coefficient of friction. As the main method of wear is adhesion leading to increased wear, a less consistent and rougher surface would lead to more asperities to be in contact and subsequently more wear and friction.

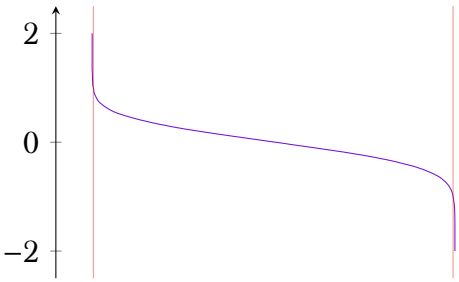

(a) Aluminium - Honed

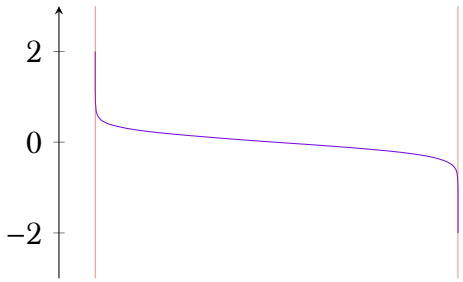

(b) Aluminium - Unhoned

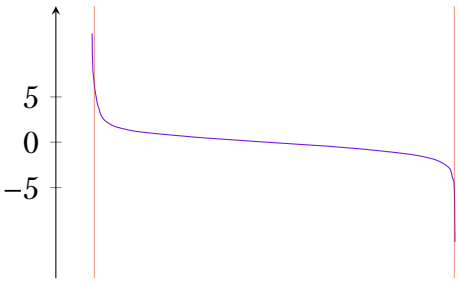

(c) PPA - Honed

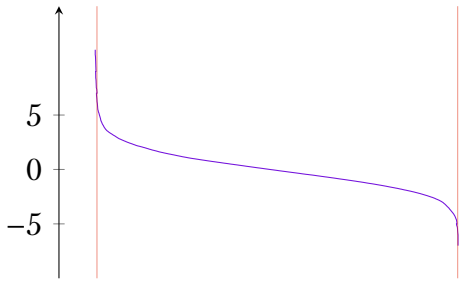

(d) PPA - Unhoned

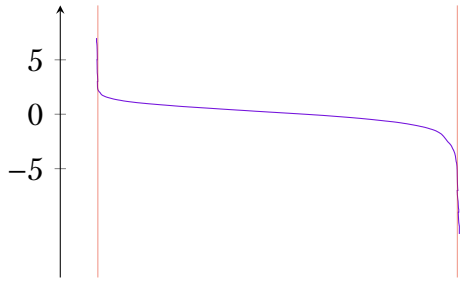

(e) PTT - Honed

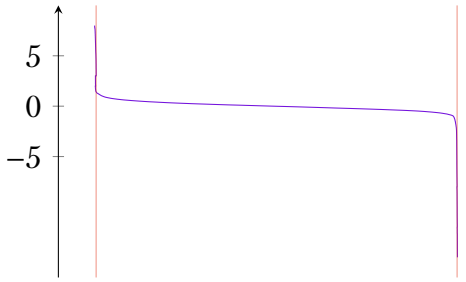

(f) PTT - Unhoned

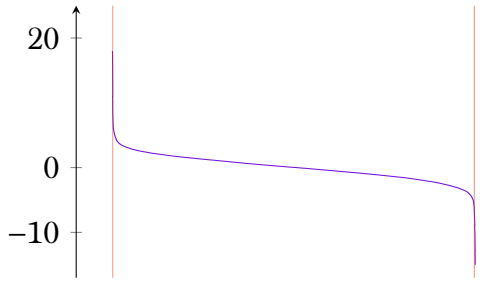

(g) PEEK - Honed

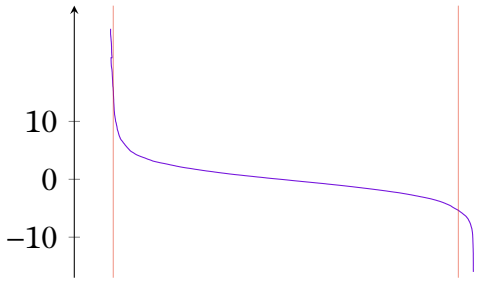

(h) POM - Honed

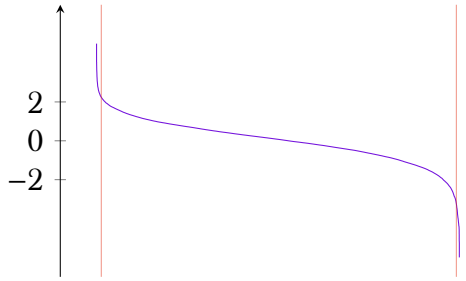

(i) POM - Unhoned

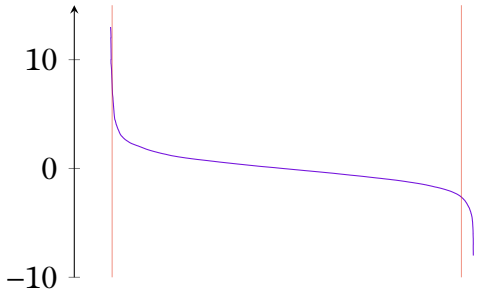

(j) POM w/ PTFE - Honed

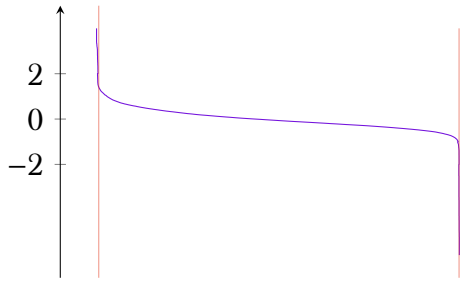

(k) POM w/ PTFE - Unhoned

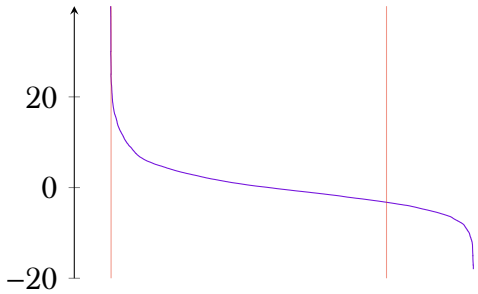

(l) UHMWPE - Honed

Figure 4.7: Abbott - Firestone curves for each material tested. In the appendices the same data is presented with identical axes to aid comparison.

Transfer Layer

Figure 4.10 shows the energy-dispersive X-ray spectroscopy (EDS) data for all of the tested materials. The elements seen in the spectra are indicated in the legend of the graphs. Every

Table 4.2: Ra and gradient of the interquartile range of the Abbott Firestone curve shown in Figure 4.7 for each material. The uncertainty in Ra is one standard deviation of the mean.

Material	**Ra (μm)**	**Gradient of Interquartile Range (μm/%)**
Aluminium Honed	0.29 ± 0.01	-0.04
Aluminium Polished	0.18 ± 0.01	-0.04
PPA Honed	0.98 ± 0.01	-0.23
PPA Unhoned	1.46 ± 0.13	-0.20
PTT Honed	0.79 ± 0.02	-0.19
PTT Unhoned	0.35 ± 0.01	-0.10
PEEK Honed	1.50 ± 0.12	-0.33
POM Honed	2.41 ± 0.37	-0.45
POM Unhoned	0.85 ± 0.02	-0.11
POM with PTFE Honed	1.14 ± 0.07	-0.22
POM with PTFE Unhoned	0.35 ± 0.13	-0.10
UHMWPE Honed	3.72 ± 0.06	-0.76

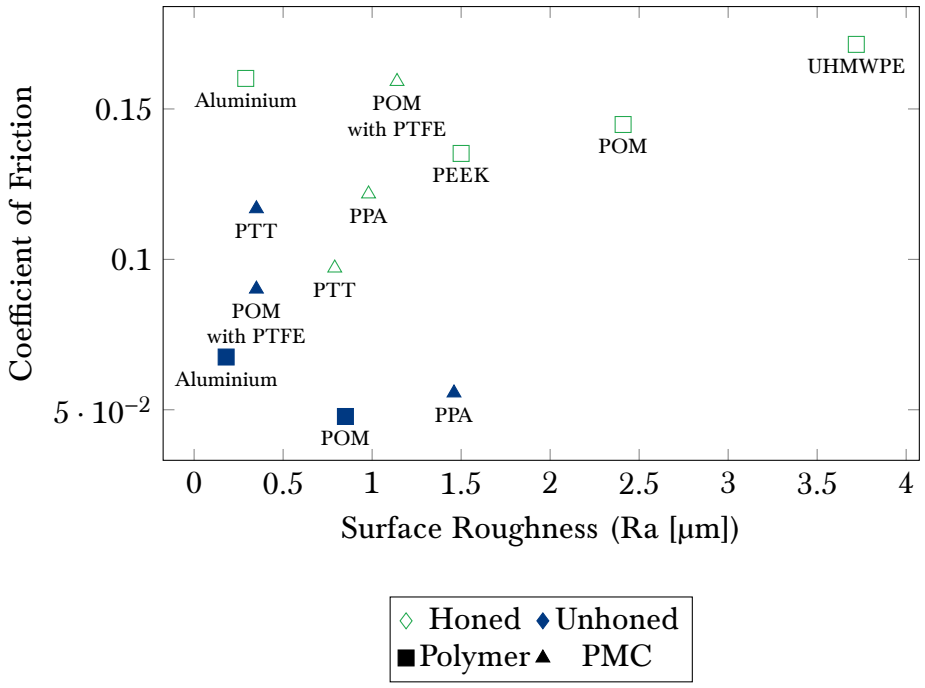

Figure 4.8: Comparison of Ra and coefficient of friction for each material honed and unhoned. Square symbols denote polymer materials and triangles polymer matrix composite (PMC). Hollow symbols are honed specimens and filled in unhoned.

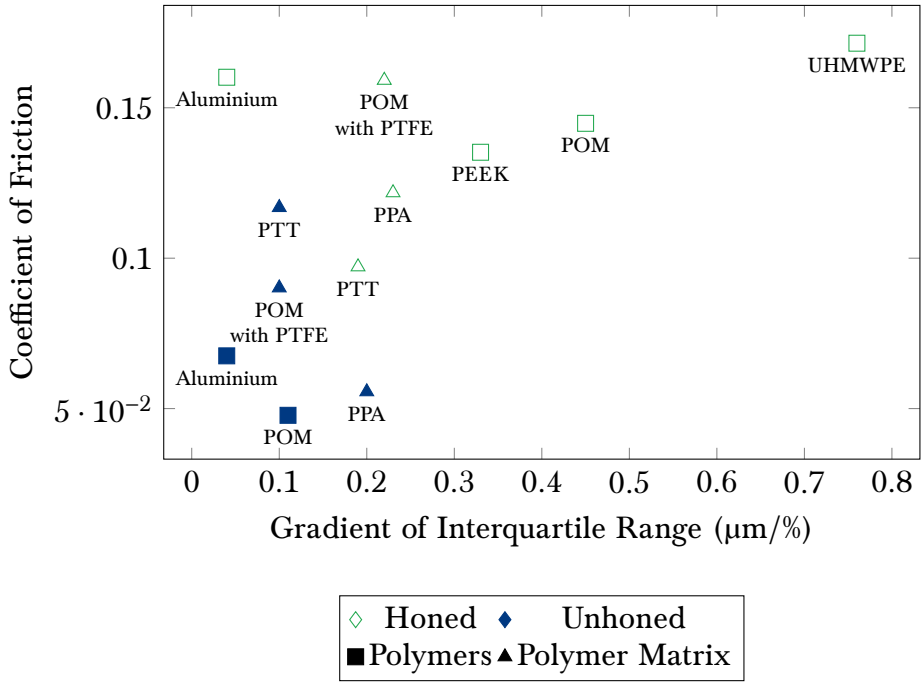

Figure 4.9: Comparison of the gradient of interquartile range and coefficient of friction for each material honed and unhoned. Square symbols denote polymer materials and triangles PMC. Hollow symbols are honed specimens and filled in unhoned.

sample had Si and S present. This was hypothesised to be due to either the degreasing solution used in the sample preparation or the lubricant used in the testing. Every sample was subject to both of the fluids and as they are present on all of the samples these peaks were discounted in the observation of a transfer of PTFE. The aluminium samples also had Na and Mg present, these are present in the aluminium alloy used in the testing. In general the materials that were honed appear to have a large spike in F and so it is inferred that there is a larger proportion by mass of PTFE present in the sample. This is an expected result as the grooves left by the process could be filled with PTFE and so a higher level of transfer occurred: leading to the potential of PTFE - PTFE contact a hugely beneficial material combination. Unhoned samples appear to have a lower proportion. The results for POM with PTFE cannot be used from these tests as the material is impregnated with PTFE. Therefore there is no way of determining if a transfer layer is present on these samples.

Unhoned POM does not display a transfer layer. This is also the material with the lowest median coefficient of friction out of all the materials at all temperatures and

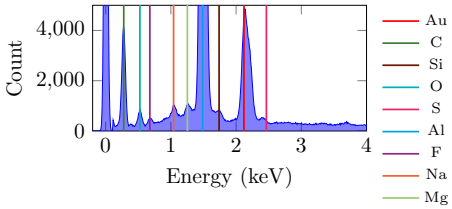

(a) Al - Honed

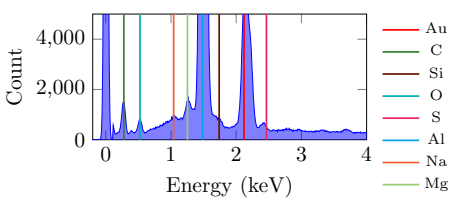

(b) Aluminium - Unhoned

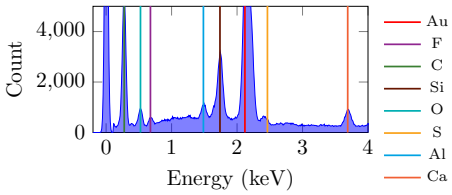

(c) PPA - Honed

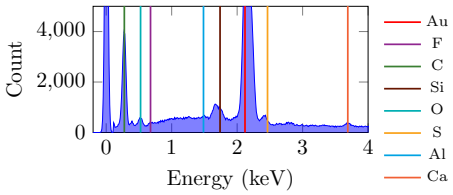

(d) PPA - Unhoned

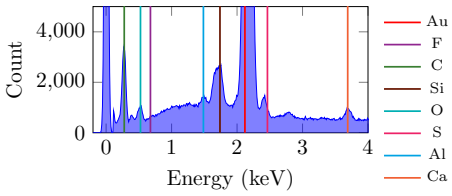

(e) PTT - Honed

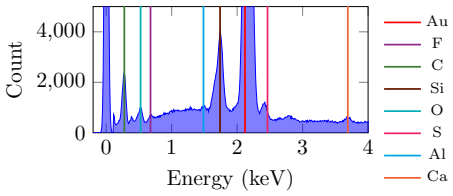

(f) PTT - Unhoned

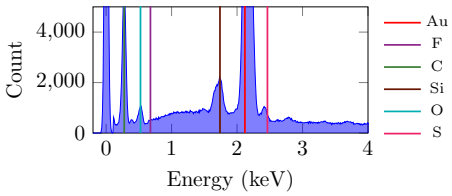

(g) PEEK - Honed

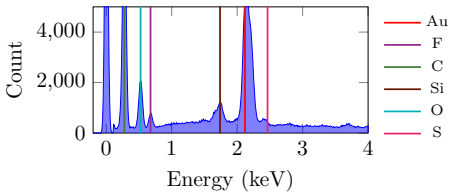

(h) POM - Honed

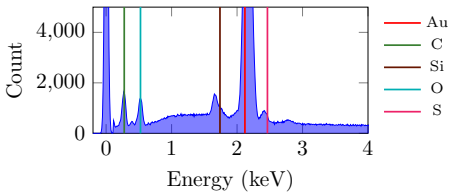

(i) POM - Unhoned

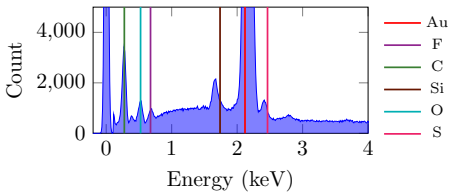

(j) POM w/ PTFE - Honed

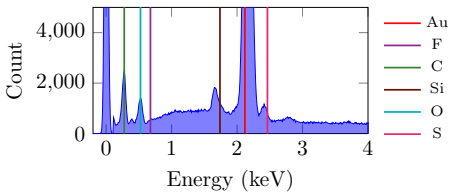

(k) POM w/ PTFE - Unhoned

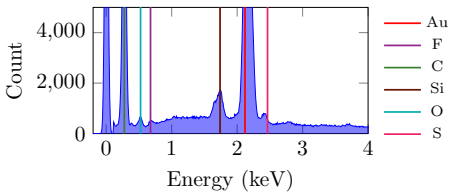

(l) UHMWPE - Honed

Figure 4.10: The EDS spectra of each of the tested materials with the principle elements indicated on at each peak.

Table 4.3: The presence of elements in the EDS analysis.

Material	Au	C	Si	O	S	F	Al	Ca	Na	Mg
Aluminium - Honed	✓	✓	✓	✓	✓	✓	✓	×	✓	✓
Aluminium - Unhoned	✓	✓	✓	✓	✓	×	✓	×	✓	✓
PPA - Honed	✓	✓	✓	✓	✓	✓	✓	✓	×	×
PPA - Unhoned	✓	✓	✓	✓	✓	✓	✓	✓	×	×
PTT - Honed	✓	✓	✓	✓	✓	✓	✓	✓	×	×
PTT - Unhoned	✓	✓	✓	✓	✓	✓	✓	✓	×	×
PEEK - Honed	✓	✓	✓	✓	✓	✓	×	×	×	×
POM - Honed	✓	✓	✓	✓	✓	✓	×	×	×	×
POM - Unhoned	✓	✓	✓	✓	✓	×	×	×	×	×
POM w/ PTFE - Honed	✓	✓	✓	✓	✓	✓	×	×	×	×
POM w/ PTFE - Unhoned	✓	✓	✓	✓	✓	✓	×	×	×	×
UHMWPE - Honed	✓	✓	✓	✓	✓	✓	×	×	×	×

preparations. The percentage overshoot and settling time was also low which suggests that the system was stable quickly. This further supports the notion of a low wear rate and a minimal transfer layer. This would suggest that the interaction with the seal would be promising: reducing wear and promoting sealing around the piston. That said a transfer layer is not necessarily a bad thing to occur: as long as the overall wear rate is low. A coating of PTFE on the aluminium samples could reduce friction and potentially lead to a lower wear rate (Dearn, Hoskins, Petrov, et al. 2013a).

Polished aluminium also did not display a transfer layer. This also coincided with a low wear rate and a low coefficient of friction. The reduced surface roughness of the aluminium potentially means that there is less asperity contact leading to less friction and adhesive wear.

Figure 4.11 shows the effect of the honing process on the polymers as examined under an SEM and annotated on each micrograph. Figure 4.11a displays significantly less glass fibre close to the surface compared to Figure 4.11b. Figure 4.11c also shows emerging glass. Figure 4.11f shows the effect of honing on the unreinforced samples. Whilst the

glass causes individual pockets of hard and soft materials the increased Young's Modulus creates a more consistent surface as less damage is done. These transitions between hard and soft surfaces cause stress concentrations in the bulk material, this effect appears to be exaggerated when the glass is exposed by the honing process showing more evidence of fatigue and wear. This can be seen in the scanning electron microscope (SEM) images; around the edges of the glass fibres fractures are present indicative of fatigue. The unhoned surface shown in Figure 4.11e appears to be a significantly more suitable surface to be a bearing surface. Despite this the surface roughness parameters in Table 4.2 do not suggest that unhoned POM will be better than unhoned PTT. The Abbott-Firestone curve for unhoned PTT has very steep ends which would suggest that there are gaps or crevices in the surface but there are not enough of these to effect the gradient of interquartile range. In comparison, the unhoned POM curve is very flat both within and outside the interquartile range, this also corresponds with low wear and friction.

As the upper specimen is extremely soft compared to the lower specimen the upper specimen will comply around the surface if there is a large gap or peak. This will be exaggerated if the lower specimen is made up of two materials of varying stiffnesses as they will comply differently and cause localised stress in the sample.

In this testing, the specimens that were tested have not previously been run against PTFE. It is expected that the phenomenon of overshoot is not limited to a traditional bedding in period that is only present once in the life of a component. Due to the viscoelastic properties of polymers when the components are not in contact the surfaces relax, this causes changes in the form and surface roughness of the material. In addition the contact area will reduce in temperature as they are not subject to frictional heating when the component is not in operation. Other factors that may change the tribological properties are the breakdown of the tribofilm and creep in the surface. When the component is operated again the surfaces will need to return to steady state, resulting in an overshoot. This overshoot is likely to be lower than that of the first operation of the component. In this testing polymer molecule orientation was not observed however this will also have an effect on the wear rate of the specimens (G. Zhang et al. 2010). This is

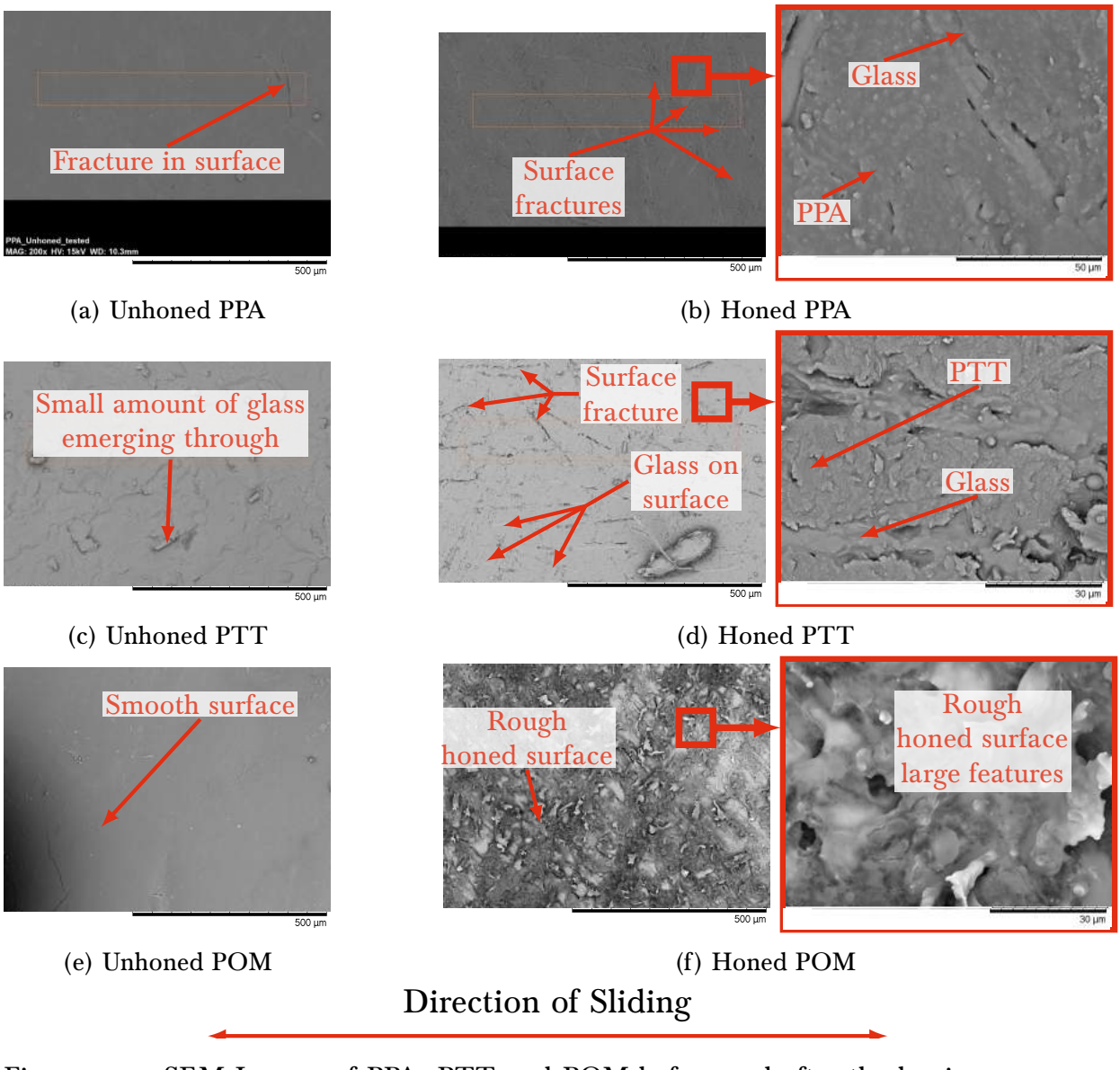

Figure 4.11: SEM Images of PPA, PTT and POM before and after the honing process. Features are marked on each micrograph.

likely to also relate to the magnitude and duration of the overshoot.

A summary of the testing is shown in Figure 4.12. This shows all data collected through this study, each thin blue line represents a different material with the two best materials and the original honed aluminum marked in bold. The area shaded in blue represents the area where the property is larger than the benchmark, the unshaded area represents the area where the property is lower than the benchmark. It can be seen that unhoned aluminium and POM outperform the benchmark.

In the context of the Dearman Engine this leads to the suggestion that in order to

reduce the largest contribution to parasitic losses either the cylinder liner should have a reduced surface roughness or be replaced with POM. There are implications on lubrication with reducing the surface roughness as there are less cavities in which to store lubricant in the bore potentially leading to areas of starvation. For this reason the replacement of the alumnium cylinder liner to one manufactured out of POM is more likely to result in desirable results.

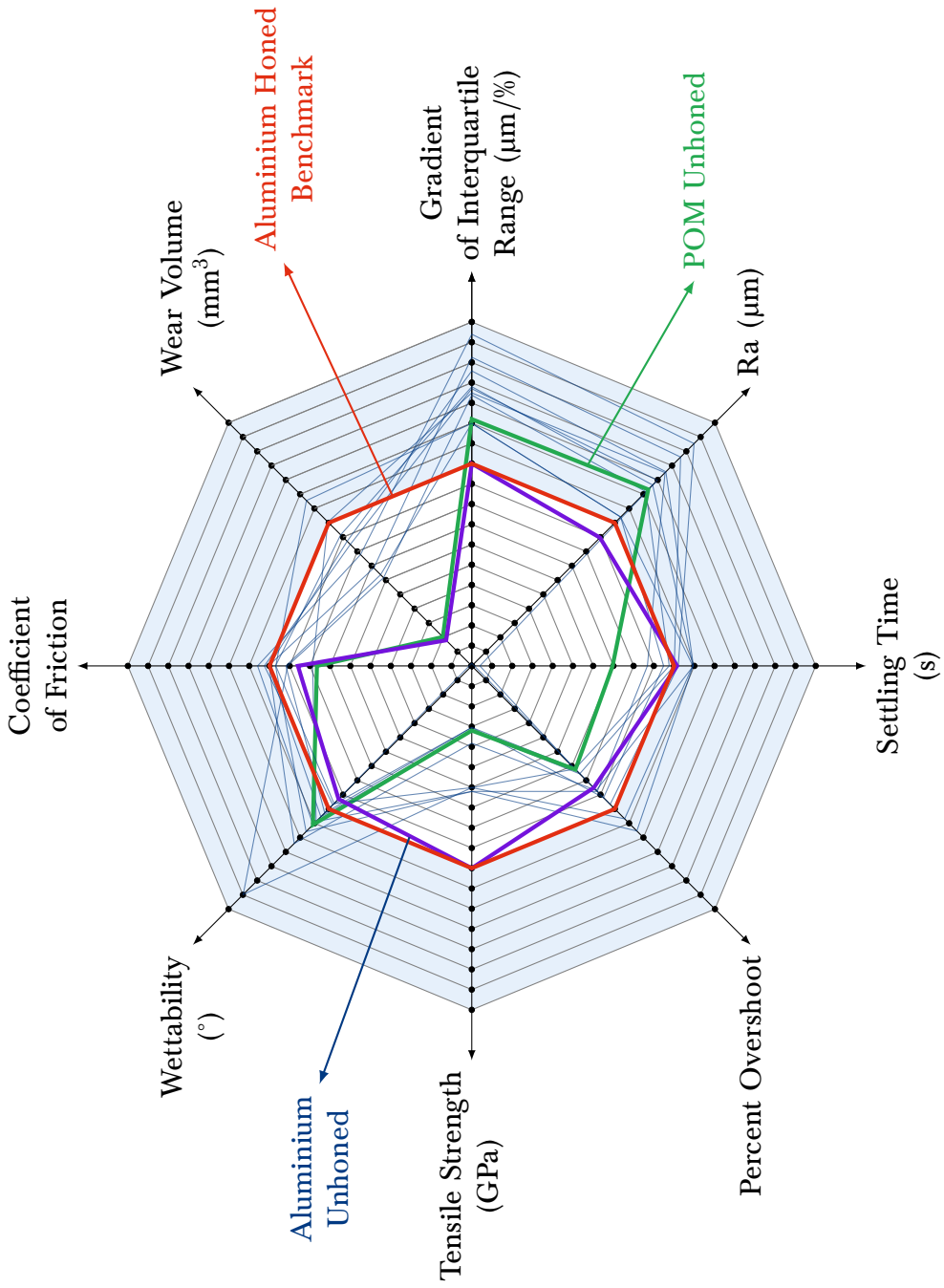

Figure 4.12: A graphical conclusion drawn from the results.

4.3 Laminated Piston Seal

Currently the piston seal employs a PMC however it was hypothesised that the materials do not need to be combined into a matrix in order to produce the same performance. The impact of PTFE-PEEK laminate (PTFE-PEEK-L) was analysed to determine if its tribological performance is better than that of a composite of the same PTFE-to-PEEK ratio.

Materials and Methods

Five different material combinations were tested: PEEK, PTFE, PTFE laminate (PTFE-L), 20% PTFE-PEEK-L and 20% PTFE-PEEK composite (PTFE-PEEK-C).

These were machined to the dimensions as shown in Figure 4.13. Where the materials have been bonded for testing, the surfaces were initially primed with a polyolefin primer (Loctite 770) and then bonded with ethyl-cyanoacrylate (Loctite 496). PTFE-PTFE-L was tested to investigate the effect of the bonding process on the sample. In order to ensure the samples were flat they were polished with an abrasive paper before they were run.

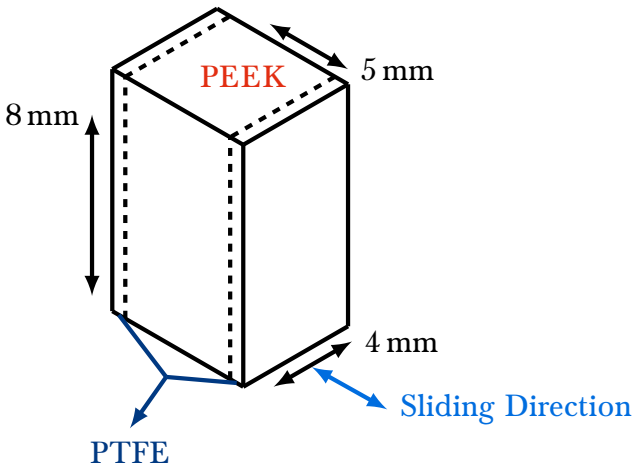

Figure 4.13: A schematic of the PTFE-PEEK-Laminated samples.

The samples were tested on the TE77 in order to measure the friction and to generate wear. A bespoke upper specimen holder was produced for the rig to hold the polymers in place. Table 4.4 shows the testing parameters used, they were selected to simulate the

worst tribological condition in the Dearman Engine, start up. The upper specimens were weighed pre-and post-test in order to quantify wear. The samples were then also examined under a SEM and analysed using EDS.

Table 4.4: The test parameters used in this research, representative of the Dearman Engine, using calculations presented in Chapter 3.

Test Frequency	4 Hz
Stroke Length	12 mm
Contact Pressure	33 MPa
Test Time	1 h
Sliding Distance	172.8 m
Temperature	Ambient
Lubricant	None
Upper Specimen	Polymer Composites/Laminates
Lower Specimen	Aluminium

Results and Discussion

Figure 4.14a shows the median coefficient of friction as measured by the TE77. It can be seen that the PEEK sample had a significantly higher coefficient of friction than the rest of the samples tested. The rest of the samples had a very similar coefficient of friction and a Mann-Whitney U test showed that there was no significant difference between the four datasets at a 95% confidence interval. This is an exciting result for two major reasons. One is that the pure PTFE sample and the PTFE-PTFE-L sample having no significant difference suggests that the process of bonding two polymers together has no effect on the coefficient of friction under these conditions. Another interesting result is that a 20% PTFE-PEEK mix produces a coefficient of friction statistically similar to a pure PTFE sample.

Figure 4.14b shows the logarithmic graviametric wear percentage after 1 h of testing. This graph shows why materials such as PTFE are commonly used as composites as the wear rate for PTFE is significantly higher than any other of the materials tested. As with

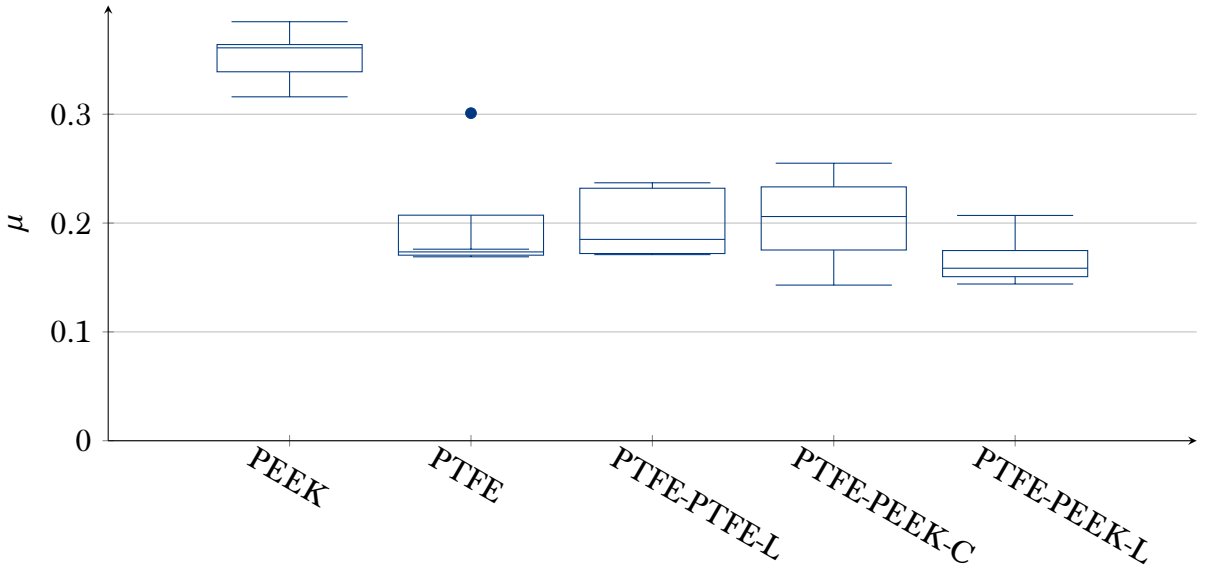

(a) Coefficient of Friction

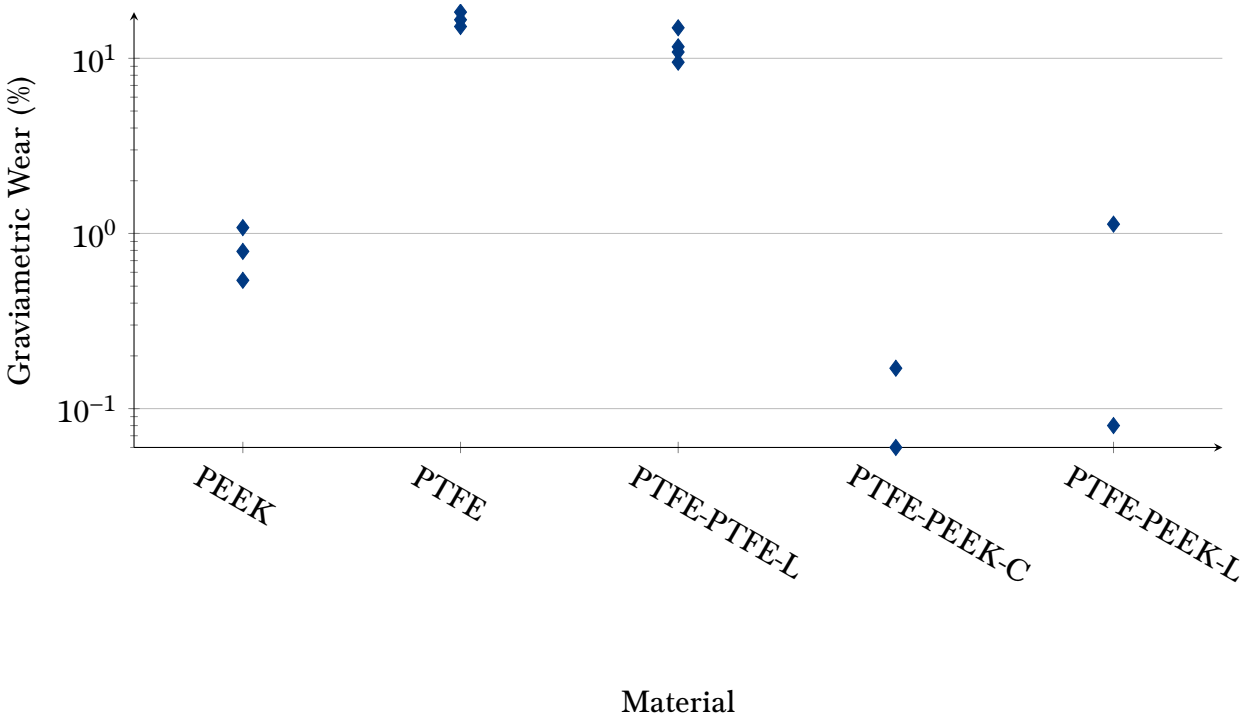

(b) Logarithmic gravimetric wear percentage

Figure 4.14: The friction and wear data for each material combination.

friction, it can be shown that bonding has no significant effect on the wear. This can be surmised due to the fact that the pure PTFE and bonded PTFE as well as the PTFE PEEK composite and laminate demonstrated no significant difference in their composite

vs laminate wear rates.

There is a wider spread of data in the PTFE-PEEK-L cases, this error may have been caused by inconsistencies in the material preparation. Samples not being perfectly flat or layers not being perfectly parallel may cause variation in the friction and wear. These errors are not of major concern as the purpose of the study is to investigate if the process will worsen the performance; which is not the case here.

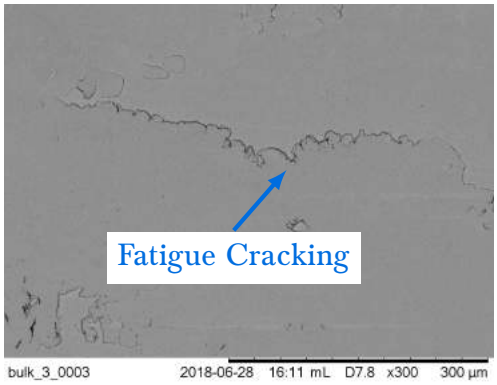

(a) PEEK

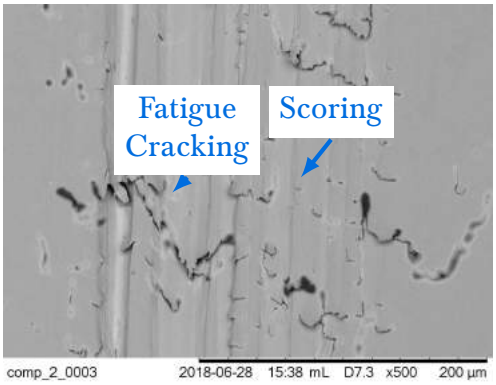

(b) PEEK-PTFE-C

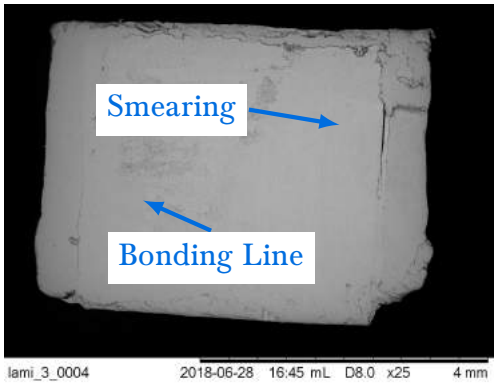

(c) PEEK-PTFE-L

Figure 4.15: SEM Images of the polymer upper samples. Subplots a) and b) were sliding vertically and c) was sliding horizontally.

As shown in Figure 4.15a, PEEK showed very little damage to the surface. There were areas of fatigue and areas of scoring. The scoring was due to the scratching of the stiffer aluminium into the PEEK surface. The areas of fatigue are small in comparison to other samples and after one hour did not appear to produce any pitting within the surface. The composite surface as shown in Figure 4.15b looks remarkably similar to the bulk of PEEK

again scoring and fatigue cracks are seen on the surface. There are areas in which the fatigue cracks have led to a small amount of pitting.

Figure 4.15c shows an overall view of a laminated upper specimen it can be seen that the surface has been subject to a large number of imperfections. Only one of the bonding lines can be seen clearly as on the other bonding line the PTFE is smeared across the top of the surface. Around the bonding surface, there does not appear to be an increase in the intensity or frequency of the fatigue cracks on the surface. The bonding line itself does not appear to be damaged and would suggest that the adhesive was suitable for the application and did not fail during testing. Again scoring can be seen on the surface parallel to the direction of reciprocation. It is difficult to separate damage produced during sample preparation and damage ascertained during testing, however, all of the samples were treated in the same manner and so it is possible to compare between samples.

Figure 4.16a shows a bar chart of the intensity of the F^- ions detected by the EDS on the lower aluminium specimens. The scan was taken in the middle of the wear track where the velocity was highest, shown in Figure 4.16b. It can be seen the pure PEEK and the PTFE-PEEK-C demonstrated either low or no intensity of F^- ions. This is expected for the PEEK as there is no material present that contains F^-. However comparing the PTFE-PEEK-C and PTFE-PEEK-L it can be seen that significantly more PTFE is transferred onto the aluminium from the laminate. This transfer layer has been shown by Dearn et al. to promote a low coefficient of friction and potentially a more stable contact (Dearn, Hoskins, Petrov, et al. 2013a). However, in both a transfer of PTFE occurs.

These results would suggest that the hypothesis that laminating makes no difference to the tribological properties of the sample compared to a composite is in part true. Whilst the friction and wear are not affected, the mechanism by which the PTFE spreads across the surface appears to be different for the laminate and composite PEEK and PTFE samples. This is difficult to examine but in a composite, PTFE is spread evenly assuming that the composite is homogeneous and therefore the PTFE is supplied to the contact from an evenly distributed source. In the laminate, PTFE is at either end of the sample and so is very easy to identify where the PTFE has come from. As it has been shown that PTFE

has a higher wear rate than the PEEK this would suggest that the edges of a laminated sample would wear quicker than the centre. One solution to this is to reduce the contact pressure incident on the PTFE by reducing the thickness of the laminates and increasing number of laminated layers.

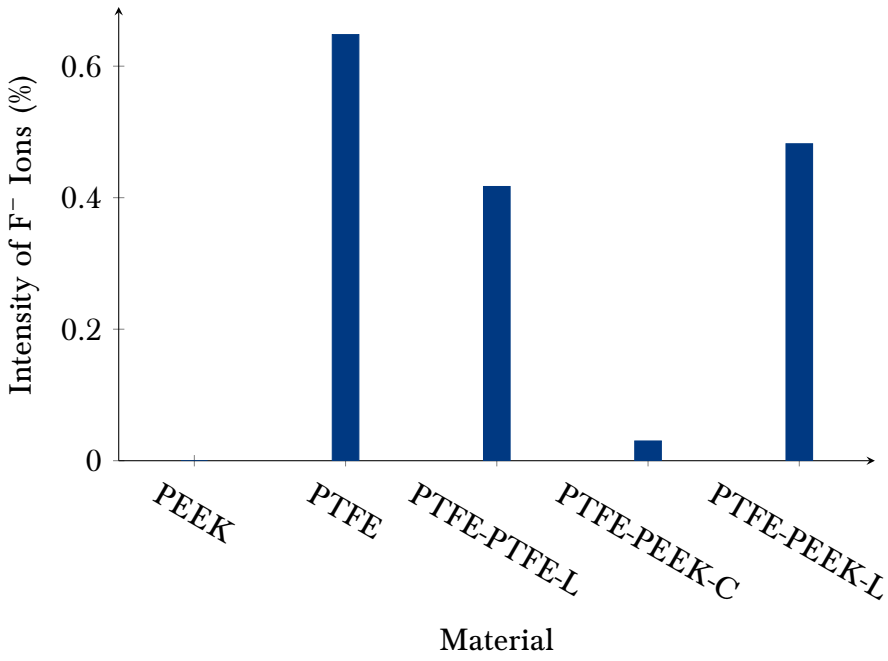

(a) A bar chart of the intensity of F^- ions as detected by the EDS for each material.

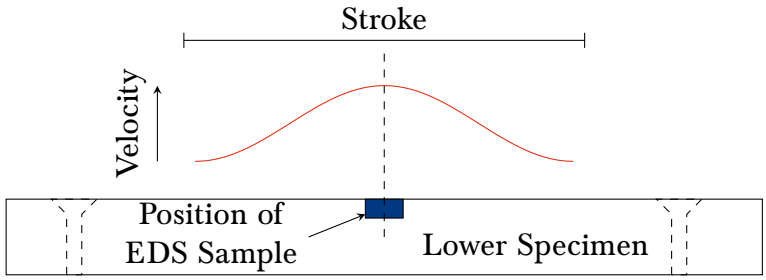

(b) A schematic of the position of the EDS analysis.

Figure 4.16: The EDS analysis of the aluminium samples.

4.4 Conclusions

Cylinder Liner

Six polymers and PMCs were tested against aluminium as a benchmark material on a tribometer with a PTFE counter surface and using other analytical techniques to determine the tribological mechanism between seal and liner at sub-ambient temperatures. This was undertaken to simulate the conditions in the cylinder of the Dearman Engine, a zero emissions cryogenic engine.

The following conclusions can be drawn:

1. A higher surface roughness prior to testing was linked to an increased coefficient of friction.

2. Temperature had a significant effect on coefficient of friction and the effects are dependant on the reinforcement of the polymer. The unreinforced materials showed a small variation with temperature but the reinforced materials showed an increase in friction with a reduction in temperature

3. A new concept of the percent overshoot of the coefficient of friction (defined as the percentage of the maximum coefficient of friction to the median coefficient of friction from each test) was introduced. The frictional overshoot correlated with wear such that higher overshoot led to a higher wear rate due to an increased flash temperature.

4. In general the materials with a higher coefficient of friction had a higher wear rate.

5. For a compliant material, reinforcement was shown not to be ideal increasing wear rate. This was the result of differing stiffnesses in the matrix causing higher levels of wear due to stress raisers in the soft PTFE upper specimen.

6. Wettability did not have a large effect on the process as most of the materials were highly oleophillic.

7. Surface roughness and the gradient of the inter quartile range of the Abbott-Firestone curve was linked with the coefficient of friction. A higher surface roughness and a less consistent profile led to an increased coefficient of friction.

8. Evidence of a transfer layer was detected by analysing the Abbott-Firestone curves and using EDS to detect F^- ions. Unhoned POM and polished Al displayed no transfer layer. This also coincided with a low overshoot and coefficient of friction.

The comparisons led to the conclusion that an unhoned POM cylinder liner would perform better under the conditions tested than the current aluminium honed surface.

Laminated Piston Seal

Five material combinations were studied in order to ascertain whether combining the polymers in a laminated material would produce similar tribological properties to composite polymers.

The following conclusions can be drawn:

1. A 20% PEEK PTFE composite under the conditions tested demonstrated a wear resistance consistent with PEEK and a coefficient of friction consistent with PTFE.

2. Bonding PTFE together changes neither the friction or wear properties of the material.

3. A 20% PTFE PEEK laminate produced statistically similar results to the equivalent composite. A comparison of the surfaces demonstrated that smearing of the PTFE across the surface occurred in the laminate material. This is important as a PTFE layer will reduce the coefficient of friction. Similar levels of fatigue cracking and scoring occurred between the composite and the laminate.

4. The PTFE encompassed within the laminate may have worn at a higher rate than the PEEK due to it being located on the leading edges of the samples. However,

increasing the number of laminating layers would reduce the contact pressure in these areas.

5. The presence of a stiff component and a lubricious component within a specimen is more significant than whether the PTFE is evenly distributed across the surface or not; meaning it is possible to use lamination as an alternative to composite materials.

This study has explored the replacement of materials within the Dearman Engine utilising the beneficial properties of polymers and their composites. A new material has been suggested for the cylinder liner along with a new methodology of creating composite materials at a significantly lower cost then a traditional PMC.

Chapter 5

Biomimetic Lubrication

5.1 Introduction

The previous chapter discussed the potential improvements to the Dearman Engine that a material replacement my lead to. An alternative to the material replacement and redesign of the engine is to address the lubricant. The aim in lubricant replacement within the Dearman Engine is to produce a 'single fluid engine'. This is an engine where the lubricant and heat exchange fluid (HEF) are the same fluid. A combined fluid will have a reduced need for auxiliary components. Reducing the auxiliary component mass of the TRU will increase the fuel efficiency of the prime mover.

The following chapter presents an analysis of two potential sources of a combined lubricant and heat exchange fluid: Pectin and bovine serum albumin (BSA). These were selected as they are water soluble and had potential to increase the lubricity of water. This was motivated by the original HEF used by Dearman — water.

5.2 Materials and Methods

Lubricant Preparation

Four lubricants were tested, two based on BSA and two on pectin, in two concentrations: $1\,\mathrm{mg\,ml^{-1}}$ and $5\,\mathrm{mg\,ml^{-1}}$. These concentrations were selected to be identical to previous work into aqueous solutions of BSA analysing the performance of these lubricants under boundary lubrication with unidirectional sliding in order to compare the results (Ahlroos et al. 2011). The BSA (Bovine serum albumin solution, 22% in saline, contains azide, aseptically filled, Sigma Aldrich, Darmstadt, Germany) and pectin (Pectin from citrus peel, Sigma Aldrich, Darmstadt, Germany) were mixed with deionised water in sterile tubes to the desired concentrations. The pectin solutions were mixed at 70 °C for 24 h. The solutions were agitated thoroughly both after initial mixing and before each test in order to ensure homogeneity. The samples were then frozen in the tubes, containing 5 tests worth of lubricant, until 24 h before each test.

Tribological Experimental Configuration

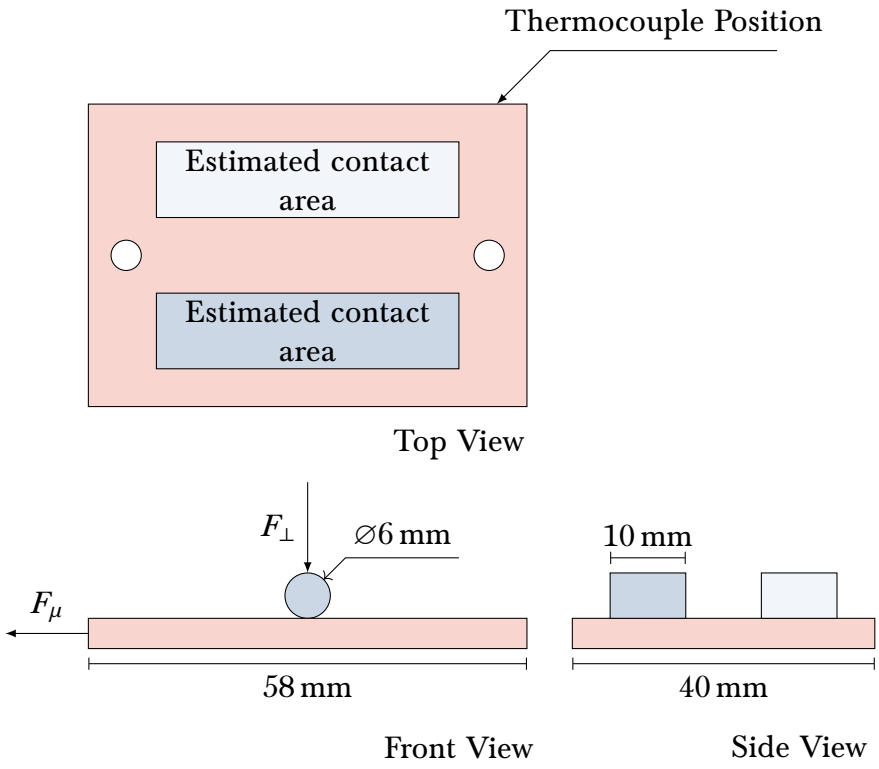

Figure 5.1: The tribological experimental configuration. Showing the location of the temperature measurement, the size and location of the wear tracks in the top view and the size of the upper specimens in the front and side views.

Figure 5.1 shows the experimental configuration used to generate friction and wear, on a TE77 high speed reciprocating rig (Phoenix Tribology, Hants, UK). The cylinder (shown in blue) is loaded with the desired force and reciprocated at the required frequency against a plate (shown in green). Metals were used to negate any viscoelastic effects of the supporting surfaces in the examination of the lubricants. The cylinder was manufactured from hardened AISI 52100 chrome steel. The plates were manufactured from SS 440C stainless steel. Two tests were performed on each lower plate with the wear tracks at least 10 mm apart. The temperature of the plate was measured using a thermocouple positioned as annotated in Figure 5.1.

Table 5.1 shows the parameters used during the testing. The force, frequency, lubricant concentration and type were all varied at two levels resulting in 16 different experiments with 5 repeats of each. The contact pressures were selected as the lowest pressure possible

Table 5.1: The parameters used in testing.

Parameter	Value		
Stroke Length (mm)		21.5	
Test Time (h)		1	
Testing Temperature (°C)		25	
Volume of Lubricant (ml)		8	
Force (N)	5	/	310
Equivalent Contact Pressure (MPa)	76.4	/	601.2
Frequency (Hz)	5	/	10
Lubricant Concentration ($mg\,ml^{-1}$)	1	/	5
Lubricant Type	Pectin	/	BSA

from the TE77 and to simulate a mechanical contact such as a cam and follower in an internal combustion engine (Priest and Taylor 2000).

In order to control the statistical independence of the data the order of the experiments was randomised with regard to the force and frequency. The BSA tests were run separately from the pectin tests to reduce the risk of cross contamination between tests. Every five tests the concentration of the lubricant was changed. This meant that the lubricant could be kept frozen until it was needed but still allowing for the tests to be statistically independent. Each test performed on every lower specimen was performed using the same concentration so there was no cross contamination on the sample.

5.3 Results and Discussion

Table 5.2 shows the median coefficient of friction, maximum temperature, median contact potential and median frictional energy dissipated for each lubricant and applied force as listed in Table 5.1. The reported uncertainty in Table 5.2 is one standard deviation of the mean. The frictional standard deviations shown in Table 5.1 are all at least two orders of magnitude smaller than the mean which represents a clear consistency in the testing

procedure and lubricant performance. The median coefficient of friction was used as it best describes the steady state value of a test and discounts the bedding in period.

Each test performed at 5 N has a higher coefficient of friction than the test performed at 310 N, although the difference is reduced in the pectin based lubricants. This would suggest that the coefficient of friction of the pectin solutions are not as dependent as BSA on the applied load at the observed conditions.

Previous literature has shown that the concentration of BSA in deionised water does not impact the resulting coefficient of friction in a unidirectional sliding test at low velocity as the temperatures involved do not change the chemical structure of the BSA. This testing was conducted at a contact pressure of 585 MPa, sliding velocity of $0.100\,\mathrm{m\,s^{-1}}$ and at 22 °C and resulted in a coefficient of friction of ≈ 0.3 (Ahlroos et al. 2011). The results from this study also suggest that the friction of BSA is not affected by concentration in the range of $1\,\mathrm{mg_{BSA}/ml_{H20}}$ to $5\,\mathrm{mg_{BSA}/ml_{H20}}$. However, in this range it is evident that a higher concentration of pectin results in a lower coefficient of friction at both contact pressures simulated.

Table 5.2: A statistical summary of the tribological testing showing median friction - $\widetilde{\mu}$, maximum temperature - $\hat{T}$ (°C), median contact potential - $\widetilde{V_{CP}}$ (mV) and median frictional energy dissipated - $\widetilde{E_{\mu}}$ (J). Each value quoted is the mean of each statistic from individual tests with an uncertainty of one standard deviation.

Lubricant	Force (N)	$\widetilde{\mu}$	$\hat{T}$	$\widetilde{V_{CP}}$	$\widetilde{E_{\mu}}$
1mgmlBSA	5	0.51 ±0.05	27.0 ±1.1	2.3 ±0.1	89.0 ±8.1
	310	0.17 ±0.03	39.8 ±8.3	2.0 ±0.1	2,280 ±370
5mgmlBSA	5	0.50 ±0.05	26.4 ±0.7	2.2 ±0.1	90.6 ±11.4
	310	0.15 ±0.01	37.5 ±3.6	2.0 ±0.2	1,920 ±160
1mgmlPectin	5	0.52 ±0.06	25.9 ±0.3	1.8 ±0.2	101.1 ±10.1
	310	0.29 ±0.04	32.5 ±3.4	1.5 ±0.2	3,810 ±460
5mgmlPectin	5	0.37 ±0.03	25.7 ±0.5	1.7 ±0.2	69.4 ±2.0
	310	0.18 ±0.01	28.8 ±2.2	1.6 ±0.2	2,370 ±170

The lowest observed coefficient of friction at 5 N was the 5 mg ml^{-1} pectin, at 310 N the 5 mg ml^{-1} BSA. At 5 N the distinction between lubricants and concentrations is more clear. In terms of coefficient of friction it is clear that the optimum lubricant tested is the 5 mg ml^{-1} pectin.

There is no distinction in the frictional data between the tests conducted at 5 Hz and those at 10 Hz as denoted by the magnitude of the standard deviation. This implies that the lubricants are quasi-newtonian and do not undergo any major chemical changes due to a higher shear rate within the lubricants (Mang 2007).

Table 5.2 also reports the maximum bulk temperature reached by the plate specimen in the top corner as annotated in Figure 5.1. The 5 N tests have very similar distributions in temperature and average values of just above the testing temperature of 25 °C. The BSA tests conducted at a higher contact pressure result in a higher temperature at the thermocouple.

5 mg ml^{-1} pectin showed no major difference in the average temperature at each condition. This would suggest that the lubricant was not as effective at removing the heat from the contact zone. As discussed in section 2.4, the chemistry of pectin is not effected by temperature.

As BSA is a protein it suffers from denaturing at a specific temperature, this changes the tertiary structure of the protein and impacts the conductivity, making the thermal properties of the solutions highly temperature and concentration dependant. BSA denaturing occurs around 50 °C to 70 °C and increases the thermal conductivity (Kyoo Park et al. 2011). Denaturing of a protein is permanent and so returning the solution to a lower temperature will also benefit from this structural change, increasing the ability of the solution to conduct temperature away from the contact zone, reducing thermal and tribological damage to the surfaces. Higher volumes of lubricant will improve the ability to conduct heat away from the contact area, reducing this effect however denaturing of the protein will not have a negative effect on the tribology of the contact.

Median contact potential ($\widetilde{V_{CP}}$) values are representative of the film thickness between the two contacting surfaces. The contact potential of each lubricant cannot be compared

directly as the dielectric constant of each fluid will change with concentration and biological additive. It can be seen that the pectin based lubricants vary less in their median values as indicated by the reduced standard deviation. Whilst it is not possible to compare between each lubricant the major overriding conclusion from analysing this data is that the film thickness of the BSA is less consistent under testing. However both fluids produced a supporting film critical to the function of a lubricant.

As is expected less frictional energy is dissipated during the lower contact pressure experiments. The disparity between the lubricant concentrations is more distinct in the pectin tests with a reduced frictional energy at $5\,\mathrm{mg\,ml^{-1}}$. The BSA lubricant tribological properties are less influenced by the concentration than pectin, this is reflected in both the coefficient of friction and the frictional energy. This may be due to differences in solubility between BSA and pectin or the hydrogen bonding present between water and the biological additive modifying the surface tension, this is discussed later in the chapter.

A major problem encountered in the tribological testing was evaporation of the lubricant due to heating of samples. This was evidenced by a reduced volume of lubricant at the end of the test and in some cases the liquid had completely been removed leaving only a residue on the surface. From qualitative observation pectin was less susceptible to this although no quantative analysis of the process was undertaken. In this testing only a small amount of lubricant was used in each test. In testing with more lubricant this evaporation will be reduced as there will be more fluid able to conduct and convect heat away from the contact. It is also pertinent that pectin's chemistry is not as sensitive to temperature, as discussed in Chapter 2.

Table 5.3 shows the mean and standard deviation of the contact angle (θ) measured every 5 s for 650 s using the method as set out in Chapter 3. The standard deviations are an order of magnitude smaller than the means demonstrating a stability in the measurement and a small amount of spreading also shown by a large contact angle. In both lubricants the increased concentration increases the contact angle.

Table 5.3: The mean and standard deviation of the contact angle and surface tension for each lubricant measured over 650 s at a sample frequency of 0.2 Hz and the measured surface tension aver a range of bubble times. $\gamma_L \cos\theta$ an indicator of interfacial energy is also presented, as contact angle and surface tension are not independent the standard deviation of the result cannot be estimated.

Lubricant	θ°	γ_L	$\gamma_L \cos\theta$
1mgmlBSA	60.4 ±5.3	73.1 ±2.1	36.2
5mgmlBSA	62.6 ±3.2	72.0 ±0.9	33.1
1mgmlPectin	62.2 ±3.2	71.8 ±0.6	33.4
5mgmlPectin	66.6 ±4.4	73.9 ±1.6	29.4

The surface tension does not follow the same trend. Increasing the concentration of BSA reduces the tension where as with pectin it increases. The key parameter in the table is the $\gamma_L \cos(\theta)$, a lower value will result in a higher film thickness and a lower friction. This comparison only describes the lubricants ability to form a film and so is only relevant at higher velocities. Therefore deviations in the $\gamma_L \cos(\theta)$ from the trends described by Table 5.2 describe the ability of the biological compounds to form a boundary lubricant.

The higher concentrations reduce $\gamma_L \cos(\theta)$ and therefore are more likely to generate a thicker lubricant film. Pectin has a lower $\gamma_L \cos(\theta)$ than BSA at both concentrations. Combined with the results presented in Table 5.2 especially when comparing the median coefficient of friction at 310 N the concentration of pectin has a larger impact on the friction and $\gamma_L \cos(\theta)$ but also results in a thicker lubricant film and a lower coefficient of friction. The variation of $\gamma_L \cos(\theta)$ with respect to concentration is lower in BSA and may explain why the coefficient of friction was less dependant on the concentration of BSA in the lubricant.

The testing has compared the friction, potential to produce wear, film thickness and ability to form a film. In each of these comparisons at the conditions tested, BSA produced results less dependent on concentration of BSA in water, however the pectin $5\,\mathrm{mg\,ml^{-1}}$ consistently produced a better tribological performance. This solution resulted in a lower coefficient of friction, frictional energy dissipation (indicative of lower surface damage)

and demonstrated an ability to operate as a boundary lubricant as well as being capable of forming a film at higher contact pressures and velocities. This was shown through both tribological testing and through the surface tension and contact angle measurements.

5.4 Conclusions

Two potential aqueous biomimetic lubricants have been analysed assessing the impact of concentration, contact pressure and sliding velocity on their tribological performance. The conditions were designed to assess the capability of the lubricants to perform in a mechanical and industrial capacity. This testing has highlighted the potential of this type of lubricant. Although more investigation and understanding of these additives is required before any implementation of pectin or BSA based lubricants; these results demonstrate that they may be possible replacements for hydrocarbon based lubricants. A summary of the main results is as follows:

1. Both lubricants tested, BSA and pectin, supported the surfaces resulting in a tribologically beneficial contact

2. The concentration of pectin has significantly more effect on the tribological properties than that of BSA

3. No major effect of velocity on the lubricant friction or film thickness was observed suggesting that there are no major viscoelastic effects in either lubricant

4. BSA demonstrated the lowest coefficient of friction under high loads; 0.17 and 0.15 at $1\,\mathrm{mg\,ml^{-1}}$ and $5\,\mathrm{mg\,ml^{-1}}$ respectively and less sensitivity to changes in concentration in all factors

5. The most promising lubricant tested is $5\,\mathrm{mg\,ml^{-1}}$ Pectin. Demonstrating a low coefficient of friction at both loads $\left(\mu\big|_{F_\perp=5\mathrm{N}} = 0.37;\ \mu\big|_{F_\perp=310\mathrm{N}} = 0.18\right)$, lower temperature rise, lower indicated wear through frictional energy dissipation and a lower $\gamma_L \cos(\theta)$

6. This investigation highlighted that these lubricants may be susceptible to evaporation, a feature of them being aqueous, however utilisation in a closed system with higher volumes of lubricant would likely result in this effect being reduced

This chapter has shown that biomimetic lubricants are able to support a mechanical contact effectively. They are ecologically sustainable and able to withstand a wide variety of contact pressures and velocities. As the lubricants are aqueous they are also potential alternatives to the HEF although more work is required in this area. A biomimetic lubricant/HEF combination would allow for the removal of the oil pump within the TRU and reduce the overall mass of the system. This is a hugely exciting area of investigation and has the potential to lead to the replacement of hydrocarbon based lubricants in other applications as well as the Dearman Engine.

Chapter 6

Velocity Dependant Friction

6.1 Introduction

In the examination of novel engines there is a large focus on data collection during durability testing. Using the Nyquist-Shannon sampling principle, the traditional methodology of data analysis ignores effects of visco-elasticity and other high frequency phenomena. The following chapter applies this theory to an analysis of the valve guides within the Dearman Engine.

The valve guides were lubricated via oil pumped into the cylinder head. The aim was to examine if the lubrication was necessary and if it was possible to remove the oil pump entirely: potentially providing a significant weight reduction in the overall system supporting the move to a single fluid engine discussed in the previous chapter.

6.2 Materials and Methods

Methods

The experimental conditions used were selected to approximate the Dearman Engine valve train on the TE77. The upper sample reciprocation frequency was 13.3 Hz (800 rpm), stroke length was 25 mm (amplitude of 12.5 mm). The 7 N normal force was equal to a contact pressure of 61.9 kPa as calculated in Chapter 3. The test duration was one hour. The tests were run at room temperature, in Chapter 4 it was shown that the tribological properties of the PEEK and POM are not significantly influenced by temperature in the range of the operating conditions of the Dearman Engine.

Lubrication

The tests were lubricated with HEF. A syringe pump (KDScientific Legato 110, Holliston, MA, USA) delivered fluid directly to the contacts at a rate of $0.2\,\mathrm{ml\,min^{-1}}$ via a tube that was attached to the moving carriage of the TE77. Homogeneity was ensured by agitating the mixture vigorously immediately before testing. During the testing the velocity and

agitation of the samples was assumed to keep the fluids from separating. Tests were also run dry for comparison.

Materials

POM and PEEK were used to manufacture dynamic upper specimens, both are engineering polymers that have been previously used and analysed for machine element design (Mark 2009; Dearn, Hoskins, Petrov, et al. 2013b; Yeo and Polycarpou 2012; Friedrich et al. 2005; Nunez and Polycarpou 2015). The static lower specimen was made from titanium; benefiting from corrosion resistance and high strength to weight ratio (K. Wang 1996). Currently the valve stems of the Dearman Engine are manufactured from titanium.

Material Preparation

After being processed into TE77 lower samples, the titanium Ti6A4V samples were ground with a Jones-Shipman 540AP surface grinder (Leicester, UK) with PBR Abrasives $24C60J5V$ silicon carbide wheel (Wolverhampton, UK). Following this, grades P140, 600 and 1200 silicon carbide abrasive papers were used to polish the surfaces to a target roughness of Ra 0.1 µm to 0.3 µm was reached, measured using a Mitutoyo Surftest SJ-310 (Coventry, UK).

Following machining, the roughness of the contact surfaces was measured. The surfaces were then refined using silicon carbide abrasive paper until the target roughness of Ra 0.3 ± 0.1 µm.

Before testing, all samples were rinsed in a dilute degreasing solution (Loctite SF0 7840). They were then placed in an ultrasonic bath with distilled water before being rinsed in ethanol to wash the abrasives off the surface before testing. Samples were left exposed to evaporate the ethanol before the experiments.

6.3 Results and Discussion

Friction

Steady State Friction

Table 6.1 lists the median coefficient of friction ($\widetilde{\mu}$) from unlubricated and lubricated tests. As expected, the coefficient of friction was significantly higher for unlubricated tests. Also, the PEEK demonstrated higher friction than the POM for the unlubricated tests which is consistent with the results shown in Chapter 4.

There was less of a distinction between the materials in the lubricated tests. In these tests, the fluid is likely to remove wear debris and create a film separating the surfaces reducing reliance on the stiffness of the surface as well as reducing the contact temperature. This observation implies that in the case that the materials are entirely in contact, the friction is dependent on the material stiffness.

Table 6.1: A summary of the steady state coefficients of friction (median) for each test showing the mean and standard deviation of the distribution of medians.

$\widetilde{\mu}$	**POM**	**PEEK**
Unlubricated	0.36 ±0.07	0.55 ±0.09
Lubricated	0.10 ±0.02	0.10 ±0.03

Friction within a stroke

Figure 6.1 shows the friction against velocity for each test with the mean trace overlaid in bold. The black line is steady-state friction. The plots demonstrate the reliance of tangential loading on the sliding speed during the unlubricated testing, showing the transition from static to dynamic frictional phases. In the unlubricated tests, there was a peak as the samples overcame the static coefficient of friction at each stationary point of inflexion during each stroke. After this point, the friction was then almost constant as the velocity increased.

The lubricated tests did not display a peak in friction at lower velocities, which would suggest that the lubricant layer does not breakdown as the direction of velocity changes; avoiding significant levels of asperity contact at the limits of the stroke. This behaviour may be because even though the samples are theoretically stationary, the lubricant is still moving relative to the surfaces due to inertia within the fluid or viscoelastic effects in the polymers.

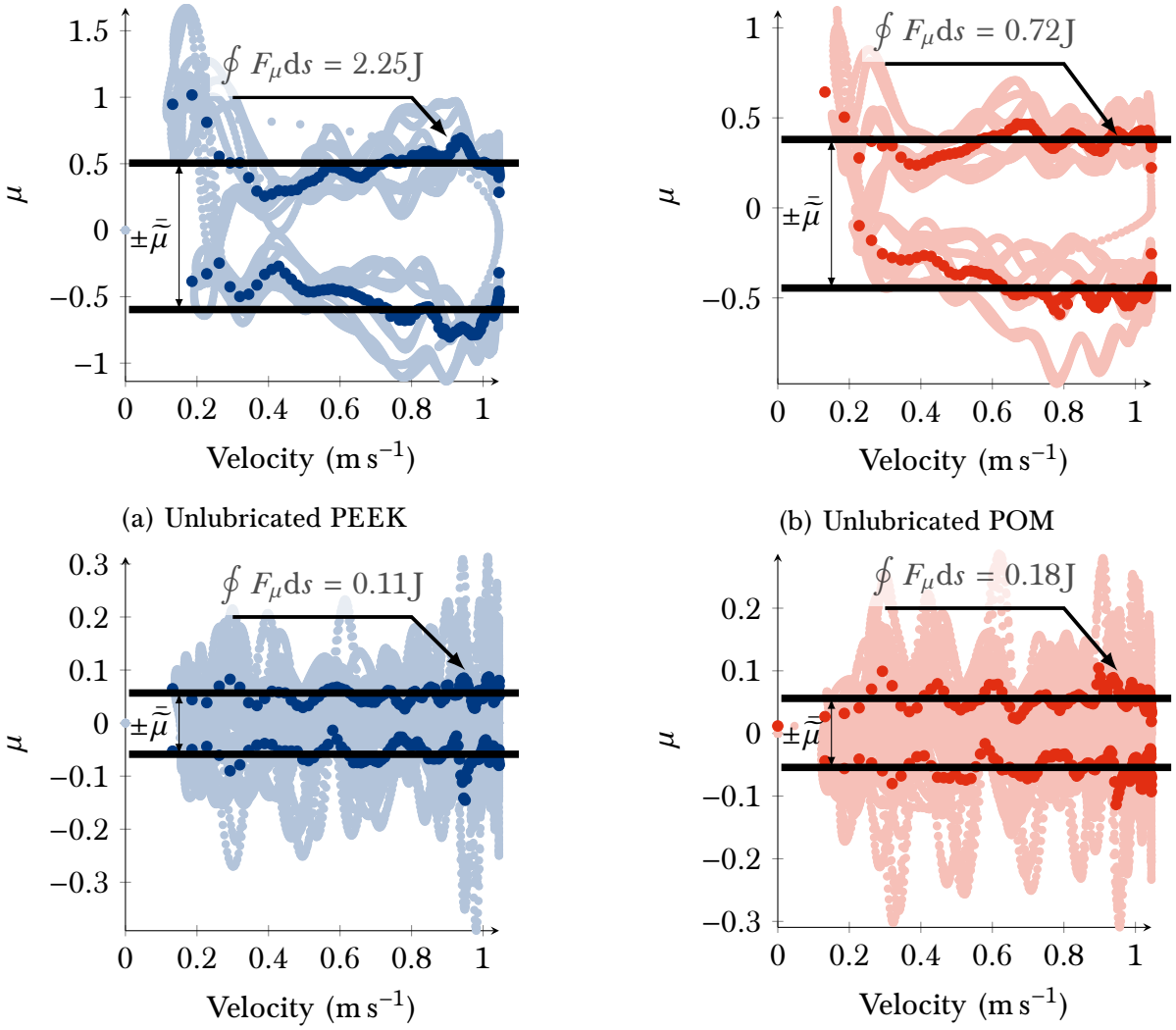

(a) Unlubricated PEEK

(b) Unlubricated POM

(c) Lubricated PEEK

(d) Lubricated POM

Figure 6.1: Friction velocity plots showing steady-state friction and energy dispersed during 65 cycles recorded at 30 min into each test. The friction during each cycle is plotted in for each material. In the darker colour the mean of all these cycles is plotted. The plots are also annotated with the steady state friction and the frictional energy dissipated as calculated by the circular integral of the mean cycle.

Frictional Energy Dissipated

Figure 6.1 also shows the frictional energy dissipated calculated from the mean stroke for each test. The unlubricated PEEK tests have a significantly higher frictional energy. A higher level of frictional energy was dissipated in the unlubricated tests. The unlubricated POM released a frictional energy about a third of that as calculated for the unlubricated PEEK. This trend is due in part due to the PEEK having a higher median coefficient of friction for each test and also higher surface energy (given in Table 3.1).

In this case, PEEK requires more energy to generate debris from the surface and so may lead to less wear; although in this application wear is not a major concern as the contact pressure is so low. Friction is significantly more important in order to reduce parasitic losses within a valvetrain. A penalty of this reduced damage is that friction is higher as a result of increased energy required to fracture inter-molecular bonds on the contact surface. Peaks are present at the start of each stroke during the PEEK tests, and these are proportionally lower during the POM tests. These factors combine to produce lower energy dissipated per stroke for POM.

The lubricated tests demonstrated similar trends, independent of the material used in testing. The lubricant removed heat and debris away from the contact zone, lowering the total amount of energy dissipated as friction, meaning that the surface free energy, an indicator of adhesive wear, was much less of a driving factor, compared to the unlubricated tests.

Because the frictional energy dissipation is calculated from HSD it describes the frictional behaviour of the system better than the coefficient of friction as calculated in the LSD. Whilst energy dissipation is directly proportional to friction, the LSD does not sample at a high enough rate to encapsulate the static-dynamic transitions and viscoelastic variations in material properties.

Surface Analysis

Neither of the polymers tested contained titanium and so EDS could be used to look for transfer of titanium onto the polymer surface. The inverse is also true, in that the titanium does not contain carbon within the alloy and so can be used to identify transfer layers of the polymers onto the counter surface. It is prudent to be cautious of using carbon as it is present in anything organic and so even handling of the specimens can lead to a false reading.

All of the polymer surfaces showed score marks across the surface, an example is shown in Figure 6.2. These grooves were in the order of 10 µm to 20 µm wide. This is consistent with the size of the abrasive on 1200 grit sandpaper (15 µm) used in the sample preparation; therefore these grooves were examined with caution in the analysis of wear mechanisms.

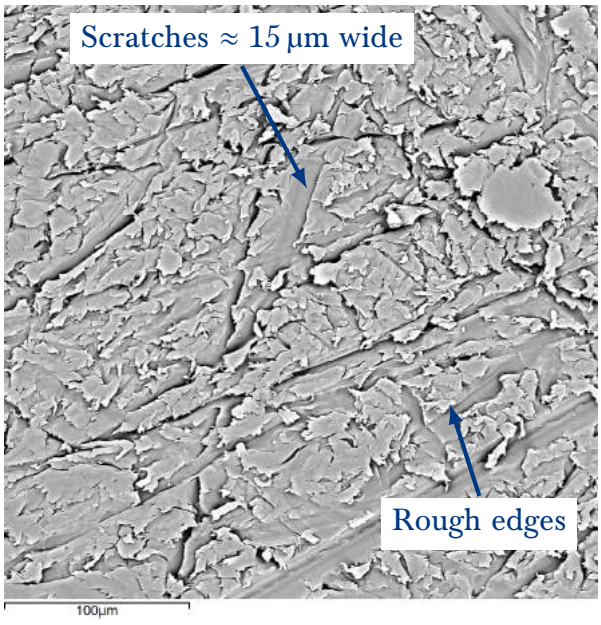

Figure 6.2: SEM image of PEEK after unlubricated testing.

The lubricated tests generated large elongated fragments of titanium, some as large as 50 µm but most were in the region of 20 µm. There was also evidence of pitting in some areas. The larger particle size would suggest higher sub-surface fatigue potentially caused by large hydrostatic pressures present in the contact (G. Stachowiak and A. Batchelor

2006, p. 636). Wear particle morphology studies are outside the scope of this study as they require a significant amount of computational effort (Eckold et al. 2015).

As the upper specimen reached its maximum velocity a wedge of lubricant is likely to have been trapped between the surfaces. This wedge of lubricant causes a high pressure spike that forces lubricant into surface cracks and exacerbates any previous damage. This explains the observation of the large pieces of titanium embedded in the polymer surface. The surface cracks themselves will have emanated from discontinuities in the surface. A pit examined on the titanium counter surface is shown in Figure 6.3.

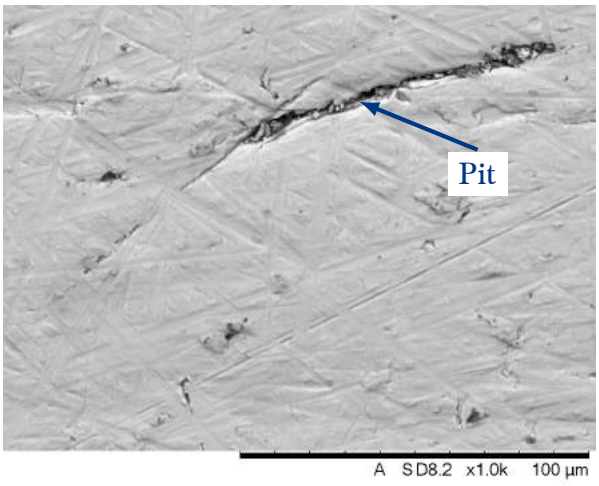

Figure 6.3: Pitting observed in titanium run lubricated against PEEK.

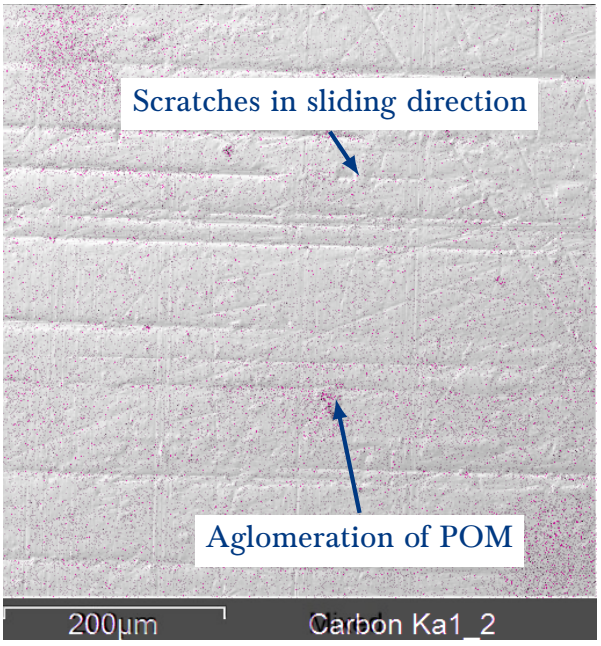

Figure 6.4: SEM image of titanium after lubricated testing against POM, carbon EDS map overlaid in red.

The titanium samples show score marks as shown in Figure 6.4. In general, those in the direction of sliding were less pronounced than the damage left by the surface preparation. There was evidence of smearing on the titanium surfaces, and this is likely to emanate from polymeric wear debris trapped between the bearing contacts. This polymer wear debris resulted in agglomerations forming transfer layers on the titanium surface Figure 6.4 shows an EDS map overlaid to support this observation.

The polymer specimens tested with no lubricant showed evidence of small fragments

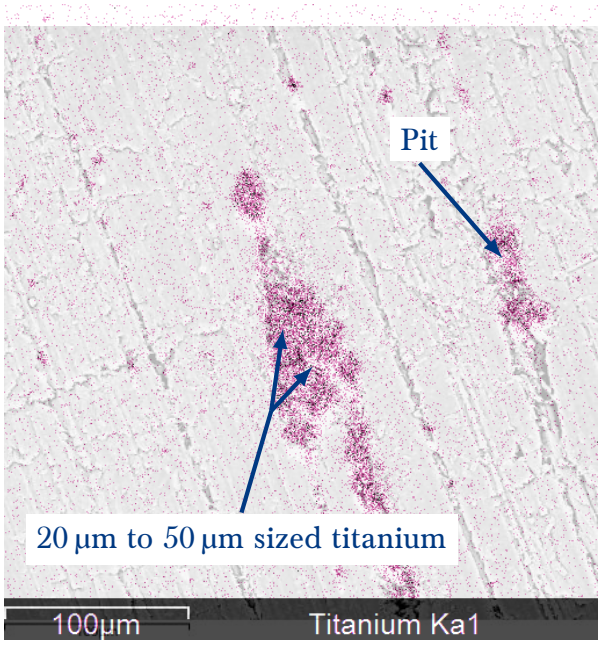

Figure 6.5: SEM image of PEEK after lubricated testing, titanium EDS image overlaid in red.

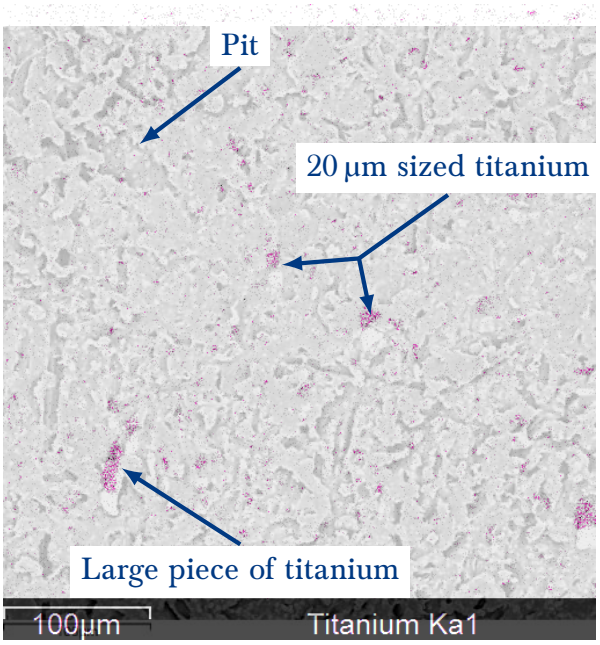

Figure 6.6: SEM image of POM after lubricated testing, titanium EDS image overlaid in red.

of titanium spread across the surface, in a similar way to the coverage of carbon on the titanium surfaces. The condition of the surfaces suggests abrasive wear with two and three body particle wear.

There were also pits observed in the lubricated titanium samples shown in Figure 6.3. These were of a similar size to the large fragments seen embedded in the polymer surfaces and were, in likelihood, formed by the same mechanism described above. The polymer counter surfaces are shown in Figure 6.7 and Figure 6.8.

Surface roughness was measured pre- and post-test for both the upper and lower specimens. Table 6.2 contains the change in surface roughness (calculated using Equation 6.1) and the variation of all the tested surfaces.

In general, the surface roughness of all the samples reduced apart from the titanium specimens run against PEEK with no lubricant. The PEEK had a higher variation in the roughness between the lubricated and unlubricated samples. The POM samples varied by a small amount between the unlubricated and lubricated tests. The standard deviations for all experiments were of a similar order of magnitude, suggesting the same level of

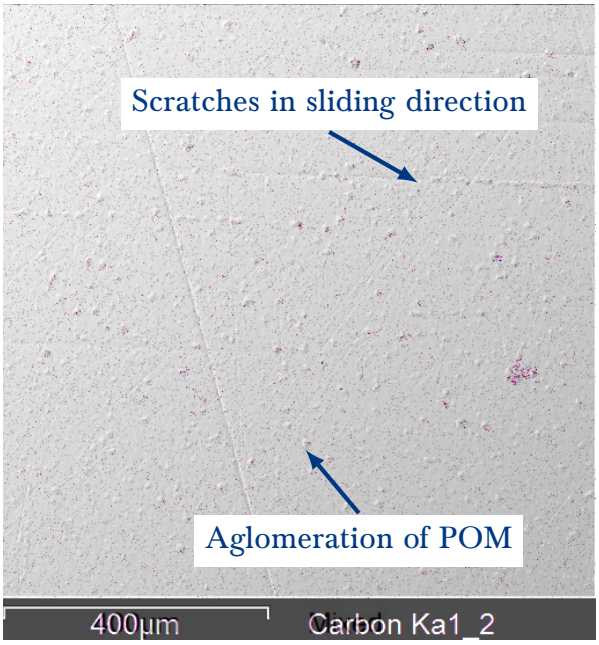

Figure 6.7: SEM image of titanium after unlubricated testing against POM, carbon EDS map overlaid in red.

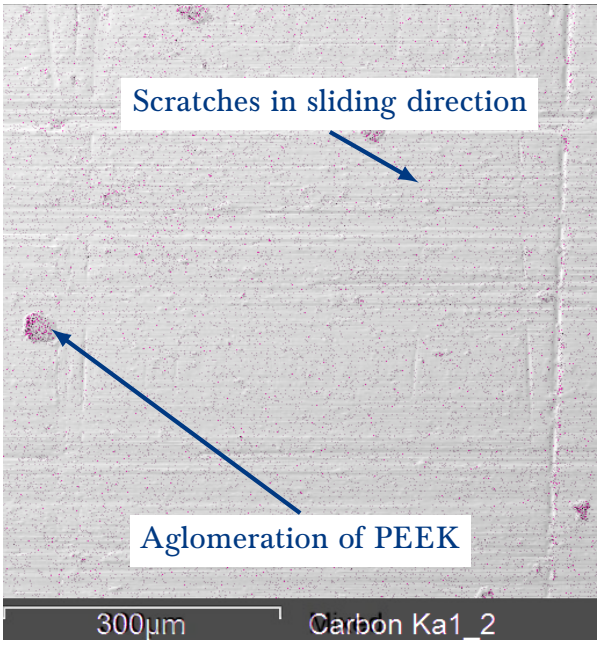

Figure 6.8: SEM image of titanium after lubricated testing against PEEK, carbon EDS map overlaid in red.

stability between the different scenarios.

$$\Delta Ra = Ra_{Pre\text{-}test} - Ra_{Post\text{-}test} \tag{6.1}$$

Table 6.2: The change in roughness and standard deviation of the upper and lower specimens over the test duration.

Upper Specimen Material	**Lubrication Methodology**	**Upper ΔRa (µm)**	**Lower ΔRa (µm)**
PEEK	Unlubricated	0.29 ±0.31	−0.06 ±0.13
	Lubricated	0.72 ±0.18	0.07 ±0.05
POM	Unlubricated	0.47 ±0.18	0.06 ±0.13
	Lubricated	0.43 ±0.43	0.09 ±0.15

This analysis utilises data sampled at 20 kHz to allow for insight into lubrication and wear mechanisms. In this manner, a diagnostic system in an industrial setting would be able to make a short high speed data recordings at periodic intervals. A system reliant on such a method would provide a similar amount of data and more insight into the

system than constantly recording at 1 Hz; for example a test run for 12 h on the TE77 generates a file that is 2600 kB. A high speed data file is 200 kB in size. This is an arbitrary measurement but hints at potential savings in storage. If a file is taken every hour over 12 h the physical size of the data would be the same as a low sample rate file, however the data recorded allows for condition monitoring of the lubricant, surface damage and other tribological phenomena. Low sample rate files only give insight into the coefficient of friction or a major tribological failure.

In running a visco-elastic material or lubricant the stick slip behaviour impacts the contact mechanics and fluid dynamics within the contact. Taking readings at a suitably chosen sample frequency leads to better insight into the mechanisms present.

6.4 Conclusions

This chapter compared the performance of PEEK and POM at low contact pressures in lubricated and un-lubricated reciprocating tests, while analysing the velocity dependent friction. Investigating the changes in friction during a stroke gives insight into the tribological mechanisms occurring during the motion of the surfaces. This method allows for the development of a diagnostic system with a greater comprehension of the tribology present in a contact. Key conclusions:

1. The transient analysis of friction demonstrated that the unlubricated samples experienced a static to dynamic transition, leading to a higher coefficient of friction at low velocities and higher frictional energy (Unlubricated: PEEK = 2.25J, POM = 0.72J. Lubricated: PEEK = 0.11J, POM = 0.18J). This is not observed in the lubricated tests.

2. Unlubricated contacts produce higher frictional losses which are dependent on the material properties such as the stiffness and surface free energy (μ_{POM} = 0.36, μ_{PEEK} = 0.55). Lubricated contacts produced a lower coefficient of friction that was influenced less by the sample materials properties (μ_{POM} = 0.10, μ_{PEEK} = 0.10).

3. Friction in the unlubricated tests increased as the sliding velocity tended to 0, contributing to higher frictional energy dissipation. This trend was not the case in the lubricated tests.

4. Extreme pressure caused by the lubricant wedge led to pitting in the Ti demonstrated by the large pieces of Ti observed embedded in the surface of the polymers.

5. Unlubricated test in-stroke friction was significantly more affected by velocity.

The method presented will accentuate the understanding of the Dearman Engine's performance, especially with the introduction of visco-elastic materials and lubricants as presented in the previous chapters.

Chapter 7

Conclusions

This thesis has explored potential developments that will reduce parasitic losses within the Dearman Engine. This has focussed on three methods: new materials, new lubricants and new designs.

7.1 Polymer Tribology: A Material Replacement Study

The first investigation was into the area where a majority of the friction had been measured previously by Dearman — the cylinder-liner piston seal interaction.

Tribological assessment of a wide variety of polymer matrix composites (PMCs), under conditions representative of the Dearman Engine, led to the selection of POM as an alternative material for the cylinder liner. POM unhoned demonstrated the lowest steady state coefficient of friction at ≈ 0.05 compared to the benchmark of ≈ 0.14 at 12 °C. In addition POM presented a short settling time and percentage overshoot: descriptors of the steady state condition directly correlated to the wear volume of the upper specimen representative of the piston seal. This testing has exposed the potential that a polymeric cylinder could have on the parasitic losses, there is another benefit: a reduction in mass of the engine. The aluminium cylinder liner has a mass of 2.208 kg, replacing the material with POM will result in the cylinder liner mass being reduced by 1.063 kg as calculated by the ratio of the densities of the materials.

The original piston seal was a polymer matrix composite of PTFE and as such there was not the same potential improvement in the tribological performance as with the cylinder-liner. For this reason an investigation into novel manufacturing techniques was undertaken. This examined the possibility that PMC's do not need to be necessarily be macroscopically homogenous but instead could consist of laminated polymers providing a lubricious layer of a soft polymer (PTFE) and a stiff matrix material (PEEK). This study showed that as long as the bonding between the layers is strong a laminated polymer can be utilised in the place of a PMC. The coefficient of friction for the PTFE-PEEK composite and PTFE-PEEK laminate were both ≈ 0.2 with a reduced wear rate when compared to PTFE or PEEK run under the same conditions. As the piston seal is operated linearly

the direction of sliding whilst reciprocating is always along the same plane. This means the laminated layers can be orientated perpendicular to the sliding ensuring the counter surface is in contact with both laminated materials during the operation. An application where this is not always the case would not benefit from this approach.

The testing of laminated polymers was conducted at 4 Hz however, the Dearman Engine operates at 800 rpm (13.3 Hz). As the tests at 4 Hz were successful the reciprocating frequency should be increased to ensure the forces through the bonded layers are not excessive and large enough to cause fracture between the surfaces.

7.2 Biomimetic Lubrication

In the TRU one of the largest and potentially unnecessary auxiliaries is the oil pump. As the motion of the crank provides splash lubrication within the main body of the engine removal of the pump would only majorly impact the valvetrain. For this reason two biomimetic lubricants were examined to see if they would operate under the harsh conditions within the crankcase: high velocity and contact pressure. In nature the most common form of lubrication is boundary and so these lubricants mimicking nature have a large potential to perform well in the valve train.

Pectin and bovine serum albumin (BSA) were selected for their ability to provide boundary lubrication in nature, pectin is found on train tracks reducing traction and BSA is partially responsible for the lubricating properties of synovial joints in mammals. Both additives were manufactured into aqueous solutions at $1\,\mathrm{mg\,ml^{-1}}$ and $5\,\mathrm{mg\,ml^{-1}}$.

The investigation demonstrated that BSA at both concentrations tested ($1\,\mathrm{mg\,ml^{-1}}$ and $5\,\mathrm{mg\,ml^{-1}}$) under high loads a coefficient of friction of 0.17 and 0.15 respectively was observed. Under low loads pectin at $5\,\mathrm{mg\,ml^{-1}}$ produced a coefficient of friction of 0.37, the lowest observed at that contact pressure, and at high loads 0.18. Each lubricant formed a lubricating film as demonstrated by the contact potential measured across the two surfaces. This led to the conclusion that $5\,\mathrm{mg\,mg^{-1}}$ Pectin was the most promising lubricant from the testing.

7.3 Velocity Dependant Friction

New materials were examined to reduce the lubricating requirements of the valve-train. These were analysed with a novel analytical method exposing the potential insight that using an appropriate sampling rate when measuring friction data can provide. This is critical when using materials and fluids that are viso-elastic in a reciprocating contact.

This led to demonstrating that by sampling at a rate above the Nyquist frequency the transition from quasi-static to dynamic can be observed. Calculation of the frictional energy dissipated and observations of the coefficient of friction at this sample rate are more representative of the physical effects being observed than observations at a significantly lower sample rate.

With the study into lubrication and novel investigative methods the potential mass reduction is less tangible. A better understanding of the friction within the valve guides and the potential lubricants in the cylinder head may lead to the possibility that the oil pump is no longer needed within the truck refrigeration unit (TRU) reducing auxiliary loads on the engine and the overall mass of the system.

All of these approaches have had the sustainable nature of the Dearman Engine at their heart. Focussing on reducing manufacturing energy costs, frictional losses and data storage requirements; all with one goal: reducing the overall weight of the TRU. The relevance of this research is wider than that of the Dearman Engine: whilst the focus of research has been into improving the efficiency and ecological footprint of the engine; most aspects of the experimental work are applicable to a wider scientific audience.

7.4 Future Work

This work is not complete: the suggested changes are not at the same technological readiness as the rest of the engine and there are limitations within the work.

As with all experiments conducted on a test rig these investigations come with limitations, in order to simplify the test conditions assumptions must be made to align

the desired loading parameters with the operating envelope of the machine. The most significant of these assumptions comes from the physical loading of the materials. On the TE77 it is not possible to dynamically load the specimens, within an engine under operation the cylinder pressure varies significantly with respect to the position of the piston. In the assessment of the cylinder liner and the piston seal the maximum contact pressure within the engine cycle was selected as the testing parameter. With the introduction of visco-elastic materials the frequency of the loading will have an effect on the static-dynamic transition in friction and the stiffness of the materials. As with the introduction of analyses at a suitable frequency, for a more accurate result the loading frequency, reciprocating frequency and sliding velocity would ideally be identical to that of the application. Within the physical footprint of the lubricant bath of the TE77 this is not possible and within the Dearman Engine, even on a test bed, there is not the sensor capability to analyse the friction at specific interfaces under realistic loading. For this reason the worst case scenario was always modelled with the assumption that at lower velocities and normal contact forces the friction and subsequent wear will be reduced.

Where possible every care was taken to align samples correctly within the TE77 specimen holders however the method through which the frictional force is measured the flatness of the lower specimen and reciprocating arm is critical to the recorded values. When samples have been manually prepared either through honing or lamination in Chapter 4 natural variation in the samples occurred which was unavoidable due to the equipment and techniques available. This variation can be seen in the results however the standard deviation is mostly an order of magnitude lower than the mean. This variable will also be observed in the final product within the tolerances determined by Dearman but is more noticeable in this style of testing as the focus in on one contact and not the multiple contacts that are found in the whole system.

Each of these investigations has been undertaken in an isolated manner despite the intention being to combine all of results to enhance the Dearman Engine. It is not possible to fully predict the interactions between each enhancement although every care has been taken to investigate compatible materials and lubricants.

In order to take the results of this thesis to an industrially viable product there is still a significant amount of work to be undertaken. With the cylinder liner and piston seal the solutions are ready to move to a component level test, gradually increasing loads and operation. Initially this would take the form of motoring an engine with the components mounted at low speeds to identify any issues with a modified manufacturing method and material.

A laminated piston seal will require a bespoke piston with which to accept the seal and provide compression perpendicular to the layer, assisting with the bonding of the lamellae; this will take a significant amount of design time to ensure the geometry is economically viable to manufacture. The effect of layer thickness, the optimum ratio and distribution of the laminated layers are also not fully understood so more laboratory work should be undertaken to fully explore this. With the addition of a more in depth analysis method and corroboration of these analyses with wear debris and surface morphology characterisation will help to develop the use of velocity dependant friction as a performance monitoring tool.

The area that is furthest away from technological readiness is the biomimetic single fluid lubricant and heat exchange fluid (HEF). Throughout this thesis the tribological performance of the fluids have been studied however the heat transfer properties have been assumed from the nature that they are largely aqueous. In order to fully assess these lubricants a more in depth chemical, rheological and thermodynamic analysis of the fluids must be undertaken. In addition only two possible sources of biological additive have been analysed. This investigation has also not addressed the impact of the chemistry on the performance of the lubricants, proteins undergo denaturing and the temperature at which BSA undergoes this is within the potential temperatures that may be seen momentarily during the operation of the engine in a contact. Denaturing is a permanent process and this will impact the longevity of the lubricant. Under the test conditions the stability of the lubricants has not been addressed, under operation in the Dearman Engine the lubricants will be used for a significant period of time (in the order of months) and under a wide variety of contacts and conditions. In order to utilise these lubricants in an industrial

setting the longevity must be understood. This will be realised through chemical and rheological analysis and extended rig testing initially and then introducing the lubricant into the Dearman Engine. Most commercial lubricants use additives to assist with reducing undesireable properties of the fluid such as corrosion, this may be necessary in the further development of the fluids but until introduction to the system under full operation some of these effects may not be observed. As the purpose of the testing was to determine if the lubricants would support a surface, viscosity was not examined however industrial development will require this to be determined at a variety of shear rates.

In conclusion this thesis has set out the groundwork for the reduction of parasitic losses in the Dearman Engine; exploring and investigating exiting developments in sustainable lubrication and potential weight reductions in the overall TRU system whilst also contributing new analytical methods to provide better understanding of the mechanisms present in visco-elastic systems. These have also had an impact wider than the scope of the Dearman Engine, whilst the material replacement studies are very focussed on the application the analysis work and the contents of the other investigations accentuate what can be found in literature and as such have relevance to the wider engineering community.

Appendix: Pugh Analysis Multipliers

Table 1: The multipliers used during the Pugh analysis for polymer selection, ordered by the magnitude of the multiplier with comments describing the thought process for assigning importance.

Property	**Mulitplier**	**Comment**
Price	10	Money is the most important factor in implementation of new technologies. Consumers are not receptive to large increases in cost without a significant and measurable improvement to performance. The cost also implies technological readiness, as a rule of thumb the greater the potential of a polymer to be mass produced the lower the cost per kg.
Bulk Modulus	10	Bulk and Shear moduli (related to Young's modulus and Poisson's ratio) describe the material response to compression and shear the two major loading mechanisms seen by the cylinder liner (Hibbler 2011, p. 680).
Shear Modulus	10	See Bulk Modulus.
Compressive Strength	10	The loading of the cylinder liner is mostly in compression from the expansion of the gas and pressure from the piston seal.

Continued on next page

Property	Mulitplier	Comment
Thermal Expansion Coefficient	10	Excessive shrinkage from poor operation may lead to seizing of the engine so minimising thermal expansion will reduce the risk of this.
Fatigue Strength	9	Durability of the components is key in the operation of the engine.
Thermal Conductivity	8	The key to the function of lubricants is to conduct heat away from a contact. The material shouldn't impede this process.
Fracture Toughness	8	Polymers have the ability to form glass like crystals creating brittle areas (Rudin 1982, pp. 394–399).
Vickers Hardness	8	An increase in hardness has been linked to a reduction in adhesive and abrasive wear (Arnell et al. 1991, pp. 68–72).
Density	7	There will be a distinct reduction in mass switching from metals to polymers however any gains from a potential material replacement must be exploited.
Poisson's Ratio	7	This is lower down the Pugh selection as it is taken account for in the bulk and shear modulus.

Continued on next page

Property	**Mulitplier**	**Comment**
Minimum Service Temperature	6	A large portion of the Dearman Engine working conditions are around ambient however there is a possibility of lower temperatures.
Specific Heat Capacity	6	Not a property directly related to tribological phenomena however the temperature rise in contact is related to the property (Carslaw and Jaeger 1959, pp. 266–268).
Young's Modulus	5	This is lower down the Pugh selection as it is taken account for in the bulk and shear modulus.
Yield Strength	5	The load state of the cylinder liner is not sufficient to cause significant plastic deformation as the liner is mostly in compression.
Tensile Strength	5	The cylinder liner is not subject to significant tension.
Glass Transition Temperature	4	The crystallinity of the polymers is encapsulated within the other properties presented.
Maximum Service Temperature	4	No excessive heating should occur unless poor lubrication occurs, there has been no evidence of this occurring in the Dearman Engine to date.
Elongation	1	Encapsulated within bulk modulus and Poisson's ratio

Continued on next page

Property	Mulitplier	Comment
Melting Point	1	No excessive heating should occur unless poor lubrication occurs, there has been no evidence of this occurring in the Dearman Engine to date.

Appendix: Abbott Firestone Curves

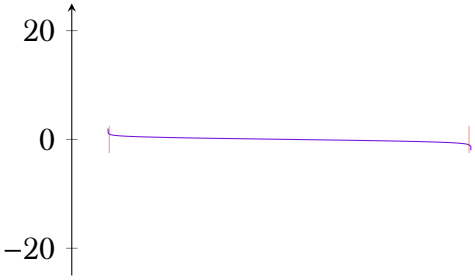

(a) Aluminium - Honed

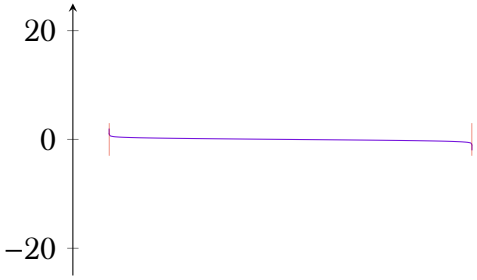

(b) Aluminium - Unhoned

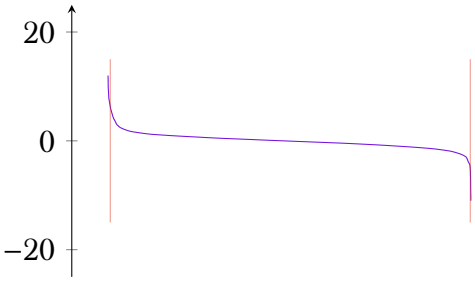

(c) PPA - Honed

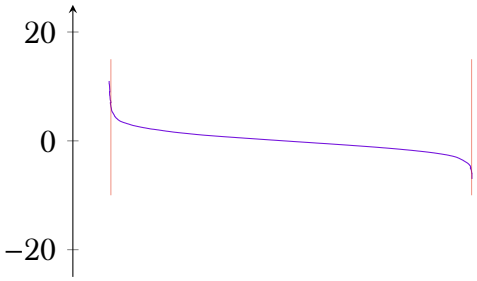

(d) PPA - Unhoned

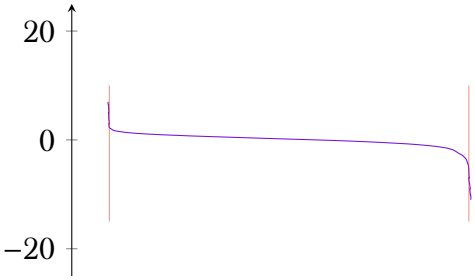

(e) PTT - Honed

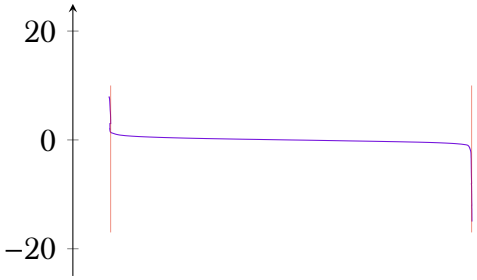

(f) PTT - Unhoned

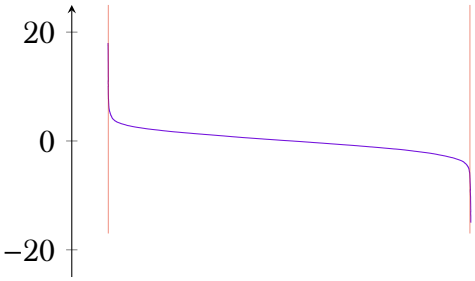

(g) PEEK - Honed

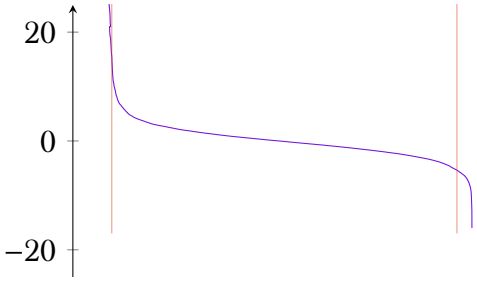

(h) POM - Honed

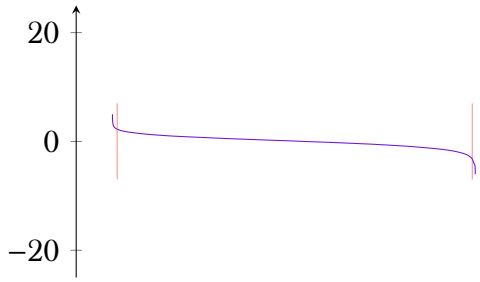

(i) POM - Unhoned

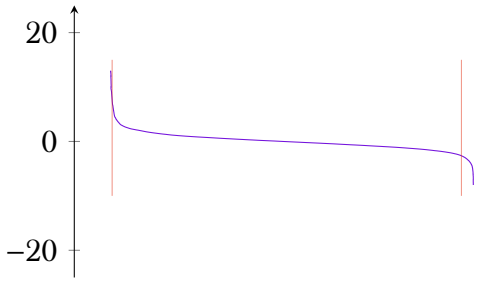

(j) POM w/ PTFE - Honed

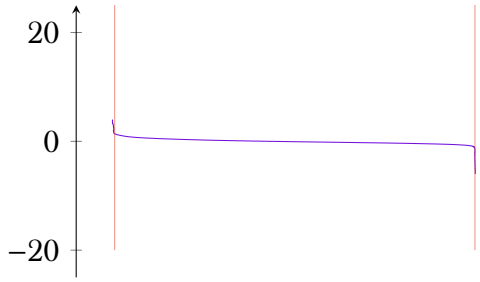

(k) POM w/ PTFE - Unhoned

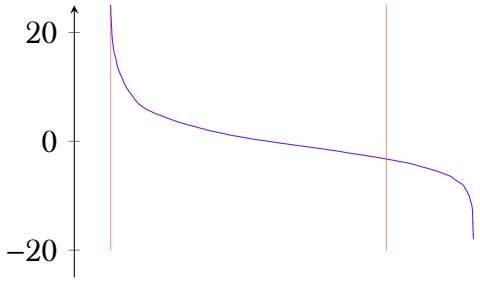

(l) UHMWPE - Honed

Figure 1: Abbott - Firestone curves for each material tested. Figure 4.7 presents the same data with differenctly sized axes to aid understanding of the form of the surface.

Bibliography

Ahlroos, T. et al. (2011). "Biomimetic approach to water lubrication with biomolecular additives". In: *Proceedings of the Institution of Mechanical Engineers, Part J: Journal of Engineering Tribology* 225.10, pp. 1013–1022. ISSN: 13506501. DOI: 10 . 1177 / 1350650111406635.

Amontons, M (1699). "De la resistance cause'e dans les machines". In: *Memoires de l'Academie Royale des Frances* A, pp. 206–227.

Arnell, R. D. et al. (1991). *Tribology: Principles and Design Application*. First Edit. London: Macmillan Education Ltd., p. 255. ISBN: 0333458672.

ASTM International, ASTM (2012). "D6079-18: Standard Test Method for Evaluating Lubricity of Diesel Fuels by the High-Frequency Reciprocating Rig (HFRR)". In: i.C, pp. 1–6. DOI: 10.1520/C0496.

Barrell, D.J.W. and M. Priest (2003). "The interaction of wear rate and friction with surface roughness for a lubricated sliding contact". In: *Tribology {Series}*. Vol. Volume 43. Elsevier, pp. 807–814. ISBN: 0167-8922. DOI: 10.1016/S0167-8922(03)80108-6.

Bart, Jan C.J., Emanuele Gucciardi, and Stefano Cavallaro (2013). "Principles of lubrication". In: *Biolubricants*, pp. 10–23. DOI: 10.1533/9780857096326.10.

Bauer, Stefan (2012). "Mass Spectrometry for Characterizing Plant Cell Wall Polysaccharides". In: *Frontiers in Plant Science* 3.March, pp. 1–6. ISSN: 1664-462X. DOI: 10.3389/fpls.2012.00045.

Bevan, Thomas (1939). *The Theory of Machines*. Third Edit. Longmans, Green and Co. Ltd.

Bhattacharyya, Souvik and Randip K. Das (1999). “Catalytic control of automotive NOx: A review”. In: *International Journal of Energy Research* 23.4, pp. 351–369. ISSN: 0363907X. DOI: 10.1002/(SICI)1099-114X(19990325)23:4<351::AID-ER497>3.0.CO;2-T.

Bhushan, Bharat and Yong Chae Jung (2008). “Wetting, adhesion and friction of superhydrophobic and hydrophilic leaves and fabricated micro/nanopatterned surfaces”. In: *Journal of Physics Condensed Matter* 20.22. ISSN: 09538984. DOI: 10.1088/0953-8984/20/22/225010.

Borruto, Adelina, Gianni Crivellone, and Filippo Marani (Nov. 1998). “Influence of surface wettability on friction and wear tests”. In: *Wear* 222.1, pp. 57–65. ISSN: 00431648. DOI: 10.1016/S0043-1648(98)00256-7.

Boyde, Steve (2002). “Green lubricants. Environmental benefits and impacts of lubrication”. In: *Green Chemistry* 4.4, pp. 293–307. ISSN: 14639262. DOI: 10.1039/b202272a.

Brown, Martyn (2008). *Chilled Foods - A Comprehensive Guide (3rd Edition)*. English. Great Abington: Woodhead Publishing CRC Press. ISBN: 978-1-84569-243-8.

Burris, David L. and W. Gregory Sawyer (Aug. 2006). “A low friction and ultra low wear rate PEEK/PTFE composite”. In: *Wear* 261.3-4, pp. 410–418. ISSN: 00431648. DOI: 10.1016/j.wear.2005.12.016.

Caffall, Kerry Hosmer and Debra Mohnen (2009). “The structure, function, and biosynthesis of plant cell wall pectic polysaccharides”. In: *Carbohydrate Research* 344.14, pp. 1879–1900. ISSN: 00086215. DOI: 10.1016/j.carres.2009.05.021.

Campbell, Neil A. et al. (2017). *Biology: A Global Approace*. Global. New York: Pearson Education Limited, p. 1498. ISBN: 10: 1292107433.

Cann, P. M. (2006). “The "leaves on the line" problem - A study of leaf residue film formation and lubricity under laboratory test conditions”. In: *Tribology Letters* 24.2, pp. 151–158. ISSN: 10238883. DOI: 10.1007/s11249-006-9152-2.

Cannaday, M. L. and Andreas A. Polycarpou (Aug. 2005). “Tribology of unfilled and filled polymeric surfaces in refrigerant environment for compressor applications”. In: *Tribology Letters* 19.4, pp. 249–262. ISSN: 10238883. DOI: 10.1007/s11249-005-7441-9.

Carrington, Damian (Sept. 2018). *Air pollution particles found in mothers' placentas.*

Carslaw, H. S. and J.C. Jaeger (1959). *Conduction of heat in solids.* Oxford.

Chattopadhyay, R. (2001). *Surface wear: analysis, treatment, and prevention.* Materials Park, Ohio: ASM International. ISBN: 0-87170-702-0.

Chian, Ri Cheng (2010). "Cryobiology: An overview". In: *Fertility Cryopreservation.* Cambridge: Cambridge University Press, pp. 1–9. ISBN: 9780511730207. DOI: 10.1017/CBO9780511730207.002.

Choudhury, Dipankar et al. (2013). "Performance of honed surface profiles to artificial hip joints: An experimental investigation". In: *International Journal of Precision Engineering and Manufacturing* 14.10, pp. 1847–1853. ISSN: 22347593. DOI: 10.1007/s12541-013-0247-z.

Chuah, T J (2012). *Engineering Polymers Seminar.* Ed. by R W Dyson. Glasgow : New York: Blackie ; Chapman and Hall. ISBN: 0-412-02081-5.

Daintith, John (1966). "Dictionary of Chemistry (6th Edition)". In: *Dictionary of Chemistry and Chemical Technology.* Elsevier, pp. 563–598. ISBN: 978-0-19-920463-2. DOI: 10.1016/B978-0-08-011600-6.50016-4.

Dearman, Peter (2006). *Engines driven by liquified or compressed gas.*

Dearn, K. D., T. J. Hoskins, L. Andrei, et al. (2013). "Lubrication regimes in high-performance polymer spur gears". In: *Advances in Tribology* 2013. ISSN: 16875915. DOI: 10.1155/2013/987251.

Dearn, K. D., T.J. Hoskins, D. G. Petrov, et al. (2013a). "Applications of dry film lubricants for polymer gears". In: *Wear* 298-299.1, pp. 99–108. ISSN: 00431648. DOI: 10.1016/j.wear.2012.11.003.

— (Feb. 2013b). "Applications of dry film lubricants for polymer gears". In: *Wear* 298-299.1, pp. 99–108. ISSN: 00431648. DOI: 10.1016/j.wear.2012.11.003.

Dentice d'Accadia, M. et al. (2003). "Micro-combined heat and power in residential and light commercial applications". In: *Applied Thermal Engineering* 23.10, pp. 1247–1259. ISSN: 13594311. DOI: 10.1016/S1359-4311(03)00030-9.

Design, Granta (2014). *CES Edupack.* Cambridge, UK.

Diversified Enterprises (2018). *Surface Free Energy Components by Polar/Dispersion and AcidBase Analyses; and Hansen Solubility Parameters for Various Polymers.*

DuPont (July 2008). *What is {PPA}?*

Eckold, D. G., K. D. Dearn, and D. E.T. Shepherd (2015). "The evolution of polymer wear debris from total disc arthroplasty". In: *Biotribology* 1-2, pp. 42–50. ISSN: 23525738. DOI: 10.1016/j.biotri.2015.04.002.

EndreSS, H. U. and S. H. Christensen (2009). "Pectins". In: *Handbook of Hydrocolloids: Second Edition* 1, pp. 274–297. DOI: 10.1533/9781845695873.274.

Fares, Mohammad M., A. K. Maayta, and Mohammad M. Al-Qudah (2012). "Pectin as promising green corrosion inhibitor of aluminum in hydrochloric acid solution". In: *Corrosion Science* 60, pp. 112–117. ISSN: 0010938X. DOI: 10.1016/j.corsci.2012.04.002.

Fennell, Daniel, Jose Herreros, and Athanasios Tsolakis (2014). "Improving gasoline direct injection (GDI) engine efficiency and emissions with hydrogen from exhaust gas fuel reforming". In: *International Journal of Hydrogen Energy* 39.10, pp. 5153–5162. ISSN: 03603199. DOI: 10.1016/j.ijhydene.2014.01.065.

Friedrich, K., Z. Zhang, and A. Schlarb (Dec. 2005). "Effects of various fillers on the sliding wear of polymer composites". In: *Composites Science and Technology* 65.15-16, pp. 2329–2343. ISSN: 02663538. DOI: 10.1016/j.compscitech.2005.05.028.

Grant, G.T. (1973). "Biological interactions between polysaccarites & divalent metal cations: the egg box model". In: *FERS Letters* 32.1, pp. 195–198. ISSN: 00145793. DOI: 10.1016/0014-5793(73)80770-7. arXiv: 0509002 [math].

Harris, H A (1974). "Lubrication in antiquity". In: *Greece and Rome* 21.1, pp. 32–36. ISSN: 14774550. DOI: 10.1017/S0017383500021665.

Hashumoto, Yoshihiro, Akihko Yoneyaj, and Yoshitaka Togari (Oct. 1989). "Design method of a quadratic performance index using a reference model". In: *International Journal of Control* 50.4, pp. 1169–1184. ISSN: 0020-7179. DOI: 10 . 1080 / 00207178908953424.

Haut Donahue, Tammy L. et al. (2003). "How the stiffness of meniscal attachments and meniscal material properties affect tibio-femoral contact pressure computed using a validated finite element model of the human knee joint". In: *Journal of Biomechanics* 36.1, pp. 19–34. ISSN: 00219290. DOI: 10.1016/S0021-9290(02)00305-6.

Hertz, Heinrich (1896). *Miscellaneous papers*. English. London; New York: MacMillan and Co.

Hibbler, R. C. (2011). *Statics and Mechanics of Materials*. 3rd Editio. Singapore: Prentice Hall, p. 877. ISBN: 9810686323.

Hoskins, T. J. et al. (Jan. 2014). "The wear of PEEK in rolling-sliding contact - Simulation of polymer gear applications". In: *Wear* 309.1-2, pp. 35–42. ISSN: 00431648. DOI: 10.1016/j.wear.2013.09.014.

Hu, Yuan zhong, Tian bao Ma, and Hui Wang (2013). "Energy dissipation in atomic-scale friction". In: *Friction* 1.1, pp. 24–40. ISSN: 22237704. DOI: 10.1007/s40544-013-0002-6.

Huang, Bill X., Hee Yong Kim, and Chhabil Dass (2004). "Probing three-dimensional structure of bovine serum albumin by chemical cross-linking and mass spectrometry". In: *Journal of the American Society for Mass Spectrometry* 15.8, pp. 1237–1247. ISSN: 10440305. DOI: 10.1016/j.jasms.2004.05.004.

Hui, Alexander Y and William J Mccarty (2013). "A Systems Biology Approach to Synovial Joint Lubrication in". In: DOI: 10.1002/wsbm.157.A.

Hutchings, I and P Shipway (2017). *Tribology: Friction and Wear of Engineering Materials*. Second Edi. Oxford ; New York: Elsevier, p. 388. ISBN: 9780081009109.

Hutchings, Ian, Mark Gee, and Erich Santner (2011). "Friction and Wear". In: *Springer Handbook of Metrology and Testing*. Elsevier, pp. 743–768. ISBN: 978-3-642-16640-2. DOI: 10.1007/978-3-642-16641-9_13.

Igobo, Opubo N. and Philip A. Davies (June 2014). "Review of low-temperature vapour power cycle engines with quasi-isothermal expansion". In: *Energy* 70, pp. 22–34. ISSN: 03605442. DOI: 10.1016/j.energy.2014.03.123.

Institution of Mechanical Engineers, Tribology Group (2014). "Tribological Design Guide Part 5: Wear". In: 1, P1–34.

International Council On Clean Transportation, ICCT (2016). *European Stage V non-road emission standards*. en. Tech. rep., p. 9.

Jain, V. K. and S. Bahadur (Jan. 1978). "Material transfer in polymer-polymer sliding". In: *Wear* 46.1, pp. 177–188. ISSN: 00431648. DOI: 10.1016/0043-1648(78)90119-9.

Johnson, Kenneth Langstreth (2003). *Contact Mechanics*. eng. 9. print. Cambridge: Cambridge Univ. Press, p. 452. ISBN: 0-521-34796-3.

Jost, H Peter. et al. (1966). *Lubrication (tribology) : education and research : a report on the present position and industry's needs*. London: H.M.S.O.

Kalin, M. and M. Polajnar (2013). "The effect of wetting and surface energy on the friction and slip in oil-lubricated contacts". In: *Tribology Letters* 52.2, pp. 185–194. ISSN: 10238883. DOI: 10.1007/s11249-013-0194-y.

Karger-Kocsis, J. and K. Friedrich (Mar. 1988). "Fatigue crack propagation in short and long fibre-reinforced injection-moulded PA 6.6 composites". In: *Composites* 19.2, pp. 105–114. ISSN: 00104361. DOI: 10.1016/0010-4361(88)90720-3.

Khedkar, Jaydeep, Ioan Negulescu, and Efstathios I. Meletis (Mar. 2002). "Sliding wear behavior of PTFE composites". In: *Wear* 252.5-6, pp. 361–369. ISSN: 00431648. DOI: 10.1016/S0043-1648(01)00859-6.

Komvopoulos, K., N. Saka, and N. P. Suh (Oct. 1985). "The Mechanism of Friction in Boundary Lubrication". In: *Journal of Tribology* 107.4, pp. 452–462. ISSN: 0742-4787. DOI: 10.1115/1.3261108.

Kotrba, Pavel (2011). "Microbial Biosorption of MetalsGeneral Introduction". In: *Microbial Biosorption of Metals*. September 2015. Dordrecht: Springer Netherlands, pp. 1–6. ISBN: 9789400704428. DOI: 10.1007/978-94-007-0443-5_1.

Kubiak, K. J., T. W. Liskiewicz, and T. G. Mathia (2011). "Surface morphology in engineering applications: Influence of roughness on sliding and wear in dry fretting". In: *Tribology International* 44.11, pp. 1427–1432. ISSN: 0301679X. DOI: 10.1016/j.triboint.2011.04.020.

Kurian, Joseph V. (Apr. 2005). "A new polymer platform for the future - Sorona?? from corn derived 1,3-propanediol". In: *Journal of Polymers and the Environment* 13.2, pp. 159–167. ISSN: 15662543. DOI: 10.1007/s10924-005-2947-7.

Kyoo Park, Byoung et al. (2011). "Thermal conductivity of bovine serum albumin: A tool to probe denaturation of protein". In: *Applied Physics Letters* 99.16. ISSN: 00036951. DOI: 10.1063/1.3652704.

Lee, P. M. et al. (Mar. 2006). "Extraction and tribological investigation of top piston ring zone oil from a gasoline engine". In: *Proceedings of the Institution of Mechanical Engineers, Part J: Journal of Engineering Tribology* 220.3, pp. 171–180. ISSN: 1350-6501. DOI: 10.1243/13506501JET148. arXiv: 0412138v1 [cond-mat].

Lehninger, Albert L. (1982). *Principles of Biochemistry*. Ed. by Sally Anderson and June Fox. 1st. New York: Worth Publishers Inc., p. 1011. ISBN: 0-87901-136-X.

Li, Z. et al. (2009). "Rolling-Sliding Laboratory Tests of Friction Modifiers in Leaf Contaminated Wheel-Rail Contacts". In: *Tribology Letters* 33.2, pp. 97–109. ISSN: 1023-8883. DOI: 10.1007/s11249-008-9393-3.

Liu, Shuhai et al. (2008). "Effect of surface physicochemical properties on the lubricating properties of water film". In: *Applied Surface Science* 254.22, pp. 7137–7142. ISSN: 01694332. DOI: 10.1016/j.apsusc.2008.05.319.

Lu, Z. P. and K. Friedrich (Mar. 1995). "On sliding friction and wear of PEEK and its composites". In: *Wear* 181-183.PART 2, pp. 624–631. ISSN: 00431648. DOI: 10.1016/0043-1648(95)90178-7.

M. Pelagade, S. et al. (2012). "Investigation of Surface Free Energy for PTFE Polymer by Bipolar Argon Plasma Treatment". In: *Journal of Surface Engineered Materials and Advanced Technology* 02.02, pp. 132–136. ISSN: 2161-4881. DOI: 10.4236/jsemat.2012.22021.

Mang, Theo, ed. (2007). *Lubricants and lubrication*. 2., comple. Weinheim: Wiley-VCH. ISBN: 978-3-527-31497-3.

Maricq, Matti (2007). "Chemical characterization of particulate emissions from diesel engines: A review". In: *Journal of Aerosol Science* 38.11, pp. 1079–1118. ISSN: 00218502. DOI: 10.1016/j.jaerosci.2007.08.001.

Mark, James E, ed. (Nov. 2009). *Polymer Data Handbook*. 2nd ed. Vol. 131. 44. Oxford ; New York: Oxford University Press, pp. 16330–16330. ISBN: 9780195181012. DOI: 10.1021/ja907879q.

Mens, J. W M and A. W J de Gee (1991). *Friction and wear behaviour of 18 polymers in contact with steel in environments of air and water*. DOI: 10.1016/0043-1648(91)90378-8.

Meuleman, P. K. et al. (2007). "Minimization of transmission errors in highly loaded plastic gear trains". In: *Proceedings of the Institution of Mechanical Engineers, Part C: Journal of Mechanical Engineering Science* 221.9, pp. 1117–1129. ISSN: 0954-4062. DOI: 10.1243/09544062JMES439.

Novak, S. et al. (2007). "The effect of residual stresses in functionally graded alumina-ZTA composites on their wear and friction behaviour". In: *Journal of the European Ceramic Society* 27.1, pp. 151–156. ISSN: 09552219. DOI: 10.1016/j.jeurceramsoc.2006.01.021.

Nunez, Emerson Escobar and Andreas A. Polycarpou (Mar. 2015). "The effect of surface roughness on the transfer of polymer films under unlubricated testing conditions". In: *Wear* 326-327, pp. 74–83. ISSN: 00431648. DOI: 10.1016/j.wear.2014.12.049.

Nyquist, H (1928). "Certain Topics in Telegraph Transmission Theory". In: *Transactions of the American Institute of Electrical Engineers* 47.2, pp. 617–644. ISSN: 0096-3860.

Ochoa-Villarreal, Marisol et al. (2012). "Plant Cell Wall Polymers: Function, Structure and Biological Activity of Their Derivatives". In: *Polymerization* September. ISSN: 18423582. DOI: 10.5772/46094. arXiv: 9809069v1 [arXiv:gr-qc].

Ogata, Katsuhiko (1997). *Modern Control Engineering*. Third. New Jersey: Prentice Hall.

Peters, Toby (2016). "Clean Cold and the Global Goals". In:

Popova, Elena and Valentin L. Popov (2015). "The research works of Coulomb and Amontons and generalized laws of friction". In: *Friction* 3.2, pp. 183–190. ISSN: 22237704. DOI: 10.1007/s40544-015-0074-6.

Priest, M and C M Taylor (2000). "Automobile engine tribologyapproaching the surface". In: *Wear* 241.2, pp. 193–203. ISSN: 0043-1648. DOI: http://dx.doi.org/10.1016/S0043-1648(00)00375-6.

Qi, Ya e., Yong Sheng Zhang, and Li Tian Hu (2012). "High-temperature self-lubricated properties of Al 2O 3/Mo laminated composites". In: *Wear* 280-281, pp. 1–4. ISSN: 00431648. DOI: 10.1016/j.wear.2012.01.010.

Ravi, S. and M. Pradeep Kumar (2012). "Experimental investigation of cryogenic cooling in milling of AISI D3 tool steel". In: *Materials and Manufacturing Processes* 27.10, pp. 1017–1021. ISSN: 10426914. DOI: 10.1080/10426914.2011.654157.

Reid, Carlton (2018). *Ride London leads to clean air (one day only) - BikeBiz.*

Roeder, Ryan K. (2013). "Mechanical Characterization of Biomaterials". In: *Characterization of Biomaterials.* ISBN: 9780124158009. DOI: 10.1016/B978-0-12-415800-9.00003-6.

Rohm, Sebastian et al. (May 2016). "Effect of Different Bearing Ratios on the Friction between Ultrahigh Molecular Weight Polyethylene Ski Bases and Snow". In: *ACS Applied Materials & Interfaces* 8.19, pp. 12552–12557. ISSN: 1944-8244. DOI: 10.1021/acsami.6b02651.

Rudin, Alfred (1982). *The Elements of Polymer Science and Engineering.* United Kin. New York: Academic Press Inc., p. 485. ISBN: 0126016801.

Rymuza, Z. (1996). "Energy concept of the coefficient of friction". In: *Wear* 199.2, pp. 187–196. ISSN: 00431648. DOI: 10.1016/0043-1648(95)06895-3.

Schertzer, Michael J. and Patricia Iglesias (2018). "Meta-analysis comparingwettability parameters and the effect ofwettability on friction coefficient in lubrication". In: *Lubricants* 6.3. ISSN: 20754442. DOI: 10.3390/lubricants6030070.

Schmidt, Tannin A. et al. (2007). "Boundary lubrication of articular cartilage: Role of synovial fluid constituents". In: *Arthritis and Rheumatism* 56.3, pp. 882–891. ISSN: 00043591. DOI: 10.1002/art.22446.

Schmitt, C., L. Aberkane, and C. Sanchez (2009). *Protein-polysaccharide complexes and coacervates*. Woodhead Publishing Limited, pp. 420–476. ISBN: 9781845695873. DOI: 10.1533/9781845695873.420.

Schnurmann, Robert (1942). "Amontons' Law, "Traces" of Frictional Contact, and Experiments on Adhesion". In: *Journal of Applied Physics* 13.4, pp. 235–245. ISSN: 0021-8979. DOI: 10.1063/1.1714861.

Schrader, M. E. (1995). "Young-Dupre revisited". In: *Langmuir* 11.9, pp. 3585–3589. ISSN: 0743-7463. DOI: 10.1021/la00009a049.

Silva, Mariana Altenhofen da, Andréa Cristiane Krause Bierhalz, and Theo Guenter Kieckbusch (2009). "Alginate and pectin composite films crosslinked with Ca2+ ions: Effect of the plasticizer concentration". In: *Carbohydrate Polymers* 77.4, pp. 736–742. ISSN: 01448617. DOI: 10.1016/j.carbpol.2009.02.014.

Sperling, Daniel and Deborah Gordon (2009). *Two billion cars: driving toward sustainability*. Oxford ; New York: Oxford University Press. ISBN: 9780195376647.

Stachowiak, Gwidon W and Andrew W Batchelor (2014). *Engineering tribology*. 4. ed. {BH}, Butterworth-Heinemann/Elsevier. ISBN: 978-0-12-397776-2 978-0-12-397047-3 978-1-299-87572-2.

Stachowiak, Gwidon and Andrew Batchelor (2006). *Engineering Tribology*. ISBN: 9780750678360. DOI: 10.1016/B978-0-7506-7836-0.X5000-7.

Stead, Iestyn M. N. et al. (2019). "Cold, clean and green: improving the efficiency and environmental impact of a cryogenic expander". In: *IOP Conference Series: Materials Science and Engineering* 502, p. 012157. ISSN: 1757-899X. DOI: 10.1088/1757-899X/502/1/012157.

Stead, Iestyn M.N. et al. (July 2019). "Towards a plastic engine: Lowtemperature tribology of polymers in reciprocating sliding". In: *Wear* 430-431.January, pp. 25–36. ISSN: 00431648. DOI: 10.1016/j.wear.2019.04.008.

Thakur, Beli R. et al. (1997). "Chemistry and uses of pectin A review". In: *Critical Reviews in Food Science and Nutrition* 37.1, pp. 47–73. ISSN: 1040-8398. DOI: 10.1080/10408399709527767.

Thomas, Alfred, Bertrand Matthäus, and Hans-Jochen Fiebig (2015). "Fats and Fatty Oils". In: *Ullmann's Encyclopedia of Industrial Chemistry*, pp. 1–84. DOI: 10.1002/14356007.a10_173.pub2.

Tukey, John (1977). "Exploratory data analysis". In:

Walshaw, A.C (1946). *Heat Engines (A first text-book)*. Ed. by Green Longmans and Co. Ltd. Reprinted. London, p. 412.

Wang, Kathy (1996). "The use of titanium for medical applications in the USA". In: *Materials Science and Engineering A* 213.1-2, pp. 134–137. ISSN: 09215093. DOI: 10.1016/0921-5093(96)10243-4.

Wang, Shiren et al. (2009). "Wettability and surface free energy of graphene films". In: *Langmuir* 25.18, pp. 11078–11081. ISSN: 07437463. DOI: 10.1021/la901402f.

Whyman, Gene, Edward Bormashenko, and Tamir Stein (2008). "The rigorous derivation of Young, Cassie-Baxter and Wenzel equations and the analysis of the contact angle hysteresis phenomenon". In: *Chemical Physics Letters* 450.4-6, pp. 355–359. ISSN: 00092614. DOI: 10.1016/j.cplett.2007.11.033.

Wrigley, E. A. (2010). *Energy and the English Industrial Revolution*. Cambridge: Cambridge University Press, pp. 1–96. ISBN: 9780511779619. DOI: 10.1017/CBO9780511779619.

Yan, Yingdi, Emil Chibowski, and Aleksandra Szcze (2017). "Surface properties of Ti-6Al-4V alloy part I: Surface roughness and apparent surface free energy". In: *Materials Science and Engineering C* 70, pp. 207–215. ISSN: 09284931. DOI: 10.1016/j.msec.2016.08.080.

Yeo, Seung Min and Andreas A. Polycarpou (Aug. 2012). "Tribological performance of PTFE- and PEEK-based coatings under oil-less compressor conditions". In: *Wear* 296.1-2, pp. 638–647. ISSN: 00431648. DOI: 10.1016/j.wear.2012.07.024.

Zhang, G., Z. Rasheva, and A. K. Schlarb (2010). "Friction and wear variations of short carbon fiber (SCF)/PTFE/graphite (10 vol.%) filled PEEK: Effects of fiber orientation and nominal contact pressure". In: *Wear* 268.7-8, pp. 893–899. ISSN: 00431648. DOI: 10.1016/j.wear.2009.12.001.

Zhang, Z. et al. (2004). "Wear of PEEK composites related to their mechanical performances". In: *Tribology International* 37.3, pp. 271–277. ISSN: 0301679X. DOI: 10.1016/j.triboint.2003.09.005.

Zhu, Yi, Ulf Olofsson, and Rickard Nilsson (2014). "A field test study of leaf contamination on railhead surfaces". In: *Proceedings of the Institution of Mechanical Engineers, Part F: Journal of Rail and Rapid Transit* 228.1, pp. 71–84. ISSN: 09544097. DOI: 10.1177/0954409712464860.